U.S. DEPARTMENT OF ENERGY

JSA

USPAS June 2015

Rutgers

RF, CRYOGENIC & OTHER METHODS FOR SRF SURFACES

Anne-Marie Valente-Feliciano

Thomas Jefferson National Accelerator Facility

MOTIVATION

Determination for SRF cavities & samples of

Superconducting properties:

- ❑Transition temperature T_c
- ❑Energy gap Δ
- ❑Coherence length ξ
- ❑Penetration depth λ
- ❑Mean free path l
- ❑Critical field H_{c1}
- ❑Critical field H_{c2}
- ❑Superheating field $H_{sh,}$Max screening field H_m

RF Performance:

- ❑Surface Resistance R_s
- ❑Quality factor Q vs E_{acc}

Through RF, cryogenic and other measurements

Quality Factor Q vs. E_{acc}

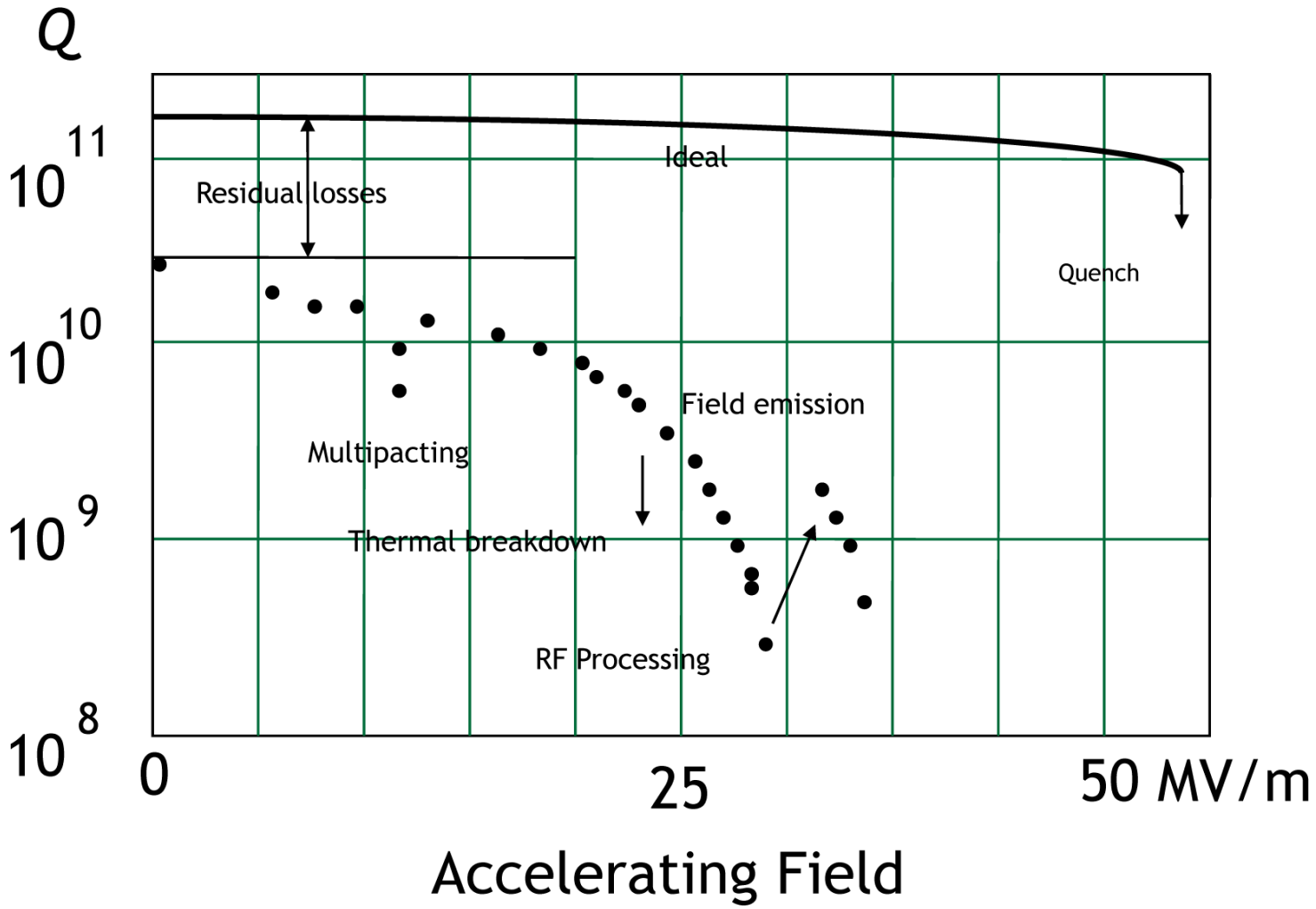

Surface Resistance

Transition temperature
Energy gap
Coherence length
Penetration depth
Mean free path

$$R_s \sim \frac{A}{T}\omega^2 \exp\left(-\frac{\Delta}{kT}\right) + R_{res}$$

In the dirty limit $l \ll \xi_0$ $R_{BCS} \propto l^{-1/2}$

In the clean limit $l \gg \xi_0$ $R_{BCS} \propto l$

R_{res}:

Residual surface resistance

No clear temperature dependence

No clear frequency dependence

Depends on trapped flux, impurities, grain boundaries, …

RF Surface Resistance of SRF materials

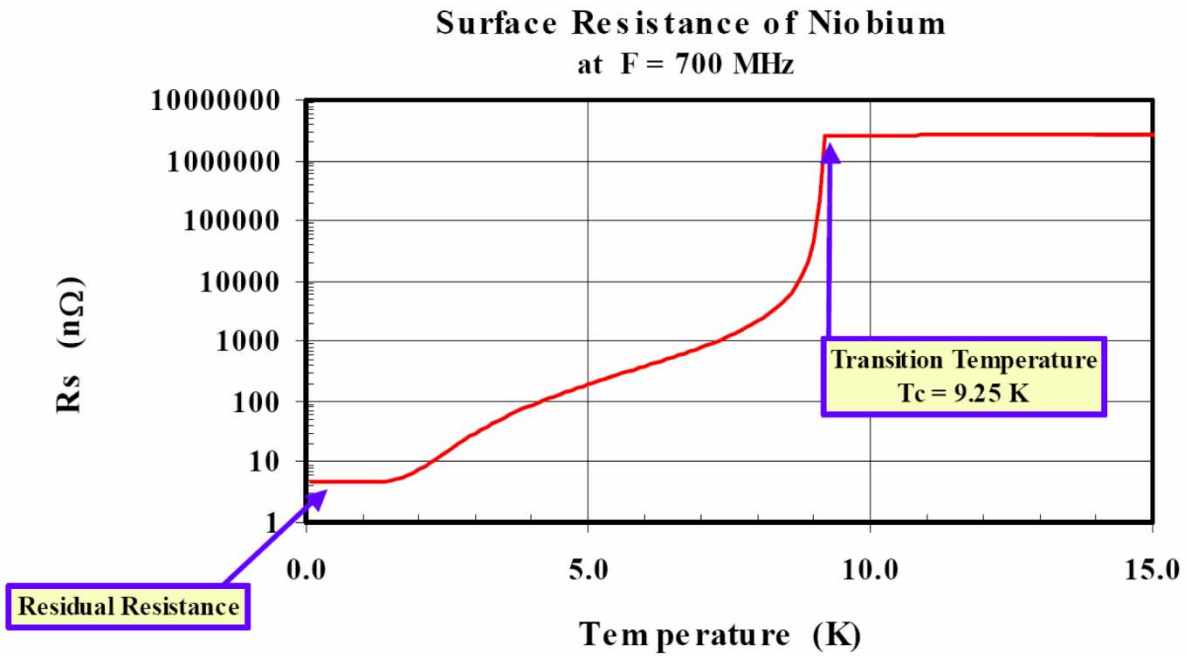

Understand the rf surface impedance of actual and candidate materials for application to particle accelerators.

Zs (*f, T, Hsurf , x, y)*

The frequency dependence of the BCS component is well behaved. ~ f^2

The temperature dependence of the BCS component is well behaved: ~ exp(-Δ/*kT) kT*

Non-linear terms in H_{surf} *are the subject of much discussion.*

Thermometric mapping indicates that high-field non-linear losses are non-uniform.

Critical Magnetic Fields

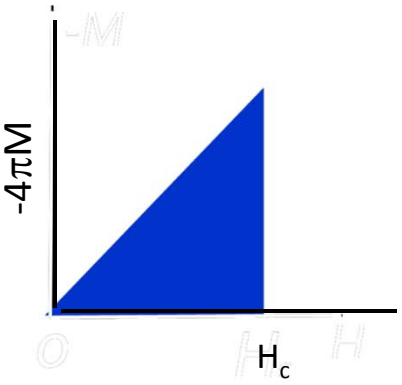

Type-I

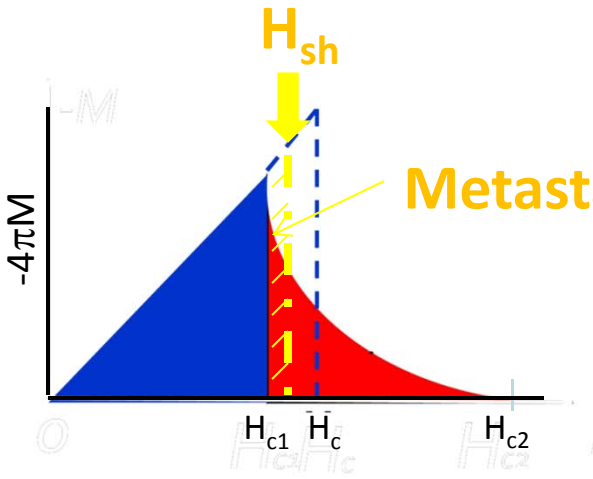

Type-II

Boundary between Type I and Type II determined by the Ginzburg-Landau parameter

$$\kappa = \lambda/\xi$$

Hc is the thermodynamic critical field

&

$H_c = H_{c2}/\sqrt{2}\kappa$

(for type-II superconductors).

- Meissner state at $0 < H < H_{c1}$
- Mixed vortex state at $H_{c1} < H < H_{c2}$
- Exponentially small R_s at $H < H_{c1}$ ($Q = 10^{10}$-10^{11})
- Drastic Q drop due to vortex dissipation at $H > H_{c1}$

The superheating field H_{sh} is the field up to which the Meissner state metastably persists above H_{c1}

For type-II superconductors, at T = O in the clean limit with a Gindzburg-Landau parameter $\kappa=\lambda/\xi \gg 1$, H_{sh} has been calculated to be ~ $0.75H_c$.

$$H_{RFcrit} \approx H_{sh}$$

RF critical magnetic field measurement

Measurement of the fundamental rf critical field H_{RFC} using high peak pulsed power to raise the cavity fields well above the CW limits.

- Depending upon the surface resistance of the cavity and the heat conduction path away from the rf surface, the temperature of the rf surface may be elevated much above the cooling bath temperature.
- The observed quench field would then be an indirect measure of the temperature dependent rf critical magnetic field.
- To circumvent the problem of localized defects, H^{rf}_c is measured in a pulsed mode instead of continuous wave. By coupling in power very strongly, the surface fields in the cavity are raised much faster ($\text{few } \mu s \text{ to } 100\mu s$) than the characteristic timescales of heat propagation. A growing normal conducting region in the vicinity of a defect doesn't have time to envelop the cavity.
- The cavity quenches due to its intrinsic H^{rf}_c while the normal zone is still small.
- The size of the normal zone is estimated by measuring the Q0 of the cavity.

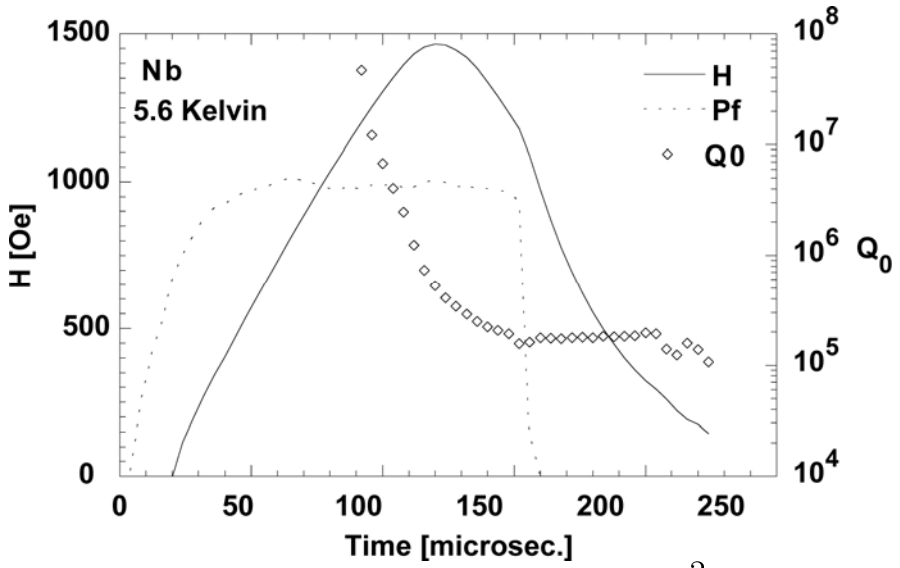

$$P_r = \left(\sqrt{P_i} - \sqrt{\omega U/Q_e}\right)^2$$

$$\frac{1}{Q_0} = \frac{2\left(\sqrt{\frac{P_i\omega}{Q_e}} - \frac{d\sqrt{U}}{dt}\right)}{\omega\sqrt{U}} - \frac{1}{Q_e}.$$

RF critical magnetic field measurement

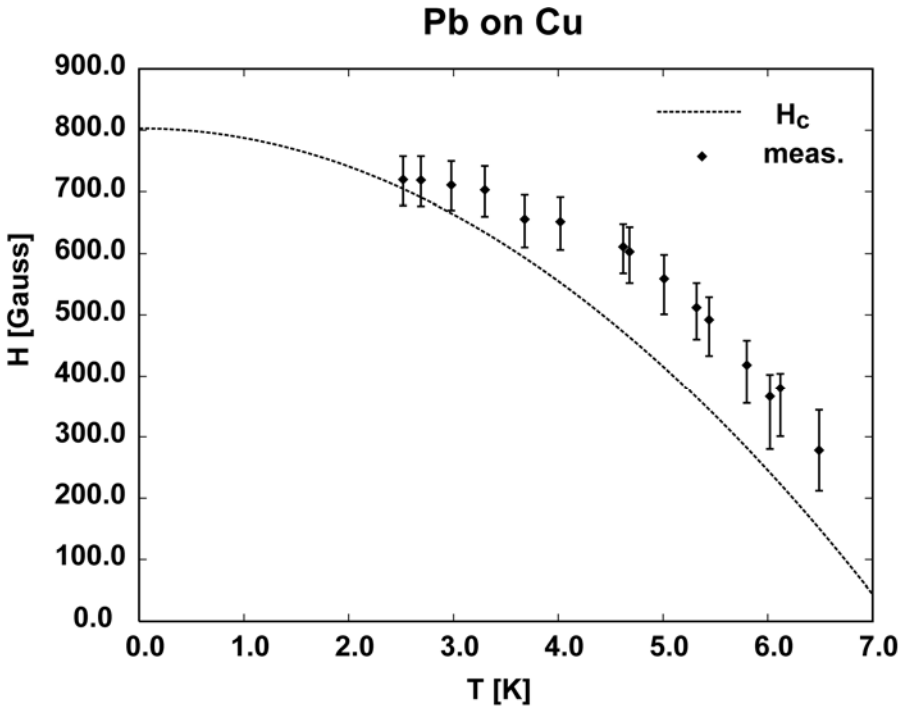

Figure 3: Measuring the H_c^{rf} of lead by pulsing a lead coated copper 1.3 GHz cavity.

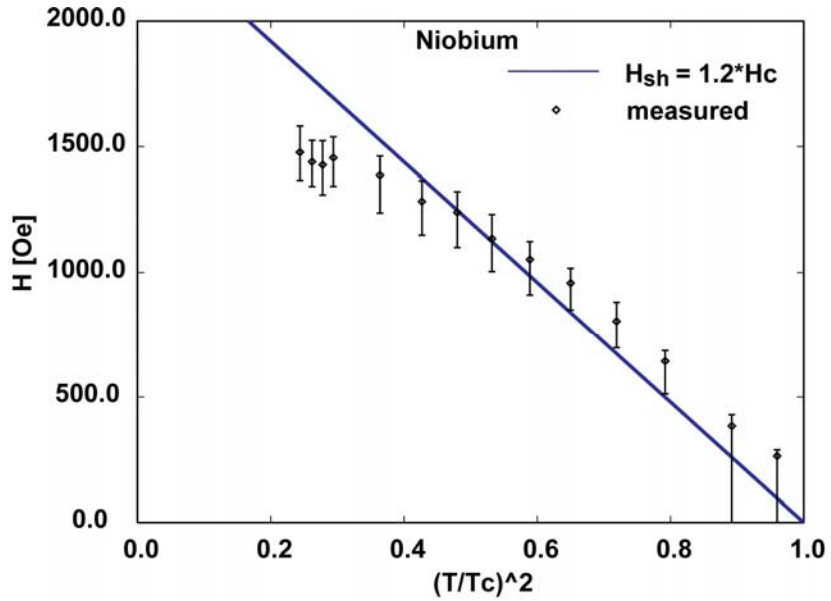

: Measuring the H_c^{rf} of niobium by pulsing a 1.3 GHz bulk niobium cavity of high RRR.

Penetration Depth λ Measurement

The variation of the cavity resonance frequency f when T approaches T_c provides a direct measurement of the temperature dependence of the penetration depth λ.

More precisely, the reactive component of the cavity surface impedance X is related to the resonant frequency *f by the formula:*

$$X = 2G\frac{(f - f_0)}{f_0},$$

where G is the geometric factor and *f0 is the frequency of an ideal cavity* (perfectly conducting). Moreover, X is proportional to the frequency and magnetic penetration depth ($X = 2\pi f m_0 l$).

Consequently, starting at an initial temperature $T_0 = 4.2K$ and recording the cavity frequency shift due to temperature variation, we can easily deduce the corresponding *:*

$$\Delta\lambda(T) = \lambda(T) - \lambda(T_0) = \frac{G}{\pi\mu_0}\frac{\Delta f}{f(T_0)^2}$$

RF measurement for Nb/Cu cavities

Surface resistance Rs measurement as a function of the RF field amplitude between 4.2 K and 1.7 K:

- Since the surface resistance at 4.2 K is much higher than at 1.7 K, the two measurements give almost uncorrelated measurements of the BCS surface resistance and of the residual resistance.
- Systematic measurement of Rs with an external magnetic flux trapped into the film when crossing the superconducting transition. Gives indications about the effect of localized defects (the pinning centers for the trapped fluxoids) on the surface resistance.
- Tc measured through the observation of the transition from the Meissner state
- λ computed by measuring the frequency shift as a function of temperature, normalized to the frequency shift of bulk niobium used as a clean limit reference ($l/\xi_0 \sim 20$).

The penetration depth is in turn linked to the electron mean free path through the formula

$$\lambda(l)=\lambda_{CLEAN}(1+\pi\xi_0/2l)^{1/2}.$$

- Approximate evaluation of the lower critical field Hc1 by using a small superconducting coil placed at the equator of the cavity in the cryostat, and by measuring the value of the punch-through field at which the surface resistance starts increasing.
- Since the field lines are distorted by the presence of the Cu cavity it is only possible to perform relative measurements, and the results must be normalized to the value measured for bulk niobium.

Thermometry/T-mapping

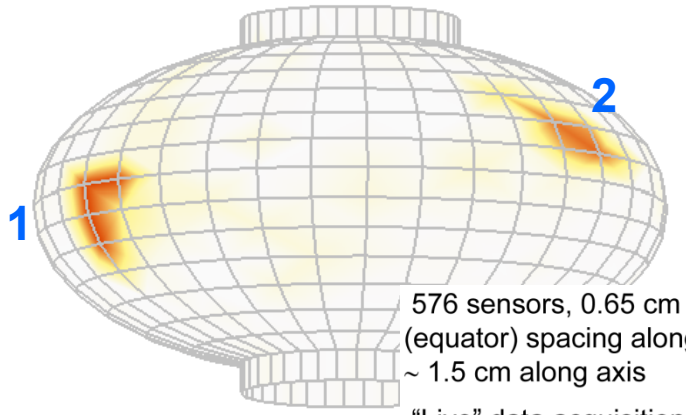

576 sensors, 0.65 cm (iris) – 1.7 cm (equator) spacing along circumference, ~ 1.5 cm along axis

"Live" data acquisition during rf test

Designed to fit CEBAF shape single-cell

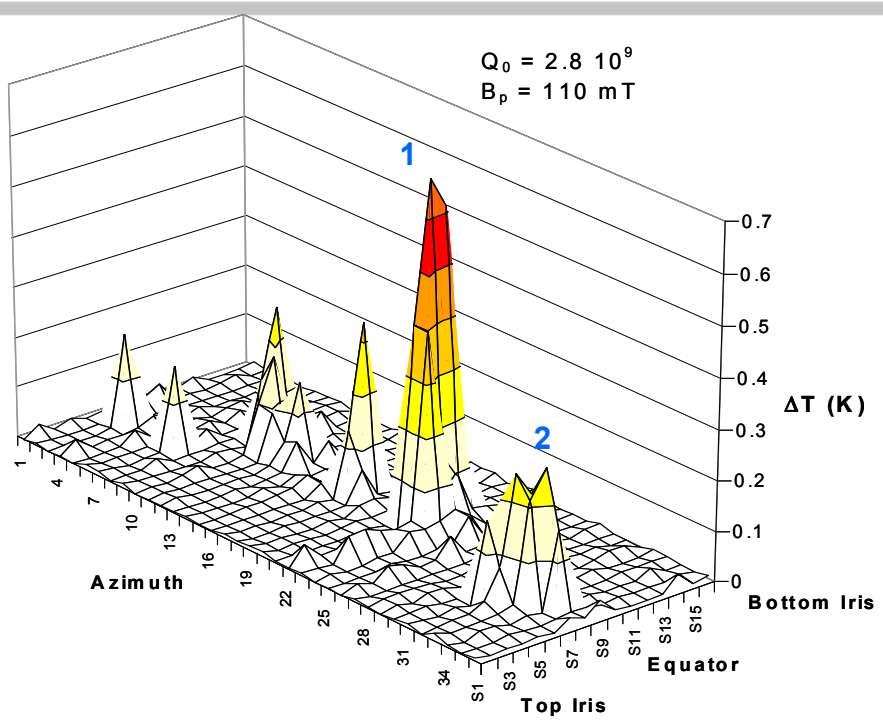

Thermometer array to detect hotspots, which ignite cavity breakdown

G. Ciovati - JLab - ODU

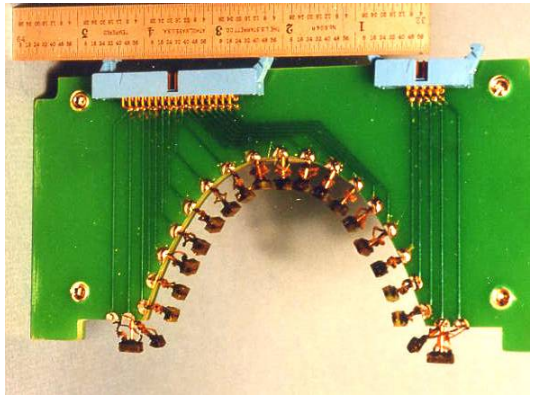

H. Padamsee - Cornell

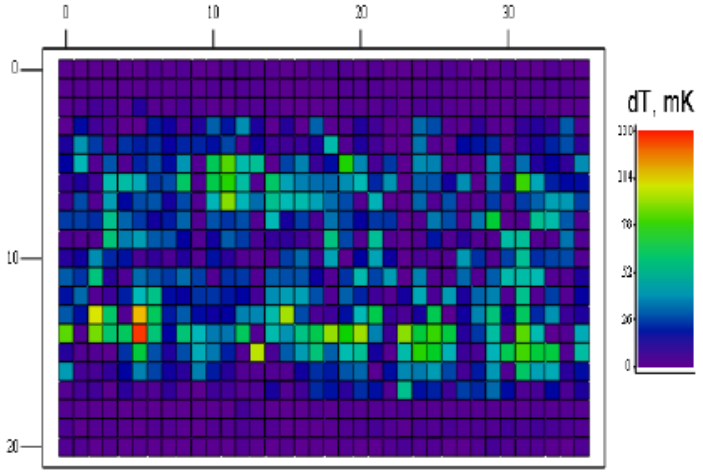

Thermometry/T-mapping

9-cell cavity assembly

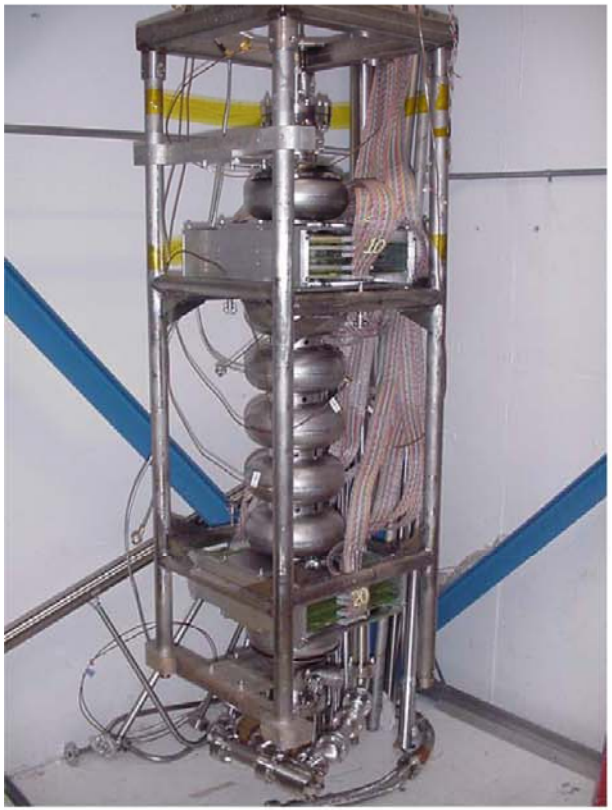

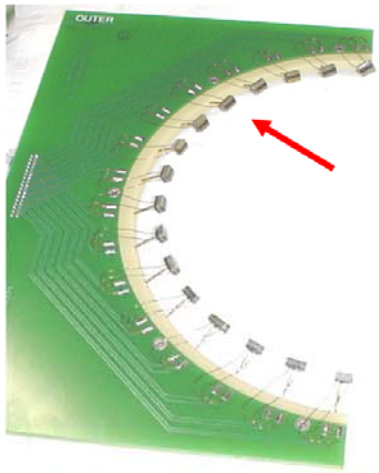

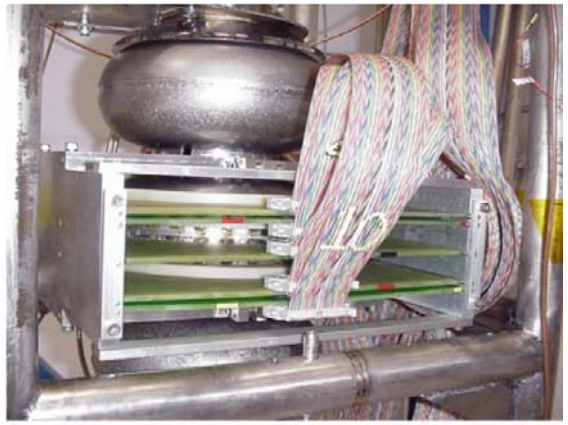

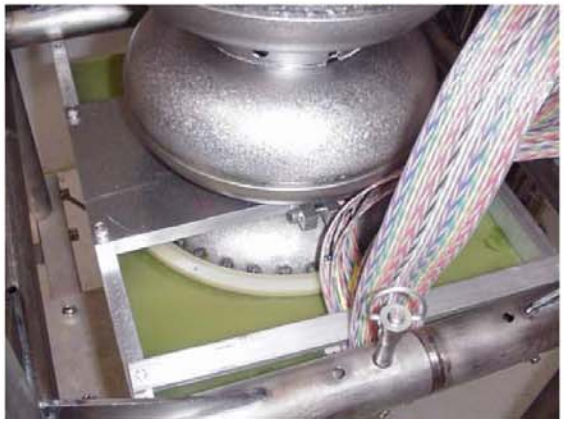

Thermometry/T-mapping

Thermometry assembled on cells #8 (bottom) and #2 (top). Cells' numbering starts from field probe side.

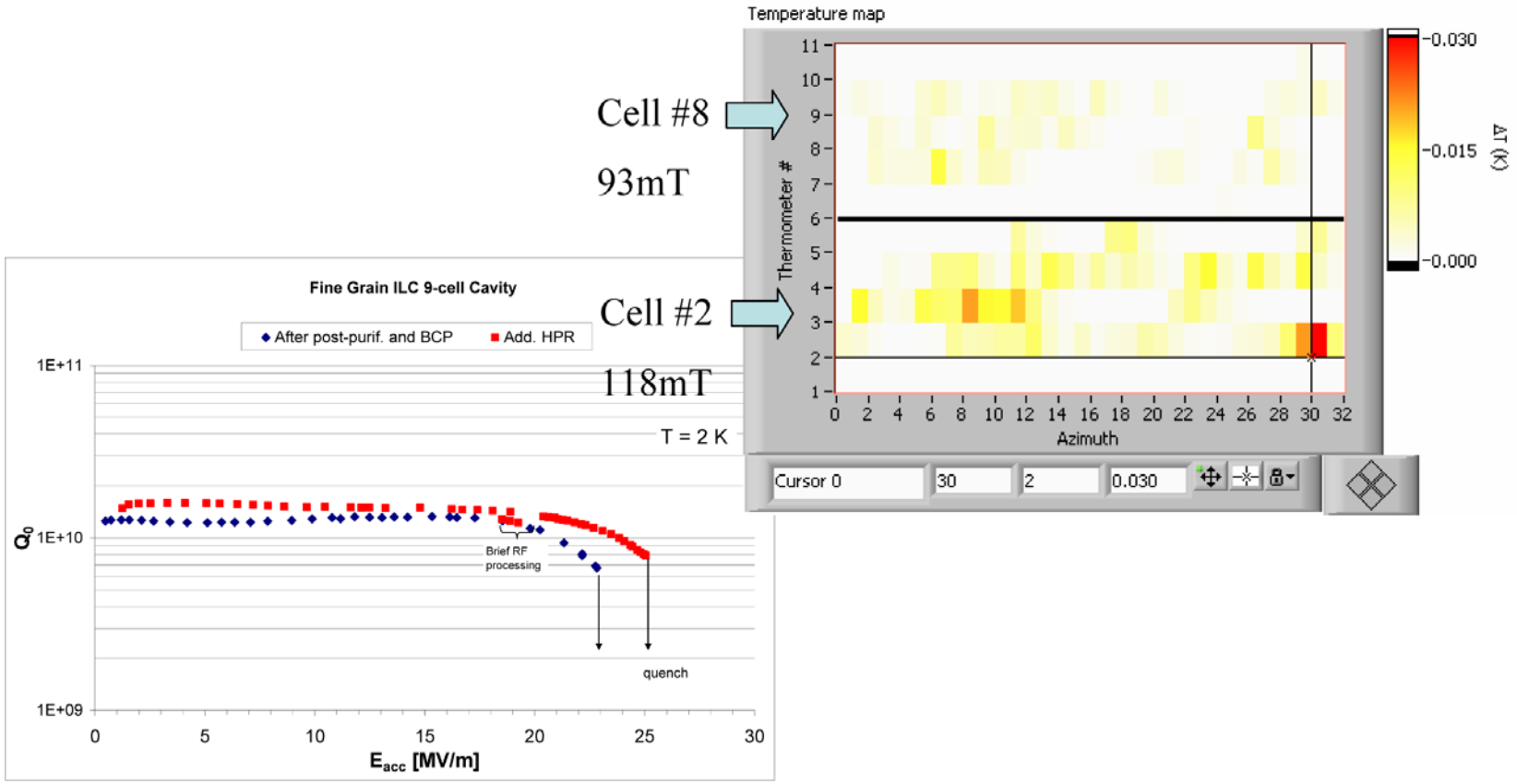

A "hot-spot" was identified on the equator weld of Cell #2 but the quench does not seem occur in either cell…

Thermometry/T-mapping

- Temperature mapping on other TM_{010} passband modes suggested that the field profile in the π-mode may not be flat
- T-maps in the 3π/9 and 4π/9 modes revealed different quench locations in cell #8 in the two modes

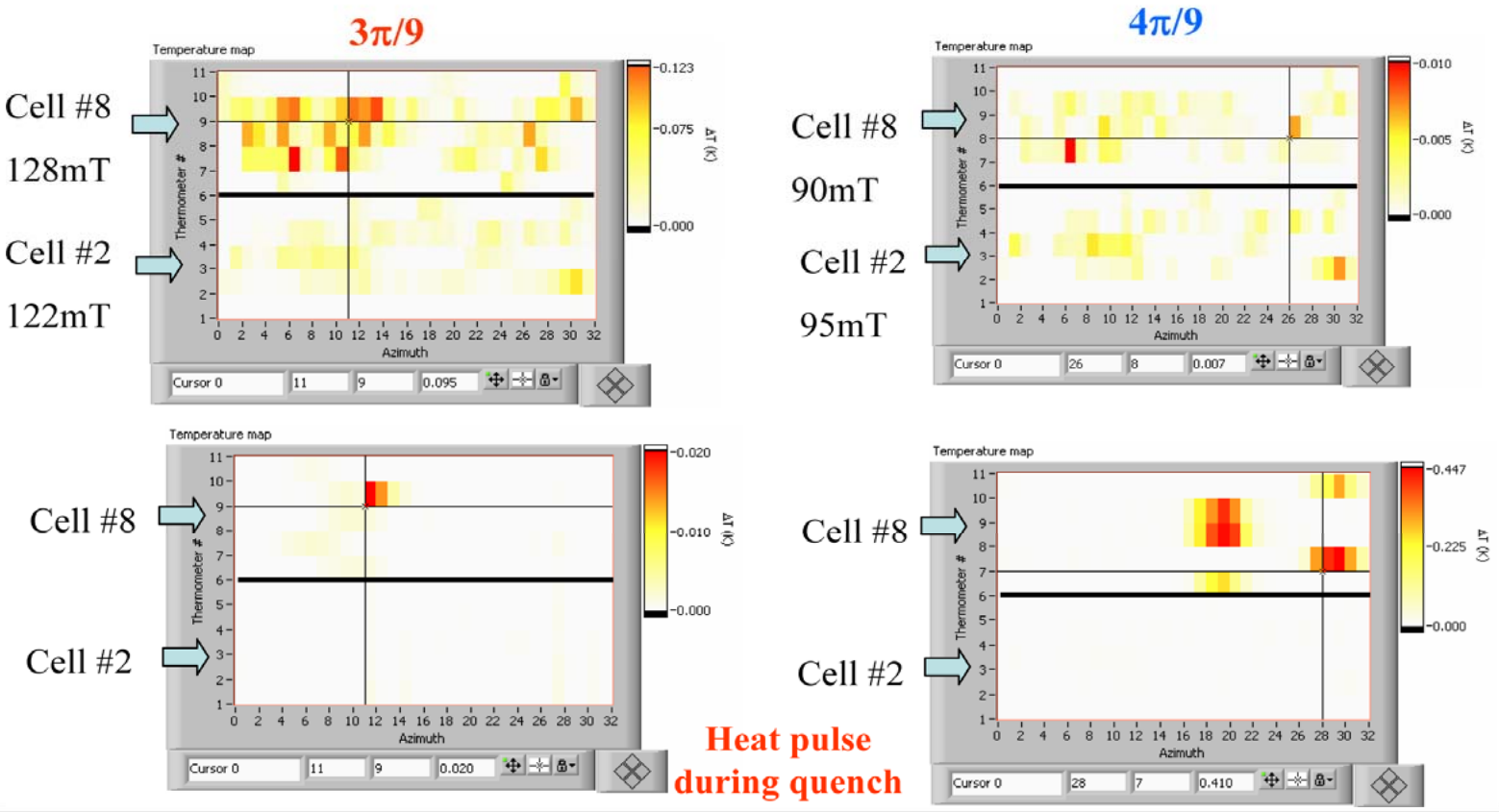

Thermometry in support of ILC

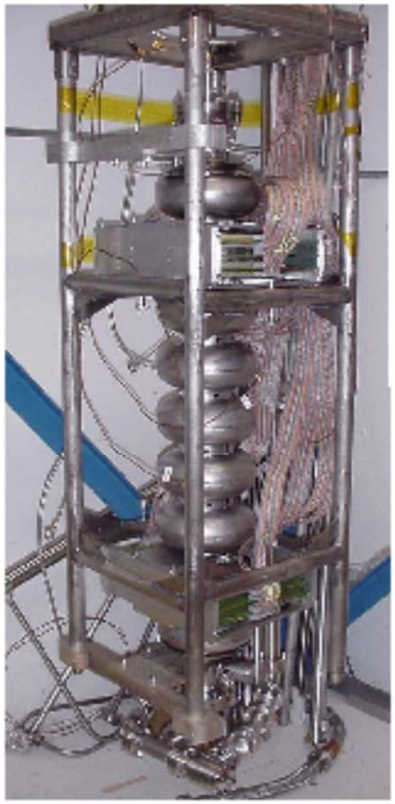

A 2-cell thermometry system for ILC 9-cell cavity was designed, built and commissioned at JLab and will be used routinely in conjunction with optical inspection of hot-spots & defects to improve understanding of thermal breakdown.

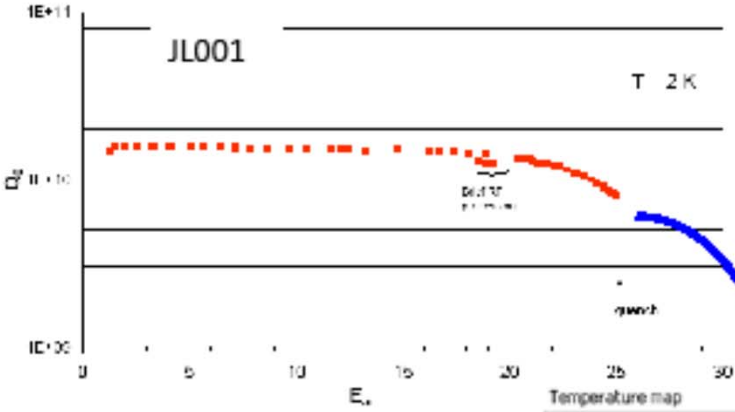

"Hot-spots" were detected near the equator weld of one of the cells, causing the Q-drop

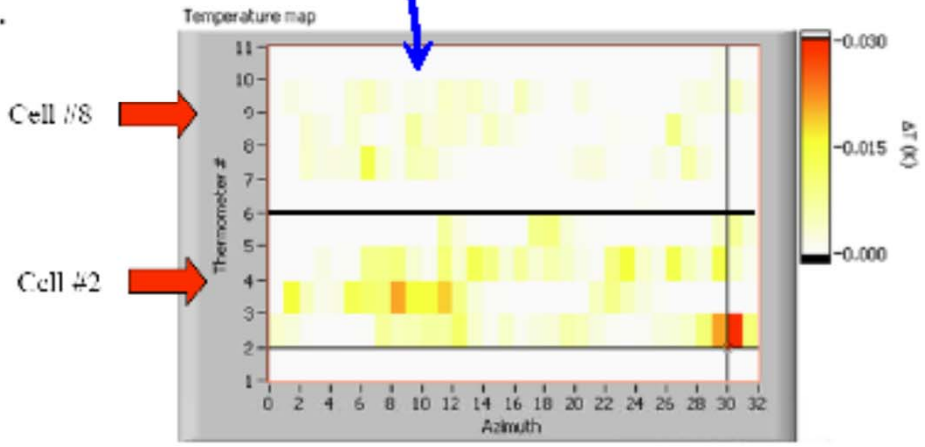

Second Sound as a Cavity Diagnostic Tool

Second Sound quench-spot location

- **Thermometry**
  - Full temperature map of the cavity at various field levels
  - Required for a detailed understanding of the cavity performance
  - Requires thousands of transducers

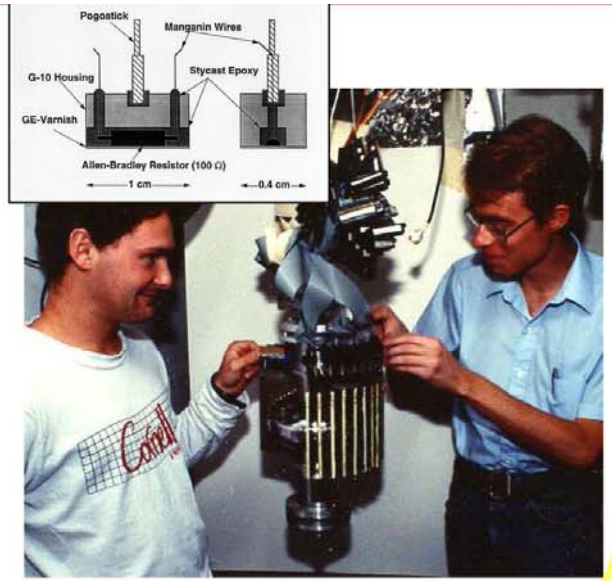

- **Second Sound**
  - Requires a few transducers (e.g. 8)
  - Simple
  - Fast
  - Accurate
  - Only locates the quench-spot
  - Convenient for the rapid testing/repair of cavities

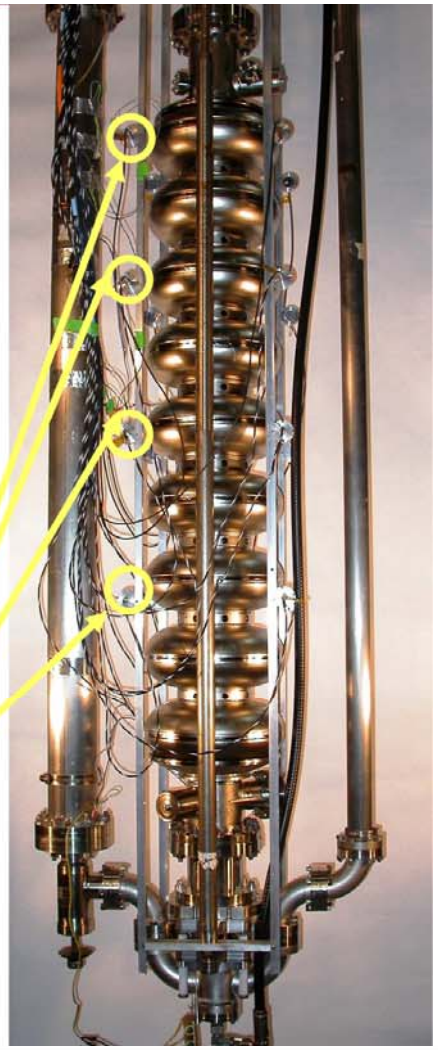

Second Sound as a Cavity Diagnostic Tool

Wave Propagation in LHe

– Normal P-r wave = 1st Sound, with velocity = ~ 220 m/s
– Below the lambda point a T-S wave can propagate = 2nd Sound, with velocity = ~ 20 m/s
– Superfluid r-T wave = 4th Sound, with velocity = ~ 200 m/s

- The detector response time can be around 0.1 msec or less which implies a spatial uncertainty of 2 to 4 mm if the start time (initiation of cavity RF field collapse) can be determined to the same timing uncertainty

- Simple defect localization schemes can be implemented by exploiting the properties of superfluid He, e.g. second sound waves.
- When a cavity quenches, typically several joules of thermal energy are transferred to the helium bath in a few microseconds.
- If the cavity is operated at T < 2.17K, the helium bath is a superfluid and a second sound wave propagates away from the heated region of the cavity.
- By locating several transducers in the helium bath around the cavity, the second sound wave front can be observed. The time of arrival of the second sound wave at a given transducer is determined by the time of flight from the heated region, which is centered on the defect causing quench.
- Measuring the time of flight to 3 or more uniquely located transducers, unambiguously determines the defect location.

Second Sound as a Cavity Diagnostic Tool

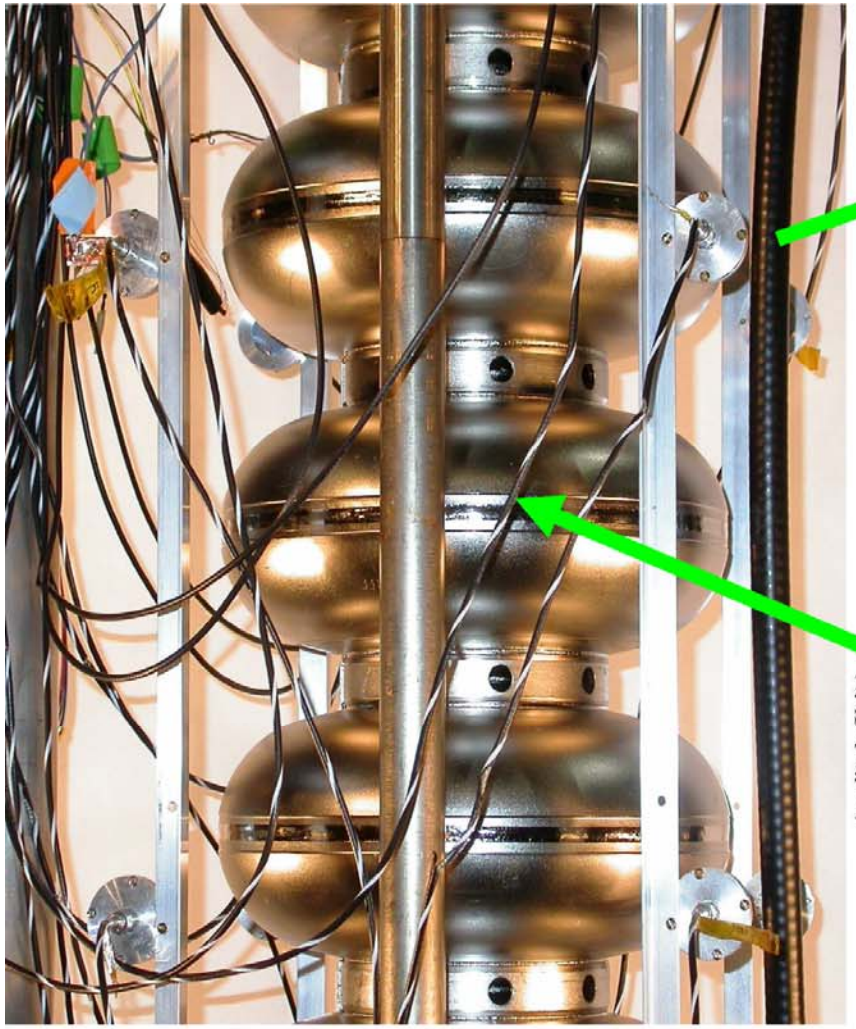

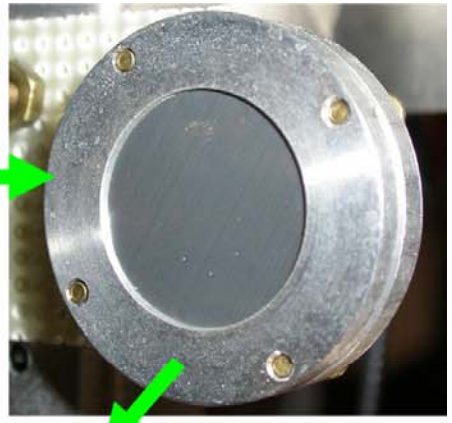

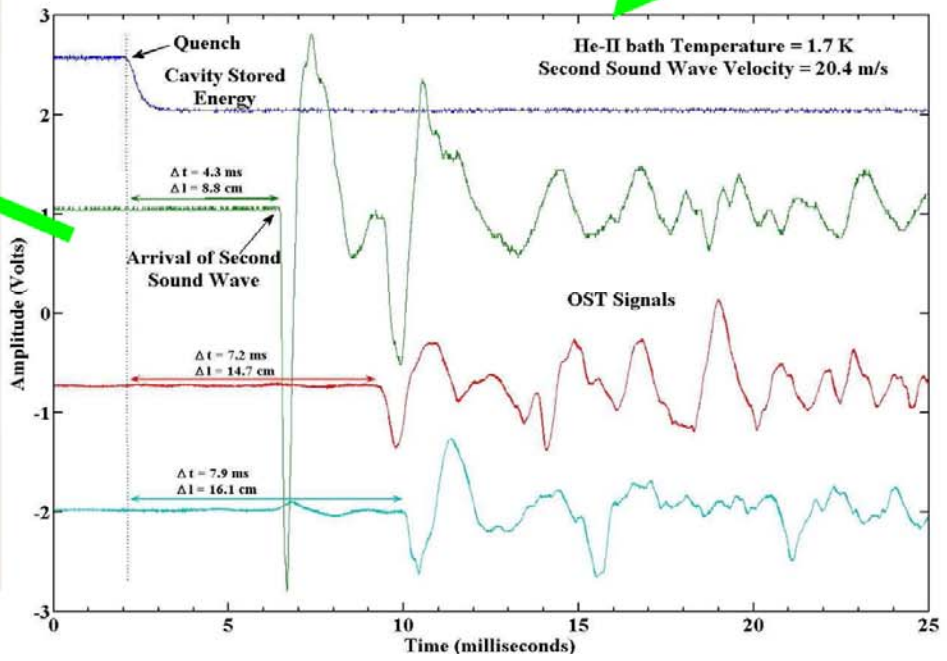

Second Sound as a Cavity Diagnostic Tool

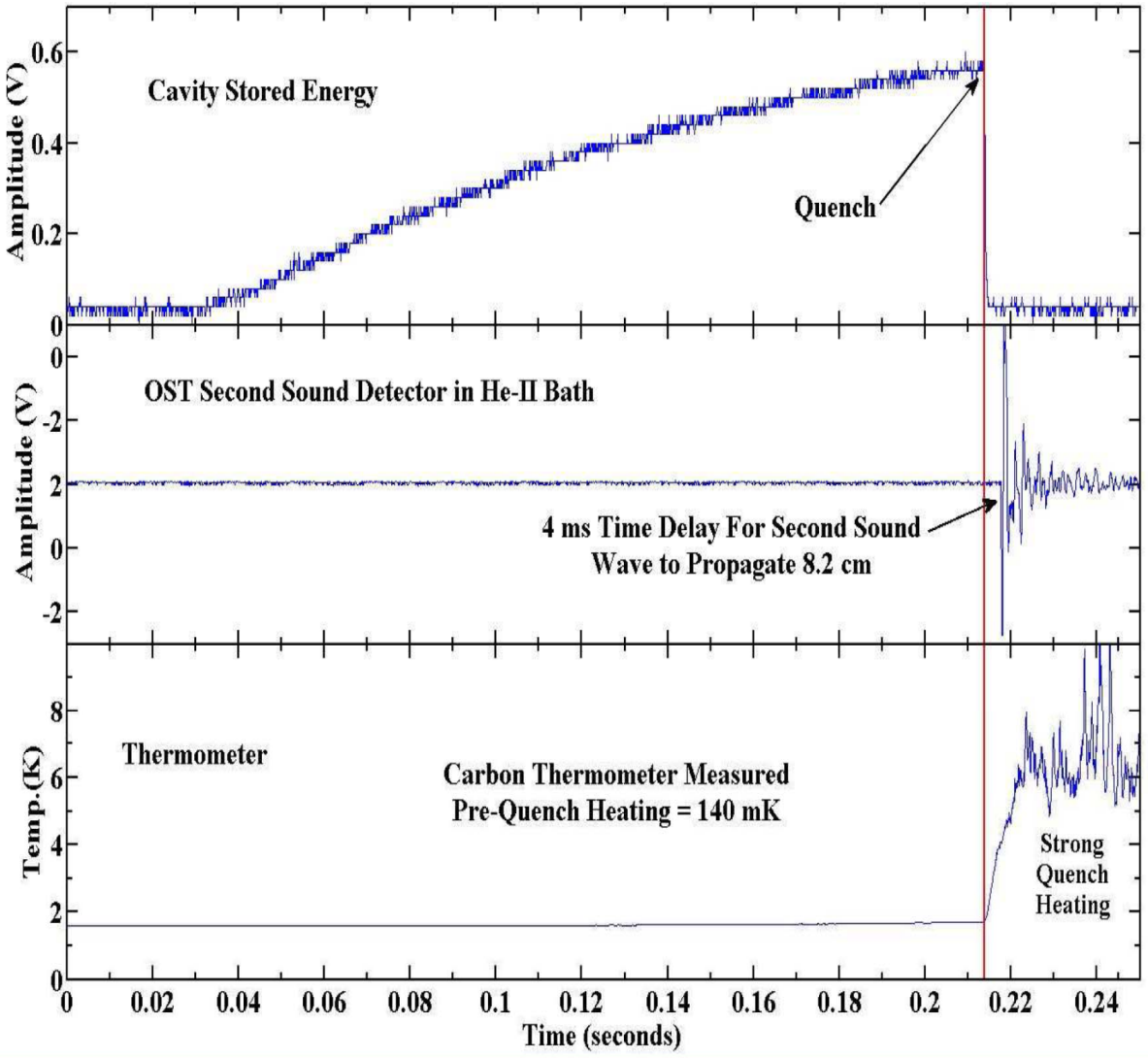

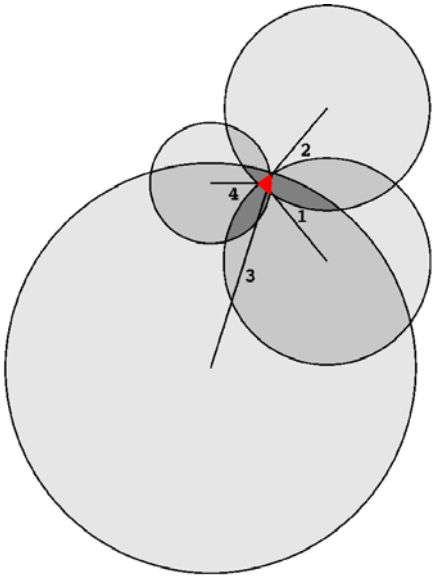

Figure 5: Spheres including the distance propagated by second sound. The intersecting volume is the most likely quench location.

Second Sound as a Cavity Diagnostic Tool

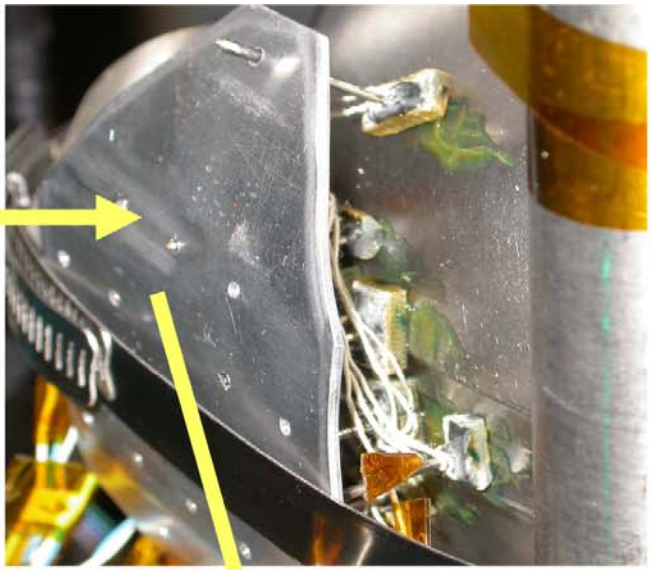

Comparison of fixed thermometer heating, 2nd sound location and Optical location. Defect heating is about 50 mK at 8 MV/m

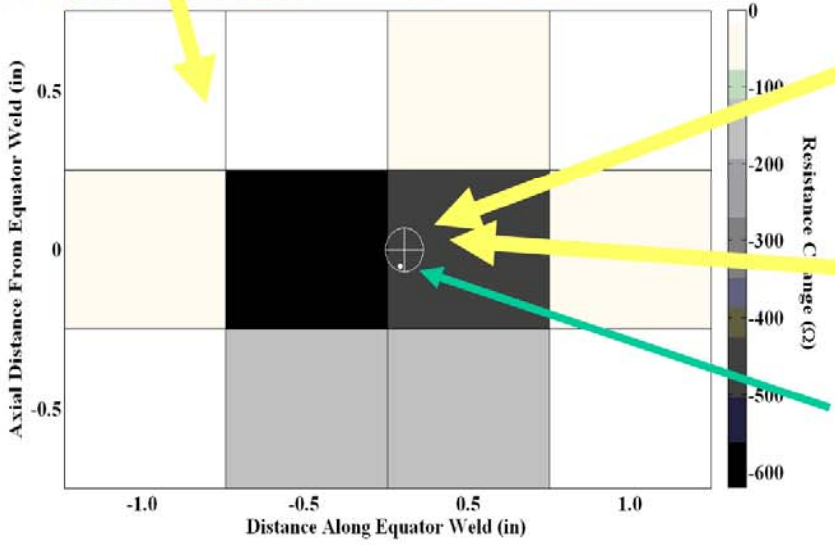

2nd Sound Defect Location

3mm radius circle around 2nd sound result

Optically Located Defect

Superheating field measurements

- Use short (~100 μs) high power pulses to drive 1.3 GHz Niobium cavity (800C, 10 μm EP, 110C bake for 48h)

(a)

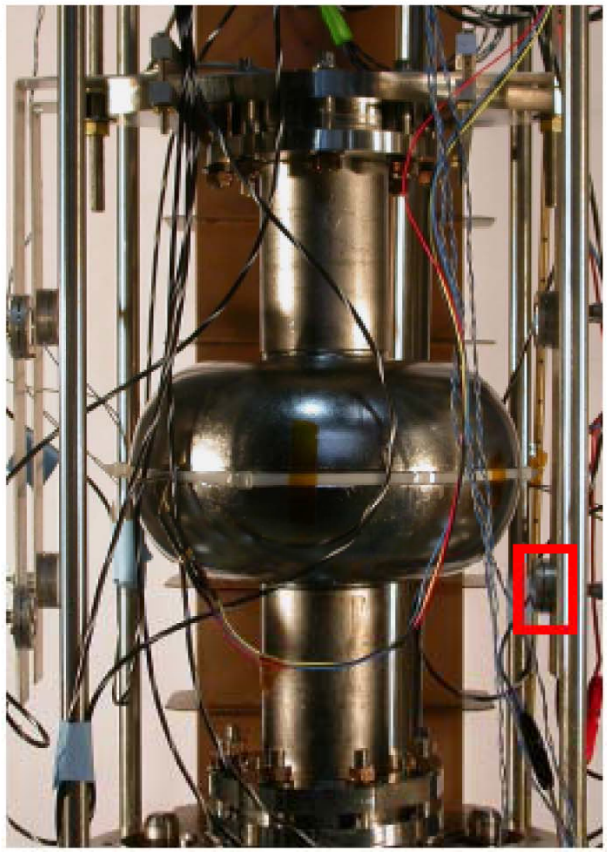

(b)

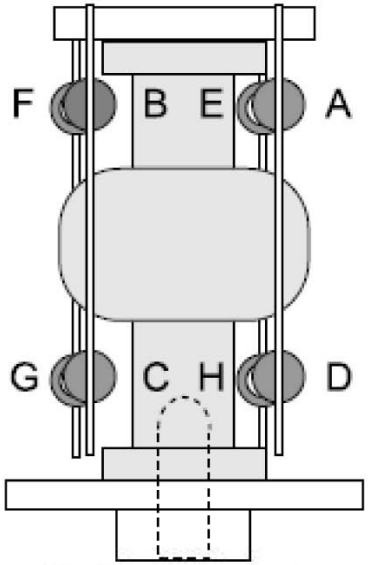

(c)

Diagnostics:

- Temperature sensors in bath and on cavity
- OST's to locate origin of quench
  -> can distinguish between quench by local defect and global phase transition at H_{sh}

H_{sh}: Pulsed Measurements

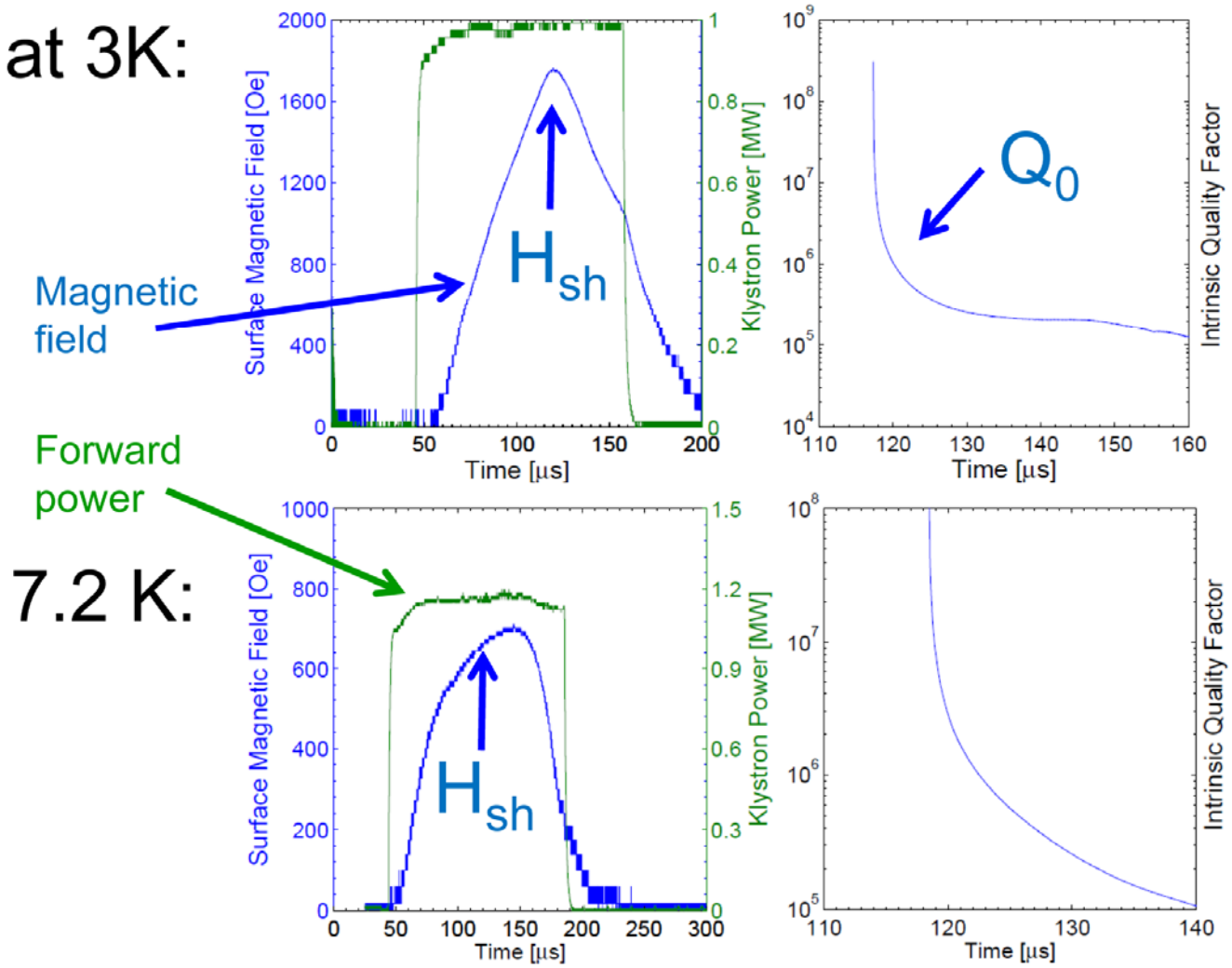

OST Data: Global phase transition

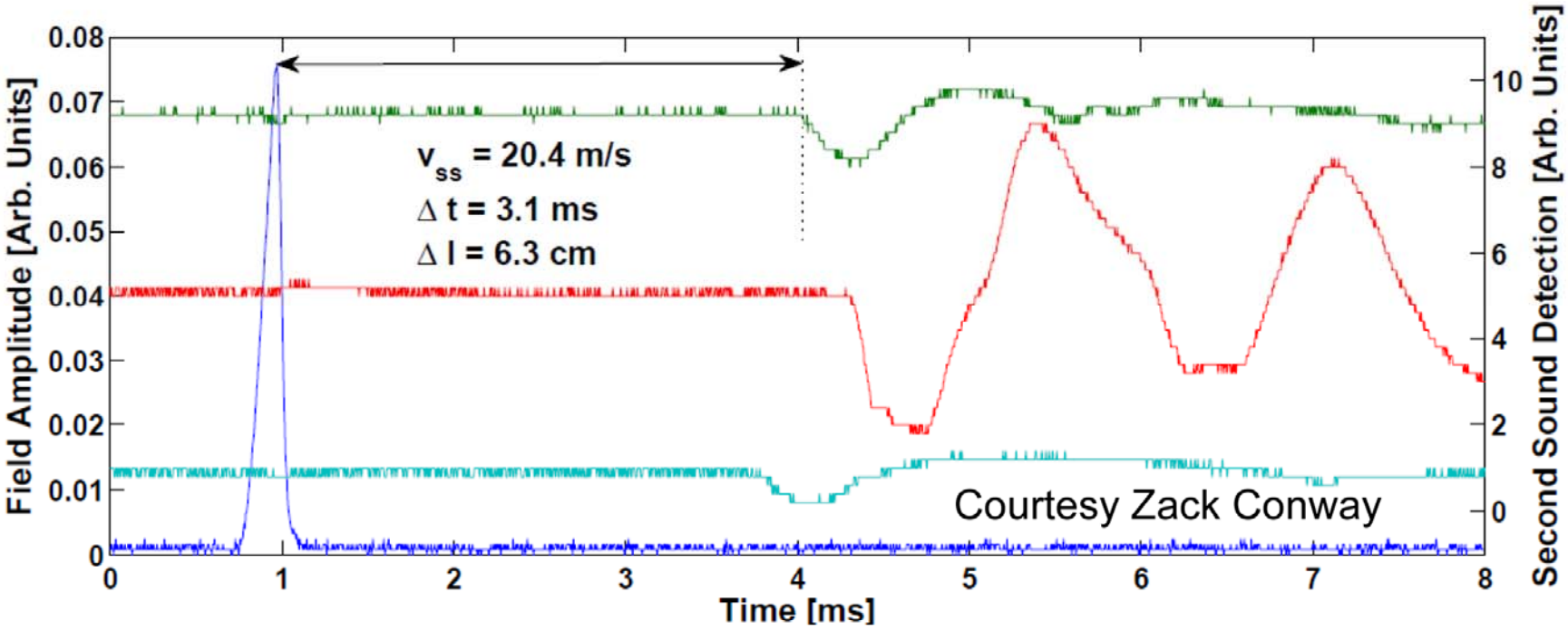

- All 8 OSTs show that second sound waves arrives first from the nearest high magnetic surface field area on the cavity, and not from a single defect location
  → global phase transition!

End result: $H_{sh}(T)$ of Niobium with $\kappa = 3.5$

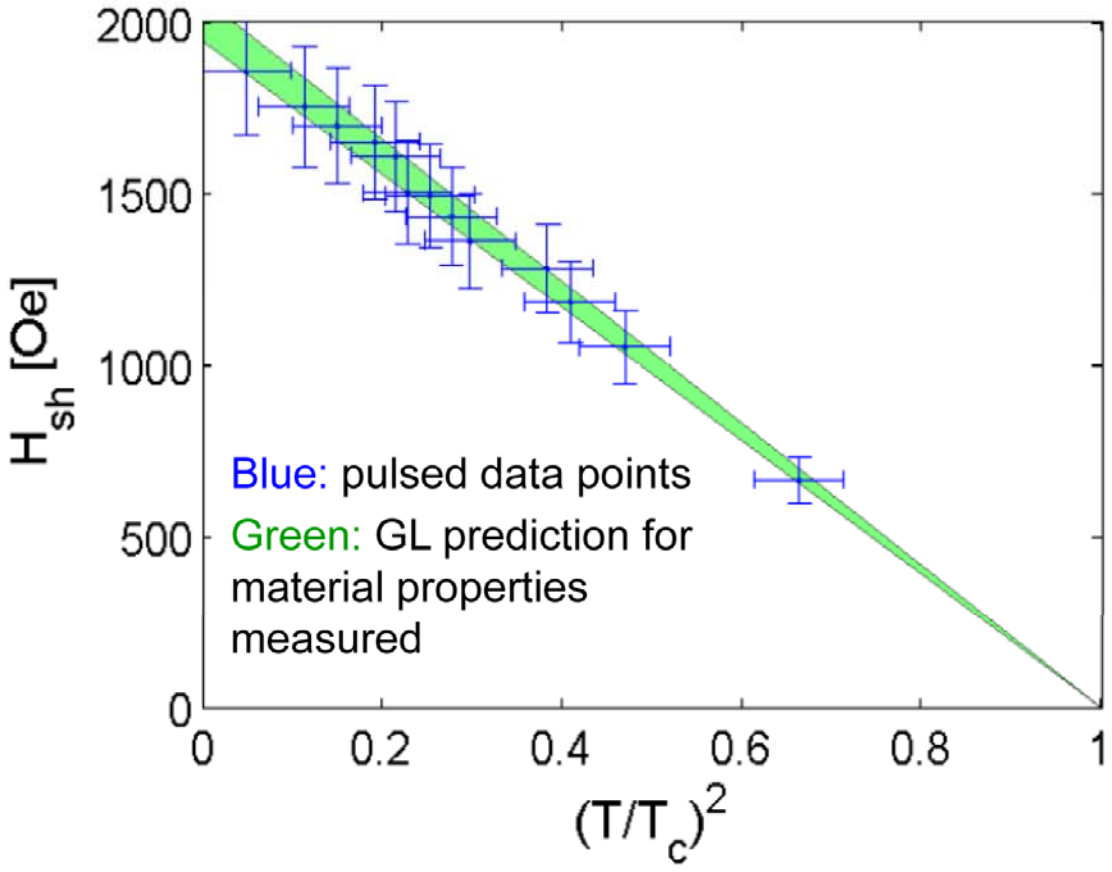

- Within ± 10% error bars:

$$H_{sh} \propto \left[1 - \left(\frac{T}{T_c}\right)^2\right]$$

down to 1.6 K

- Slop is in very good agreement with prediction from GL theory for material properties measured (κ= 3.5)

RF Surface Resistance of SRF samples

Characterization of samples vs. cavity

- ❑ Easier to create
- ❑ Easier to control
- ❑ Easier to examine (if planar and small)

⇒ Opportunity for systematic parametric studies

The practical challenge has been how to present known rf fields to samples and measure the impedance. *Pure rf techniques – make the sample part of a resonant circuit and observe the resonant frequency and Q-factor variation with temperature and field amplitude.*

RF + calorimetric techniques – measure directly the power dissipated in the sample from known rf field distribution.

TE011 cavities

- R_S can be determined by measuring Q_0
  $Q_0=G/R_S$
  - R_S may vary strongly over the cavity surface
- More convenient: Investigation of small samples
- One way TE cavity with demountable endplate
  - Large size concerning frequencies of interest for accelerator applications
  - Same field value on both endplates

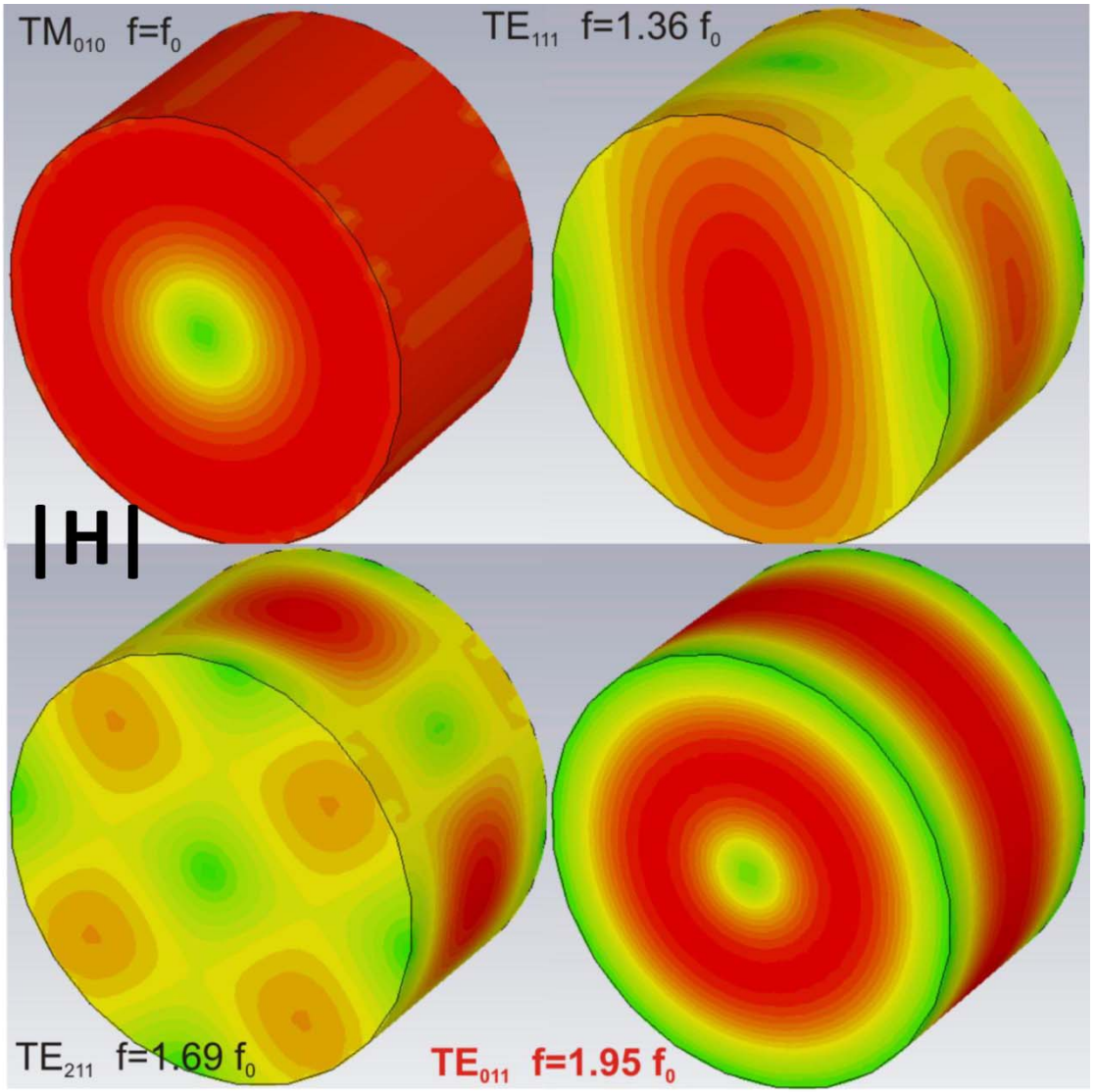

TE011 cavities

Small samples can be exposed to RF using a pill box cavity with demountable endplate

Two possible techniques
Replacement
Calorimetric

Drawbacks
Large size concerning frequencies of interest for accelerator applications
Same field value on both end plates

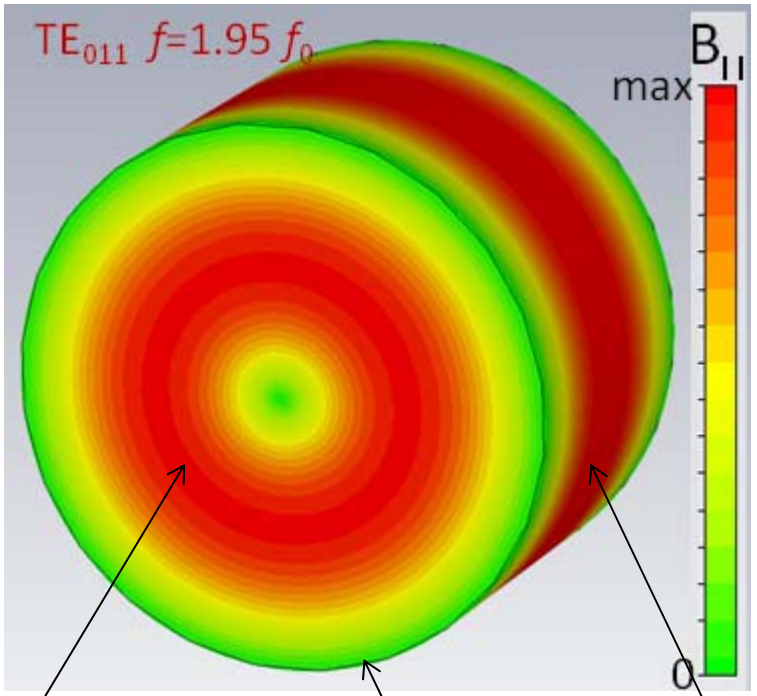

Demountable endplate

Flange

Host cavity

Surface Impedance Cavity (SIC)

Connecting Structure & Performance for SRF Surfaces

Designed to measure the RF impedance of small, flat samples

- Small, flat, controlled samples are easier to make s
- Material characterization of small, flat samples is much easier

TE_{011} sapphire-loaded cylindrical Nb cavity

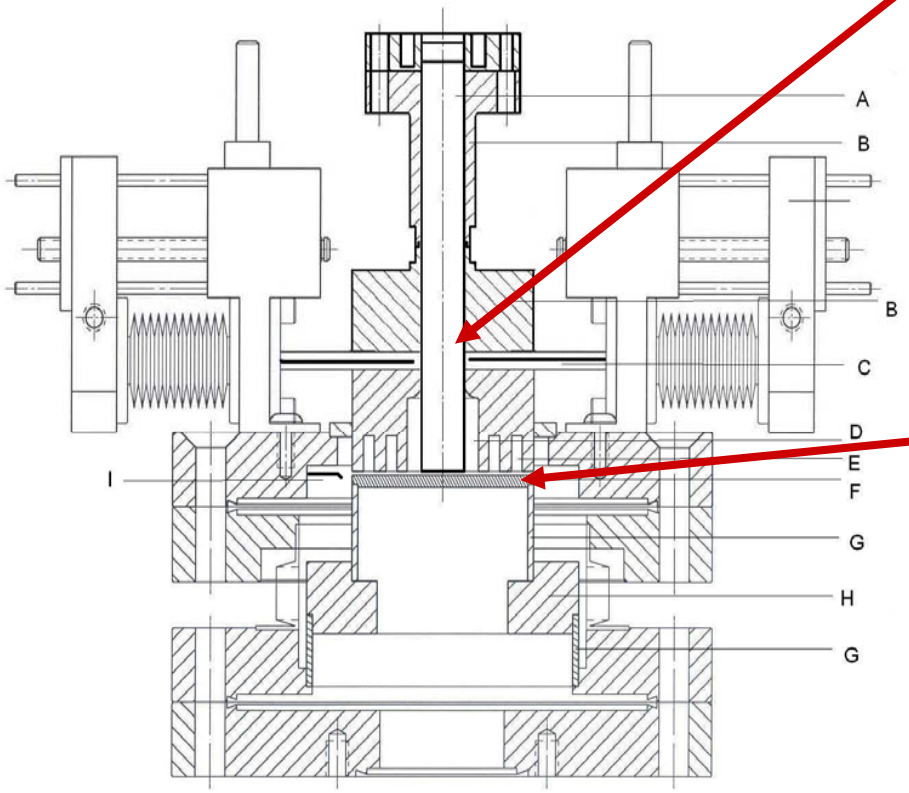

A. **Sapphire rod**

B. Nb

C. Coupler

D. TE011 cavity

E. Choke joint

F. **Nb sample on copper plate**

G. Stainless steel thermal insulator

H. Copper ring

I. Coupler near the choke joint to monitor the rf leaking from gap and choke joint.

f (GHz)	A_{Sample}	A_{rf}	$R_{\text{sens}}(\Omega)$	B_{max}
7.5	20 cm^2	**0.8** cm^2	<1e-7	?

Designed by J. Delayen, L. Phillips & H. Wang
Initially described at the SRF 2005 Workshop
http://www.lns.cornell.edu/public/SRF2005/pdfs/TuP46.pdf

SIC System

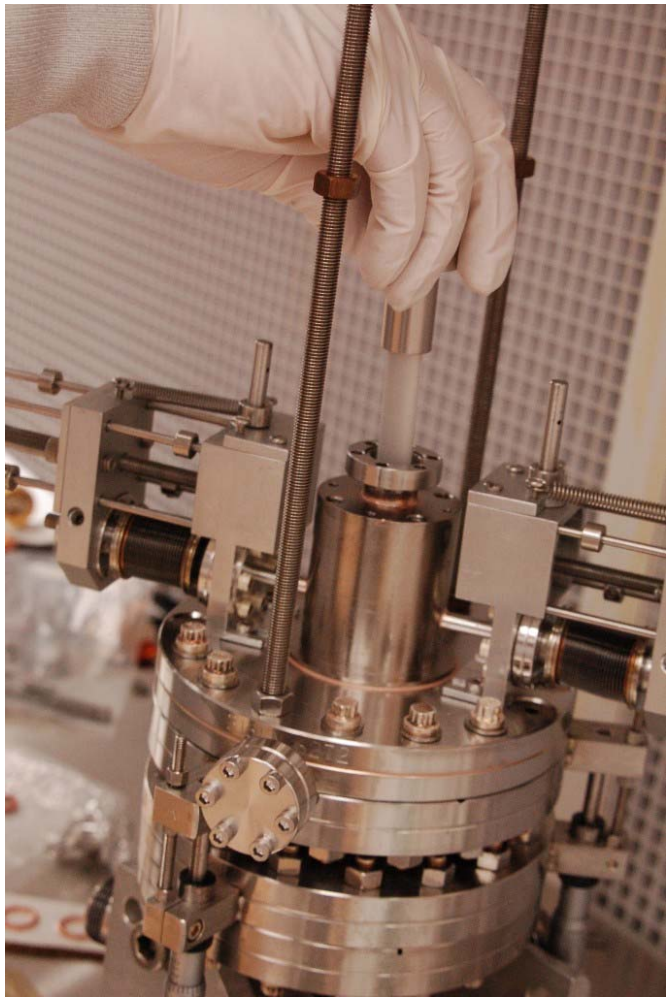

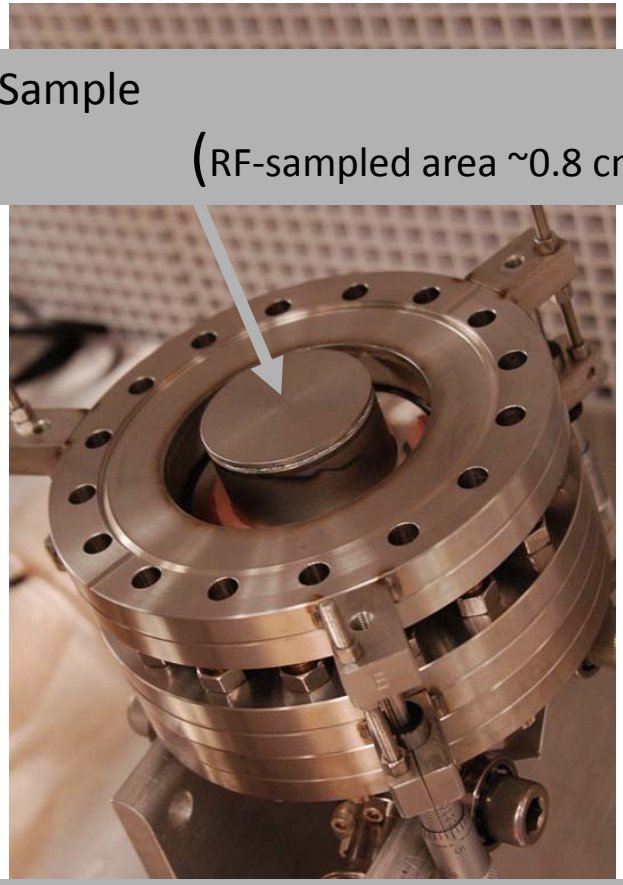

- Sapphire rod attached inside the cavity lowers resonance frequency
- Sample thermally decoupled from the cavity
- The calorimetric measurement technique is sensitive to the sample surface only while being insensitive to other cavity losses.

Calorimeter enables sample temperature to be controlled independently of balance of cavity and bath.

Measurement with the SIC cavity

✓(TE_{011} sapphire-loaded cylindrical Nb cavity) Surface impedance as a function of magnetic field and temperature from 1.9 K to 4.8 K.

✓Normal state surface impedance at 10 K, from which the surface value of electronic mean free path and surface H_{c1} can be determined.

✓Superconducting penetration depth, λ, at low field will be measured by carefully tracking the cavity frequency with temperature as the sample temperature is swept slowly back and forth across the transition temperature (SIC sensitivity: 30 Hz/nm) while the rest of the cavity is held at 2 K.

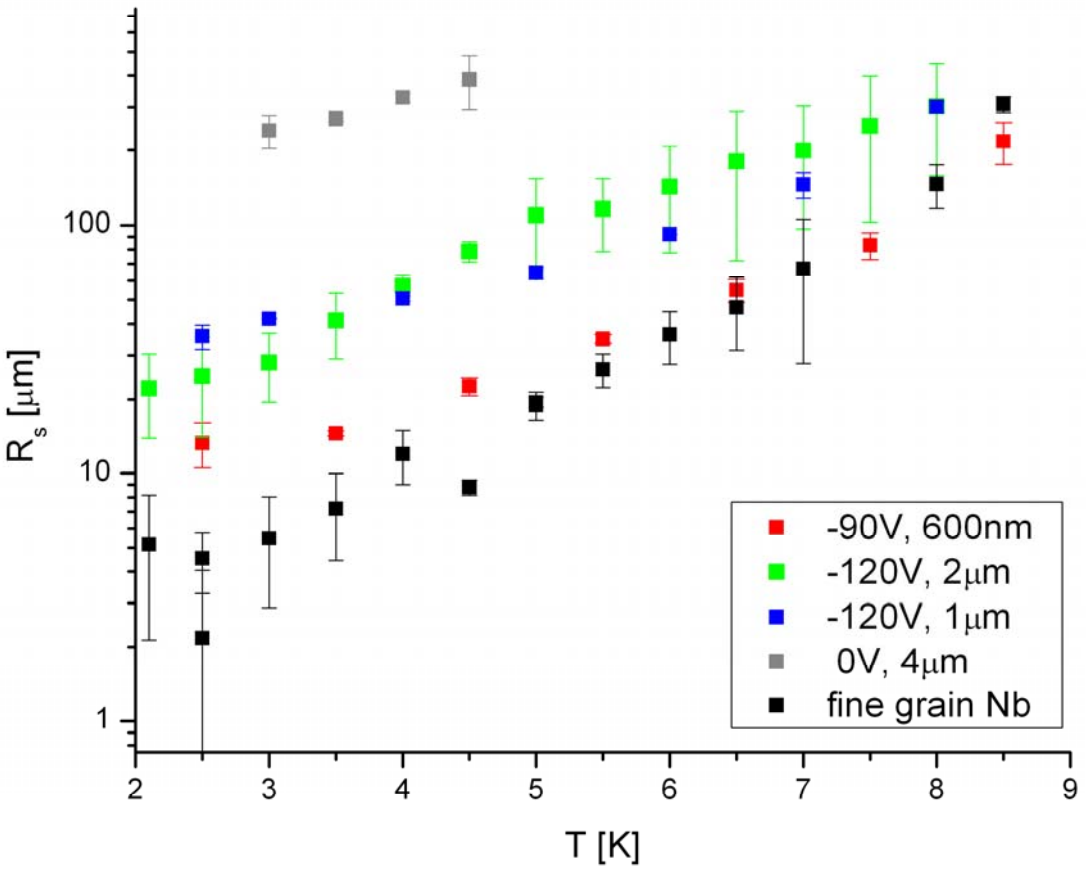

Coaxial TE011 cavity

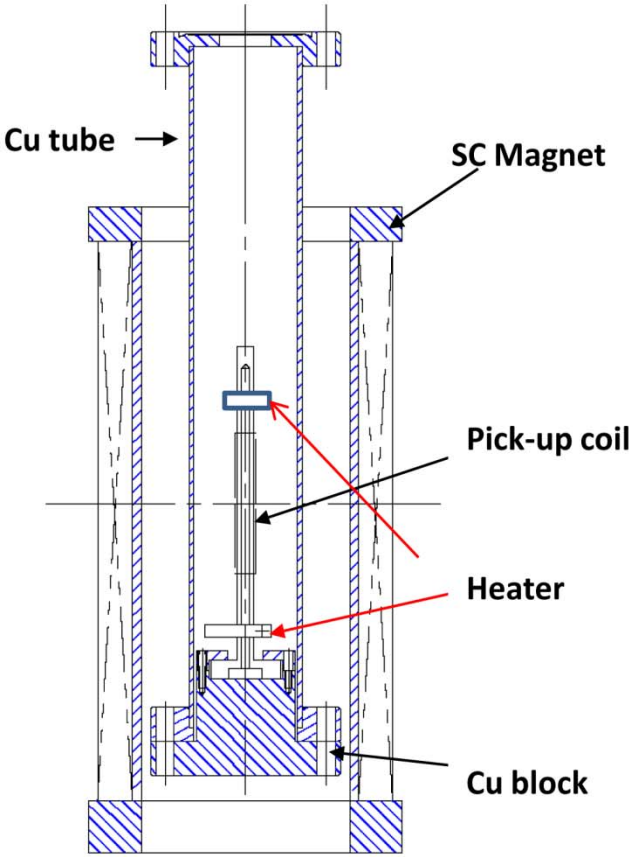

THIS INTEGRATED SYSTEM HAS BEEN DESIGNED TO MEASURE,

- DC MAGNETIZATION
- THERMAL CONDUCTIVITY
- PENETRATION DEPTH
- SURFACE PINNING CHARACTERISTICS

SUBSYSTEMS OF THE APARATUS:

SAMPLE: Φ 6mm, L=120mm, NIOBIUM ROD

HEATER: Made with constantan wire glued on a Cu block with Epoxy is clamped near the base and on the upper side of the sample rod.

TEMP. SENSOR: Two calibrated Cernox resistors are soldered with indium on two small Cu blocks which are clamped to the rod at a distance of about 40 mm.

PICK UP COIL: ~ 200 turns, 0.29 mm diameter Cu wire coil is inserted in the middle of the sample, between the two Cernox .

SC MAGNET: 1T (0.1% field homogeneity over the sample length
- made by Cryomagnetics)

Coaxial TE011

- Sample rod 6 mm diameter is inserted on centerline of TE cylindrical cavity
- Present MP limitation @ 50 mT

f (GHz)	A_{Sample}	A_{rf}	$R_{sens}(\Omega)$	$B_{max\ (mT)}$
3.54	22 cm^2	18 cm^2	?	50

Coaxial TE011 cavity

Measurement of Nb rod made with E-beam additive manufacturing (Radia Beam)

Frequency (GHz)	3.544
$B_p/\sqrt{U}$ (mT/√J)	151.8
$G = Q_0 R_s$ (Ω)	623.8
P_{sample}/P_{total}	19.3%

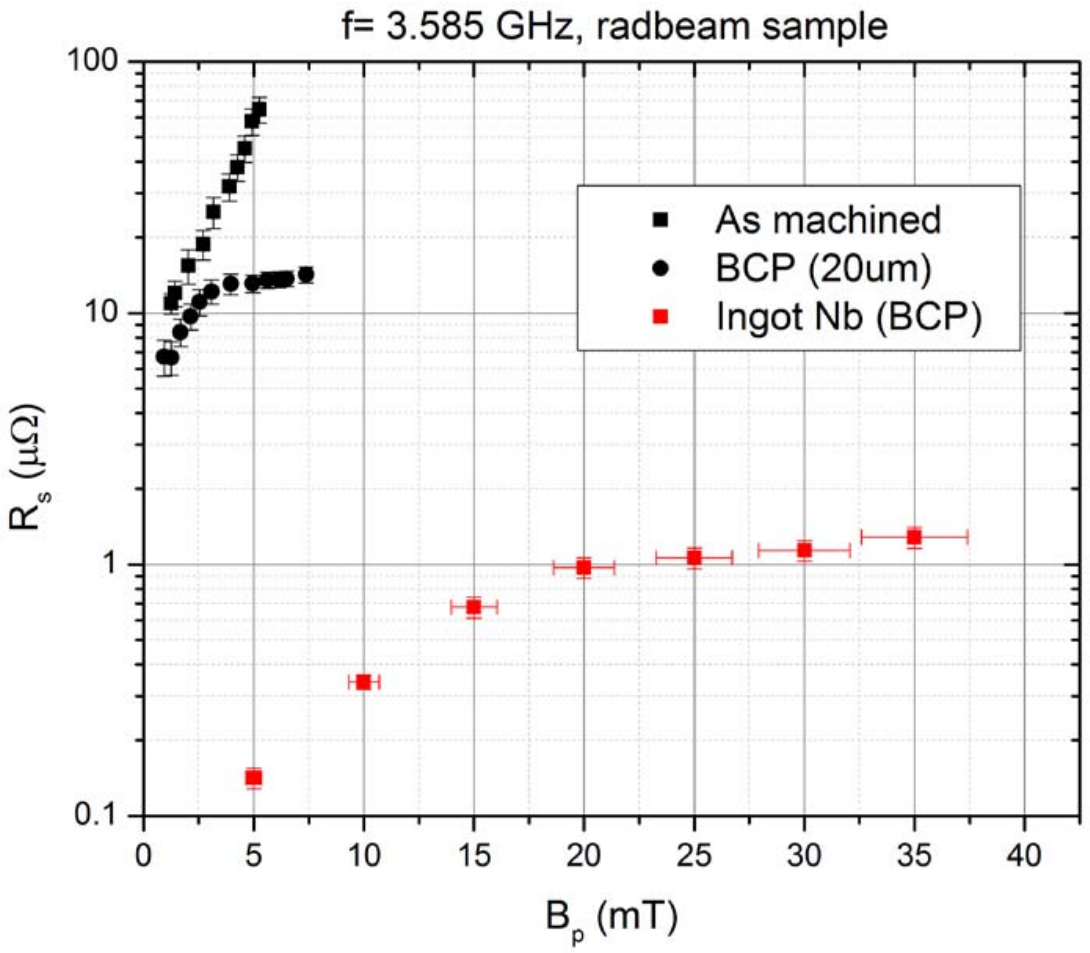

11.4 GHz mushroom Cu cavity at SLAC

High-Q cavity under TE013 like mode

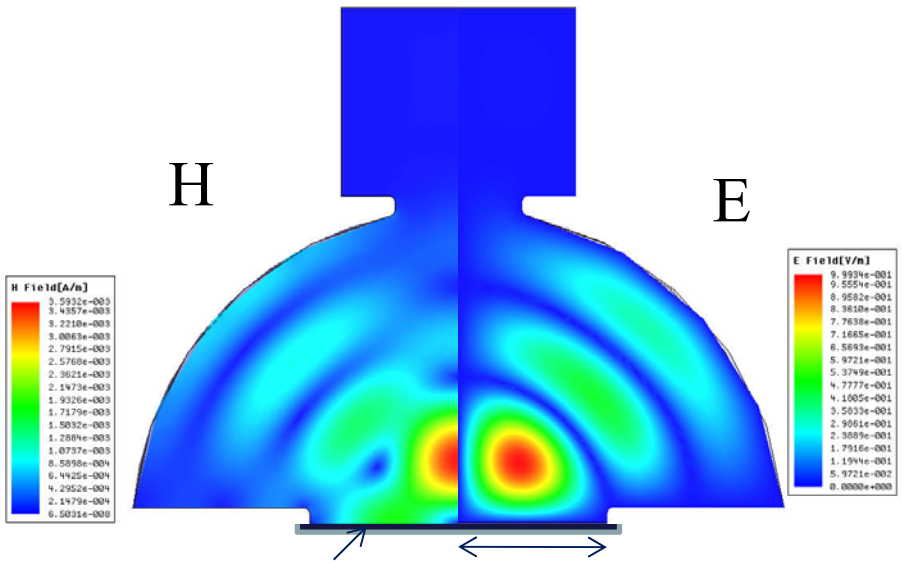

$F_{res,\ design}$=~11.399GHz
$F_{res,\ 290K}$=~11.424GHz
$F_{res,\ 4K}$=~11.46GHz

Tc~3.6μs(using Q value for copper at 4K)

$Q_{0,4K}$=~224,000
$Q_{0,290K}$=~50,000
(measured from bulk Cu samples)

Qe~310,000

$Q_{0,4K}$=~342,000
(Estimated for zero resistivity samples, using measured Cu sample results)

- High-Q hemispheric cavity under a TE_{013} like mode
  - Zero E-field on sample
  - Maximize H-field on the sample, H_{peak} on bottom is 2.5 times of peak on dome
  - Maximize loss on the sample, 36% of cavity total
  - No radial current on bottom
- Copper cavity body
  - No temperature transition or quenching
  - Higher surface impedance
  - Coupling sensitive to iris radius
- Nb cavity body
  - More precise R_s characterization

RF critical magnetic field measurements -TE013 cavity (SLAC)

System Schematic: With short pulsed power, heating effect is supposed to be eliminated, thereby the correct RF critical magnetic field can be measured

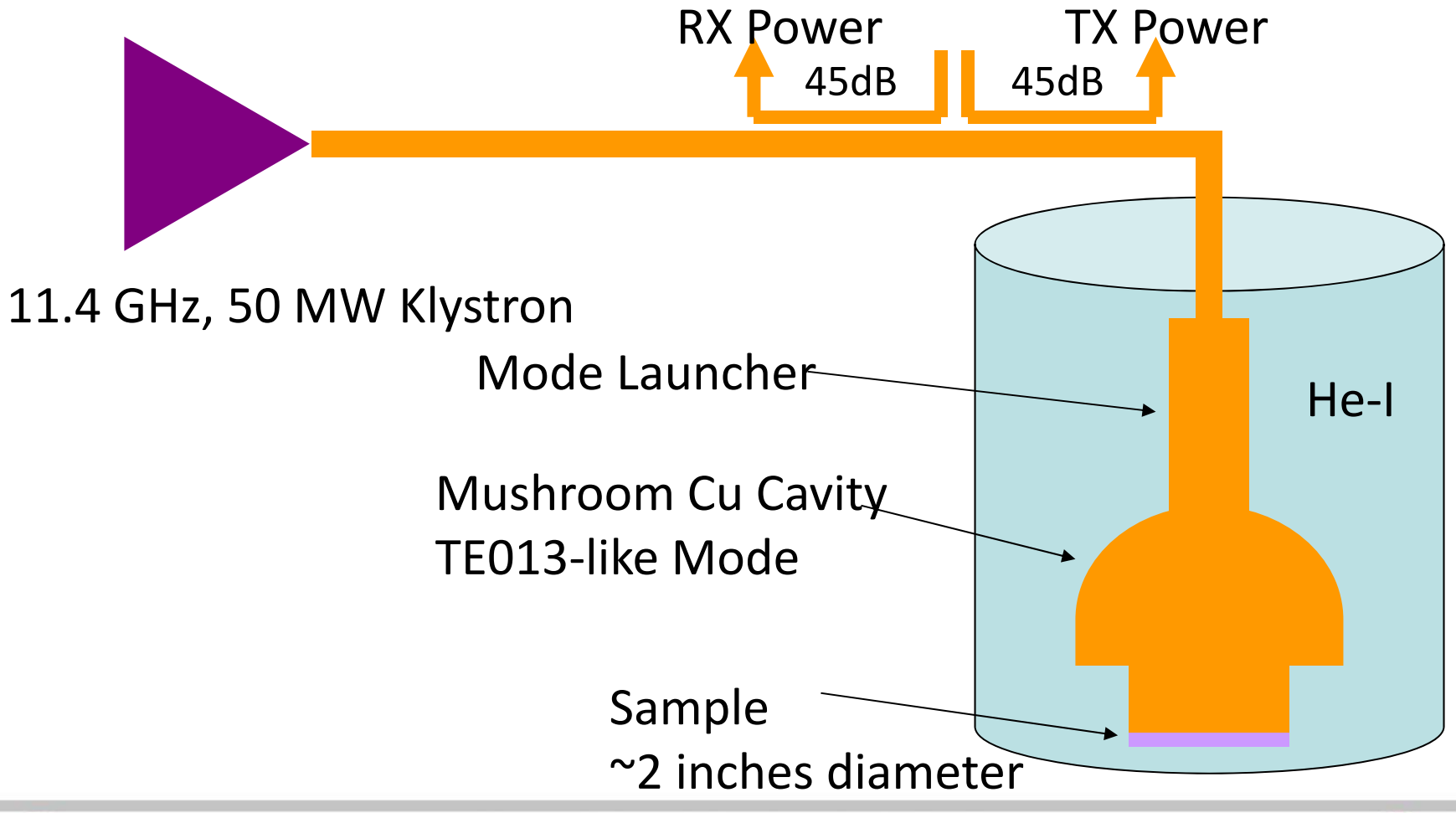

RF critical magnetic field measurements -TE013 cavity (SLAC)

A Nb sample (fine grain, RRR~250) was tested as a reference

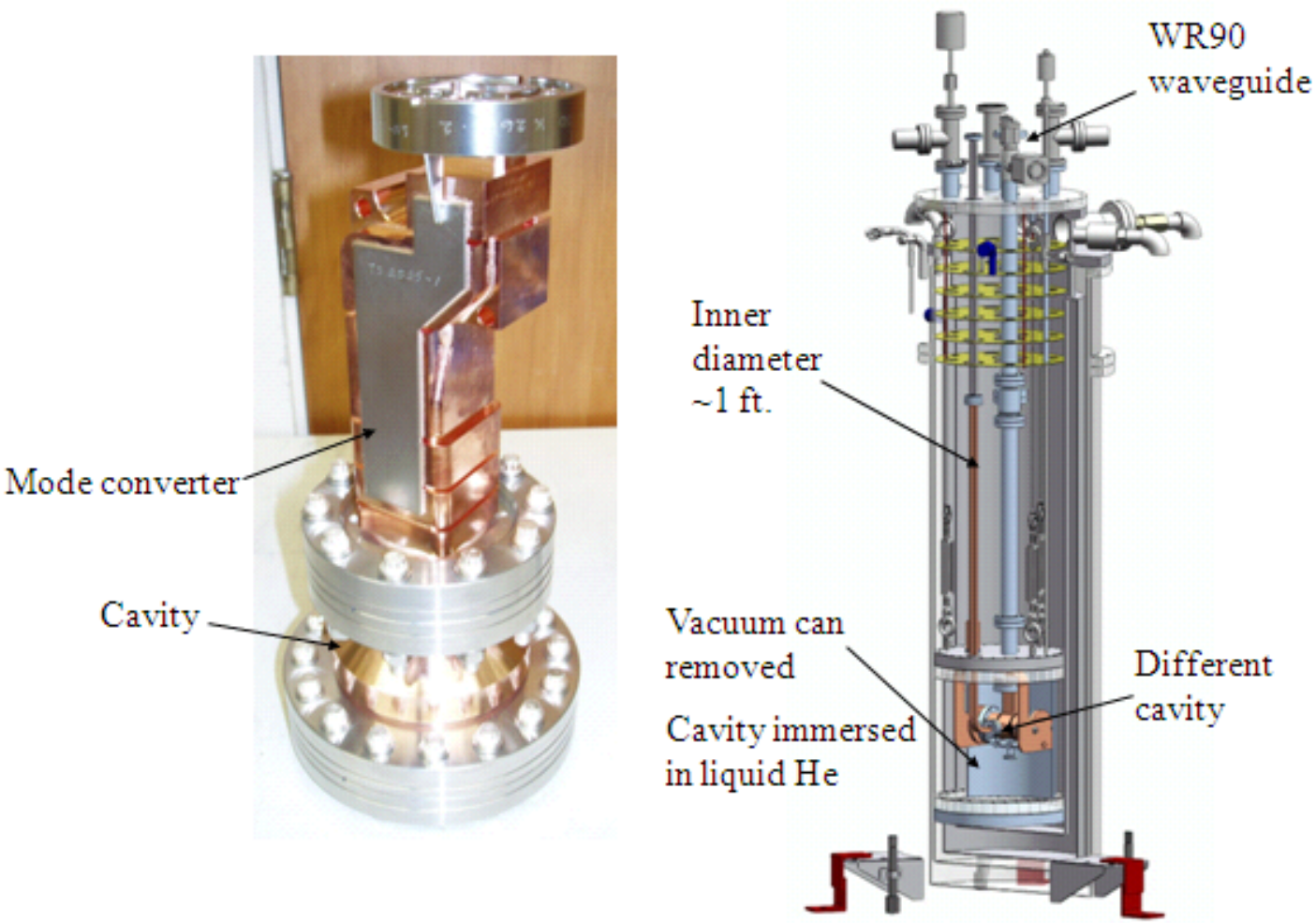

TE013 measurements

Q vs. incident power

rt of breakdown at RF
ical magnetic field at
highest field region

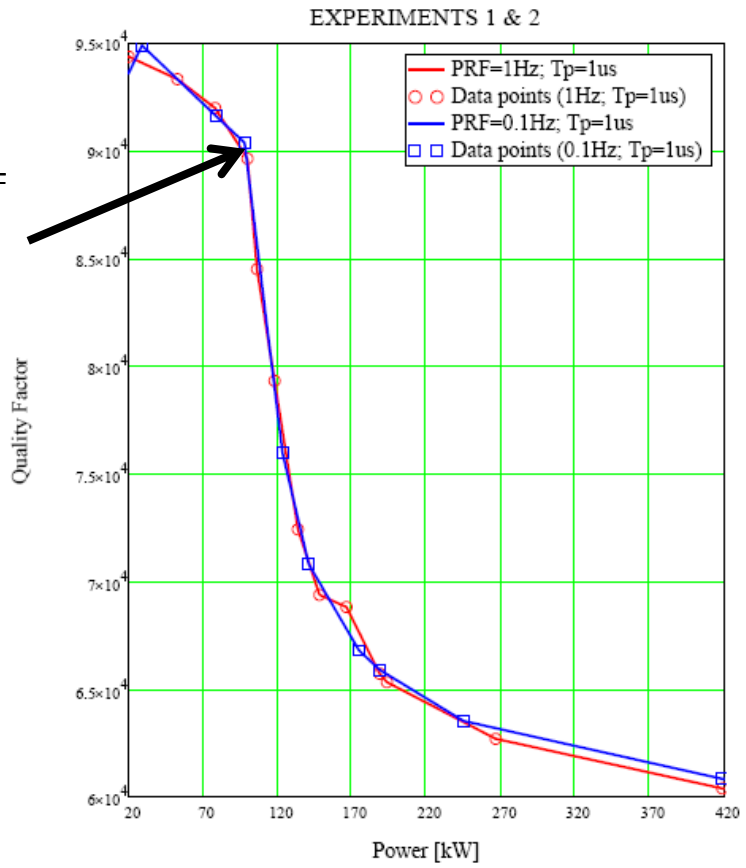

Effect of reducing pulse width from 1 to 0.5 μs

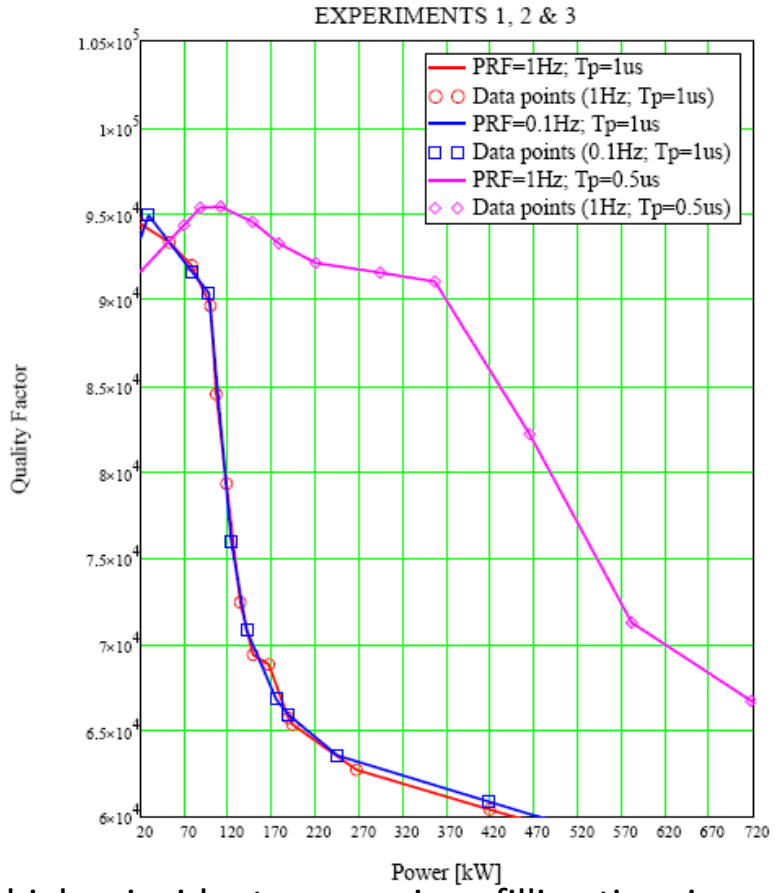

needed ~4x higher incident power since filling time is longer than pulse width

1 ms seems short enough, but we will test shorter pulses

An analytical model to simulate the results was developed and showed a good agreement

Canabal, http://laacg.lanl.gov/scrflab/pubs/ILC/LA-UR-08-2706.pdf

Cavity Model: Critical Magnetic Field

- Sample

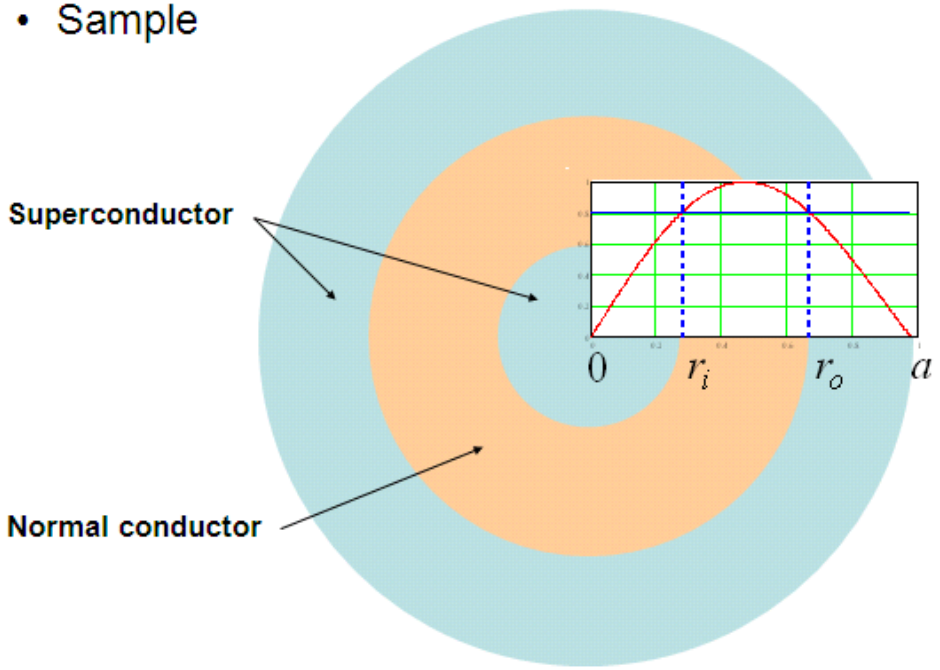

Q vs. normalized incident power with simulation (solid line). Good agreement was obtained.

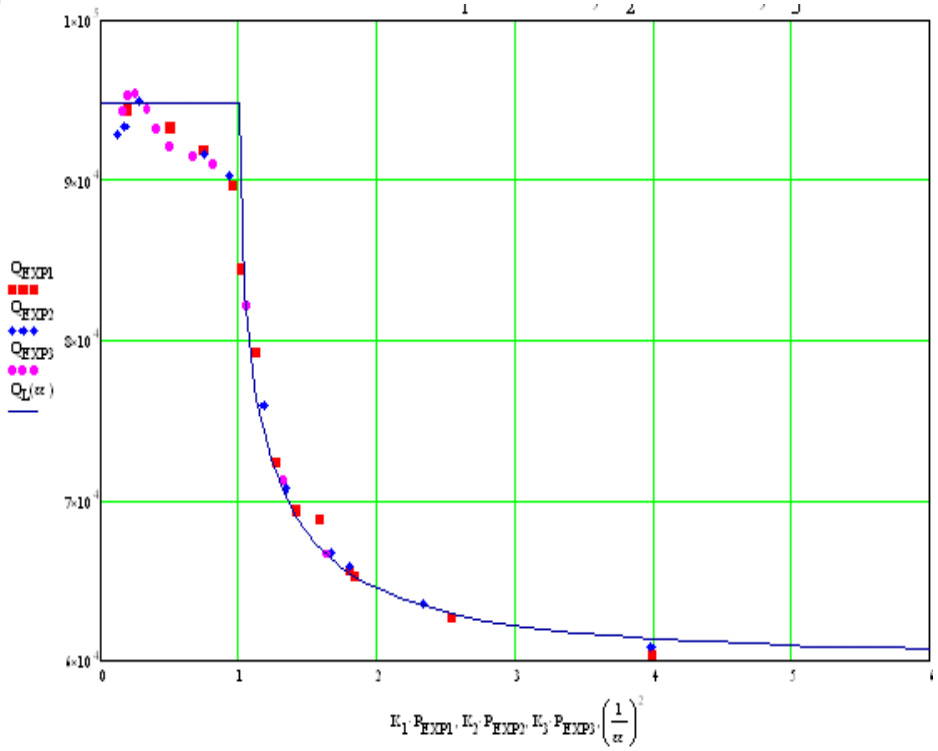

Measurement Results: Bulk Nb, low power test

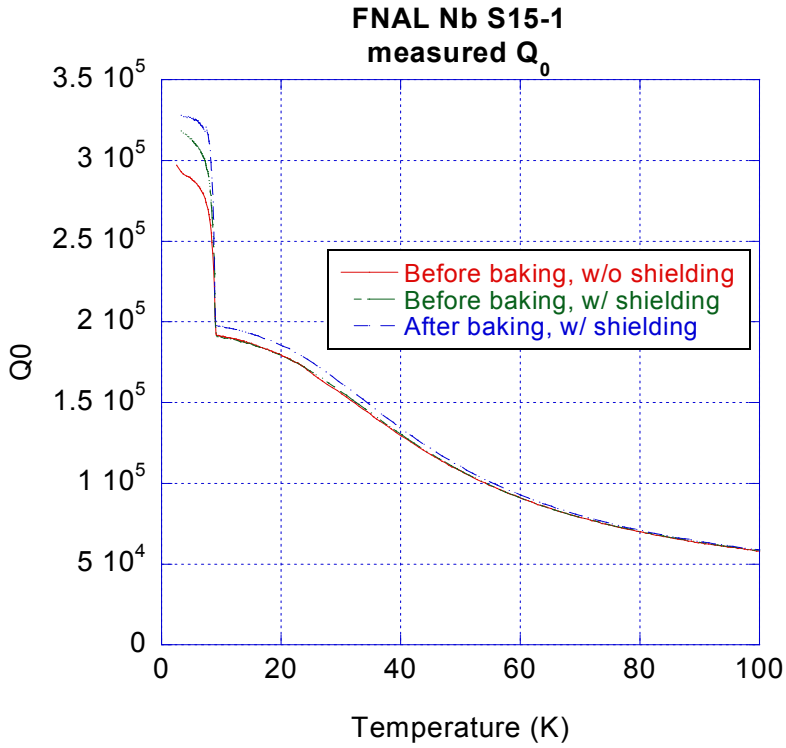

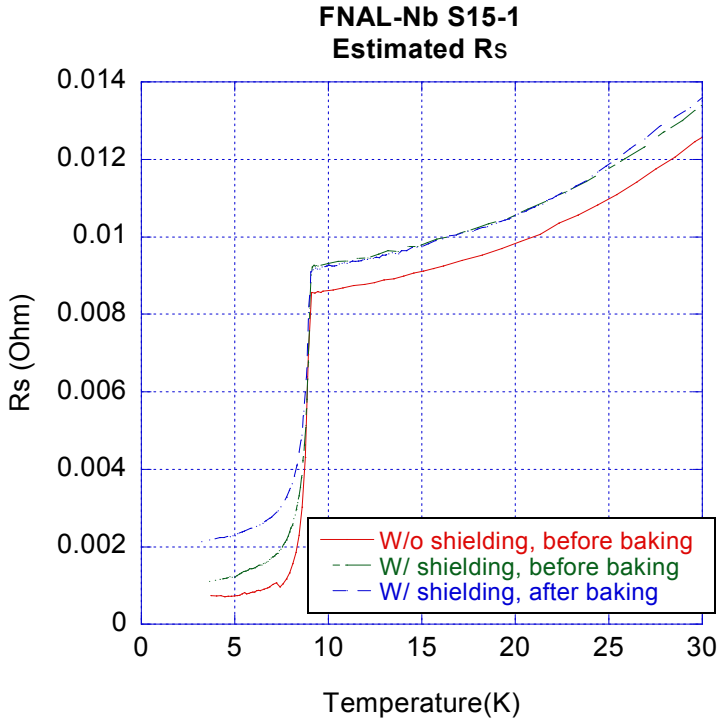

FNAL bulk large grain Nb sample

Sample surface impedance is estimated from the measured Q_0 of the cavity with Nb sample and the measured copper surface impedance.

Without magnetic shielding, the residual resistivity is high. After adding a magnetic shielding and 800˚C vacuum bake, surface impedance reduced by a factor of 3.

Measurement Results: Bulk Nb, high power test

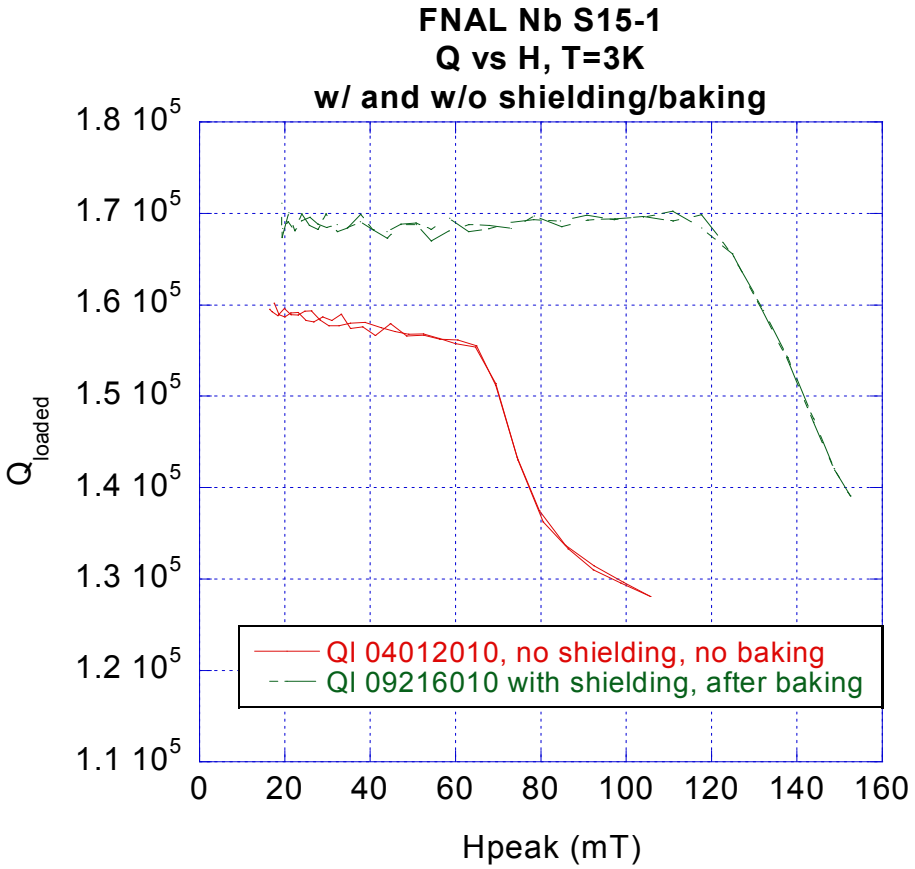

FNAL bulk large grain Nb sample

The residual resistivity is causing pulse heating and degrades the quenching field.

Before magnetic shielding and baking, the sample start to quench at ~65mT with temperature rises ~5K.

After shielding and baking, quenching starts at about 120mT when temperature rises ~3K.

- **Precisely measure the quenching field of up to 300-400mT**
- **Magnetic shielding is crucial for Nb residual resistivity. At X-band, pulse heating from residual resistivity can easily degrade the quenching field.**
- **Precision of R_s measurement is currently at the level of 0.1mΩ. It can be improved with a separate Nb cavity.**

A CRYOGENIC RF MATERIAL FACILITY AT SLAC

J. Guo *et al., SLAC (IPAC 2010 ,WEPEC073)*

Measurement of samples from different sources

Nb (FNAL)

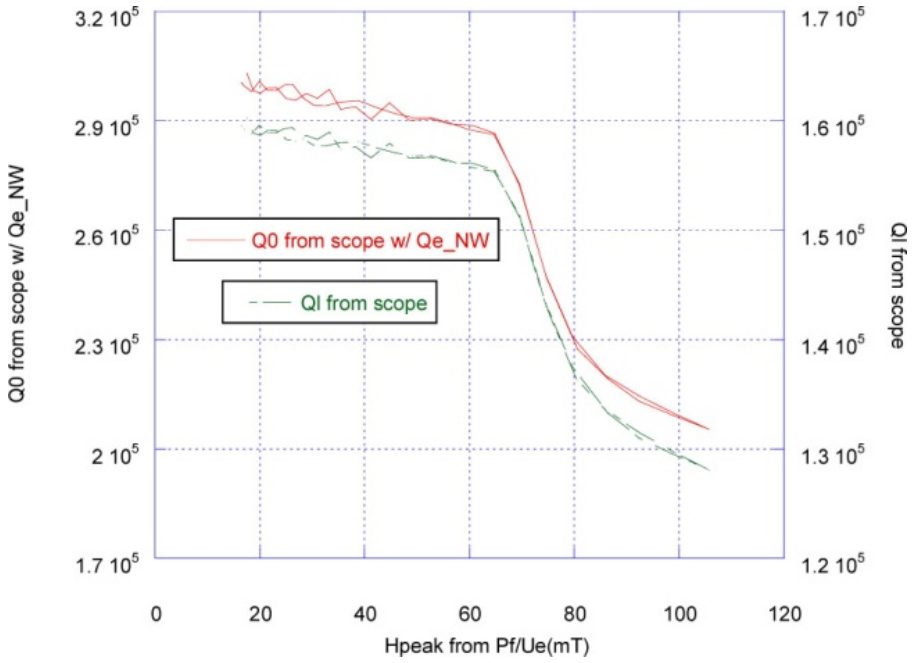

MgB2 (LANL)

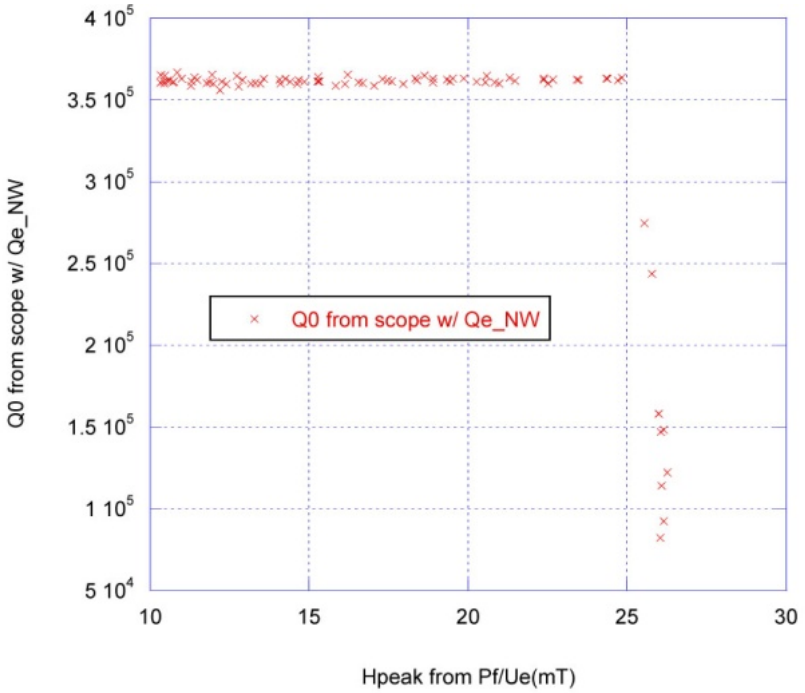

Figure 8: Q_0 vs H-field, LANL 300nm MgB2 on Sapphire

Quadrupole Resonator (CERN)

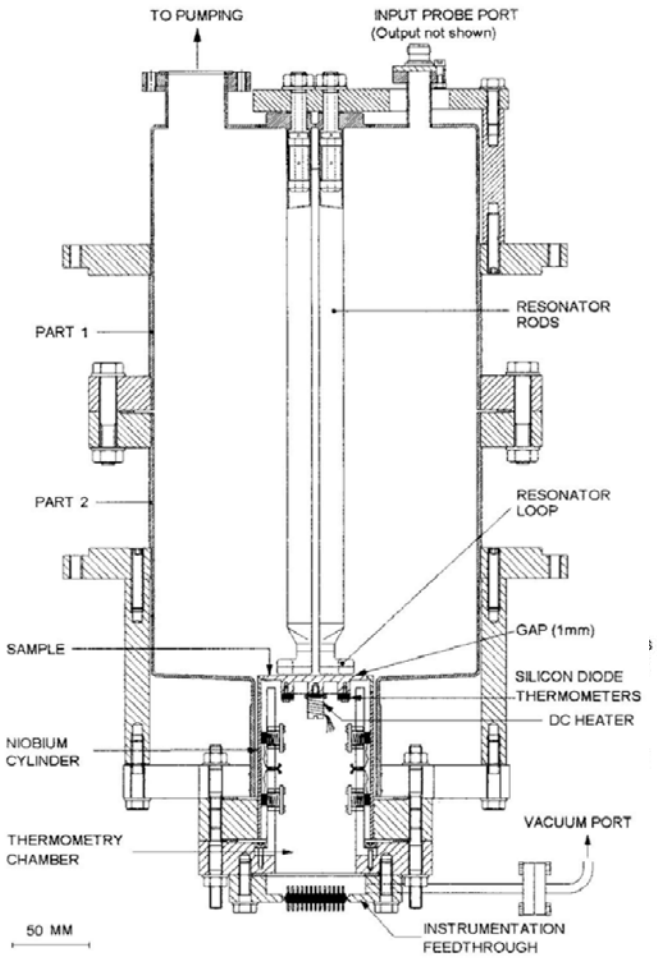

- Resonator excited in a TE_{21} like mode
- Samples attached in a coaxial structure
- Calorimetric measurements
- Resonant frequency 400 MHz (LHC)

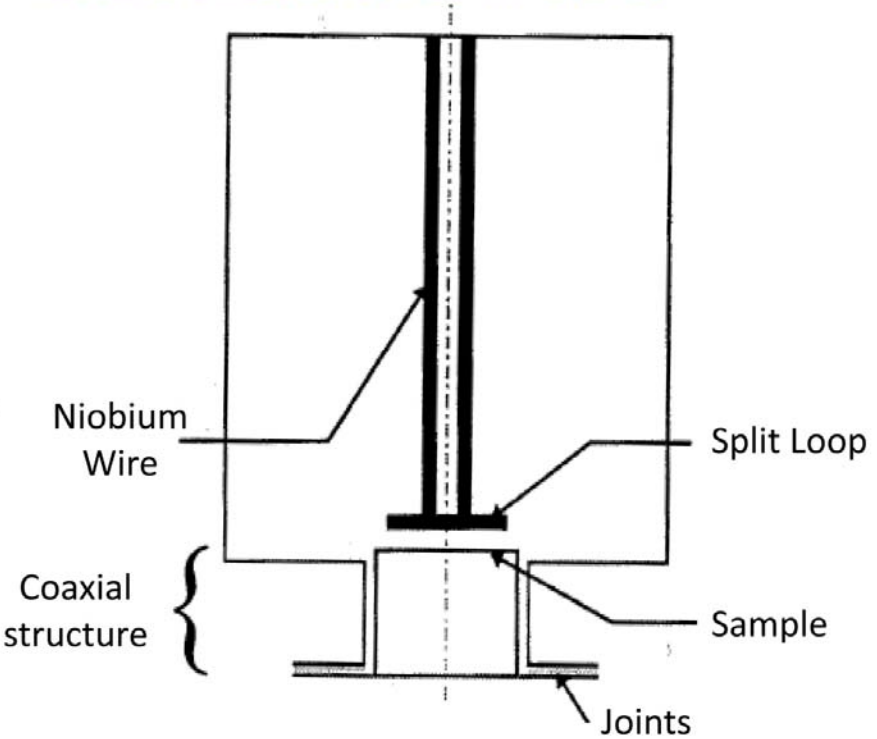

f (GHz)	A_{Sample}	A_{rf}	$R_{sens}(\Omega)$	B_{max}
0.403	44 cm^2	12 cm^2	1e-9	0.15 mT

-Very sensitive, low frequency
-Delicate structure setup
- Difficult sample preparation (EBW)

The Quadrupole Resonator

- Resonant frequencies:

  400, 800, 1200 MHz

- Same magnetic field configuration for all frequencies
- $B_{max} \approx 60$ mT
- Temperatures 1.8 -20 K
- Sample:
  - 75 mm diameter
  - Equipped with a dc heater and 4 temperature sensors

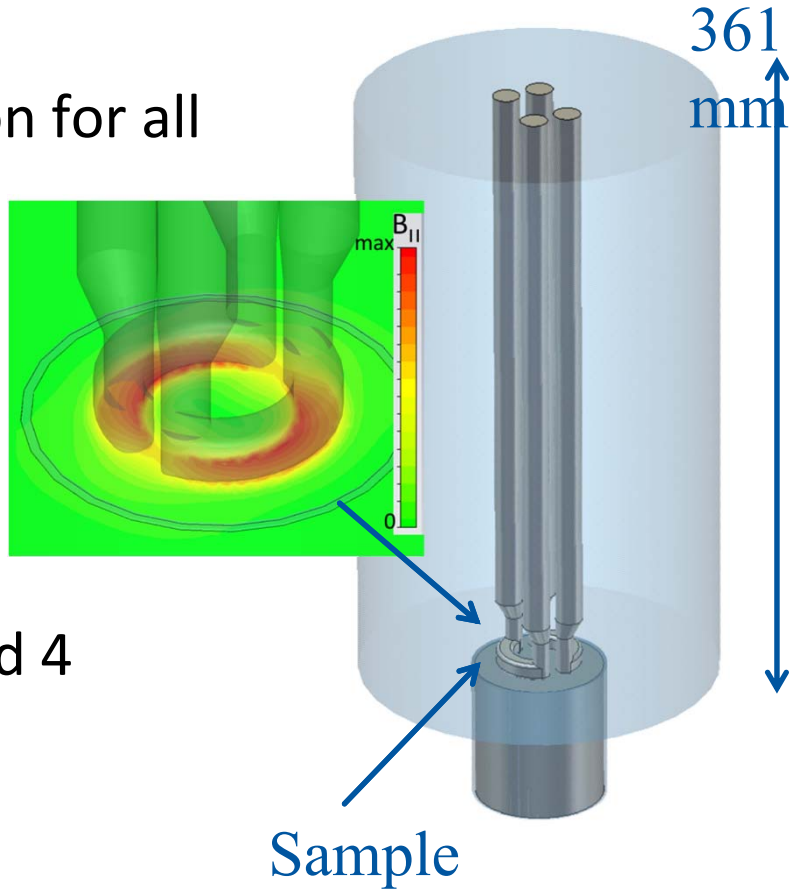

Calorimetric Method

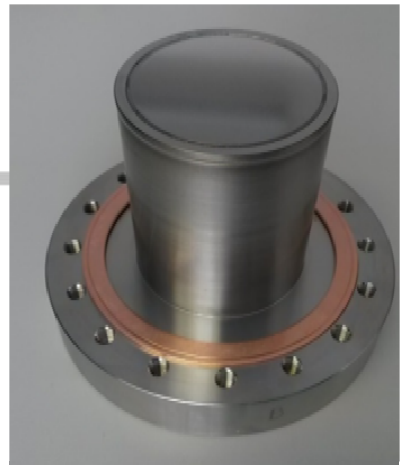

- RF-DC-compensation technique

$$P_{RF} = P_{DC,RF\_off} - P_{DC,RF\_on} \approx 1/2\, R_{Surface} \int_{Sample} H^2 dS$$

$$R_{Surface} = \frac{2(P_{DC,RF\_off} - P_{DC,RF\_on})}{\int_{Sample} H^2 dS}$$

Direct Measurement

- Measurement of transmitted power P_t
- $P_t = c\int H^2 ds$, c is calculated from CST Microwave Studio®

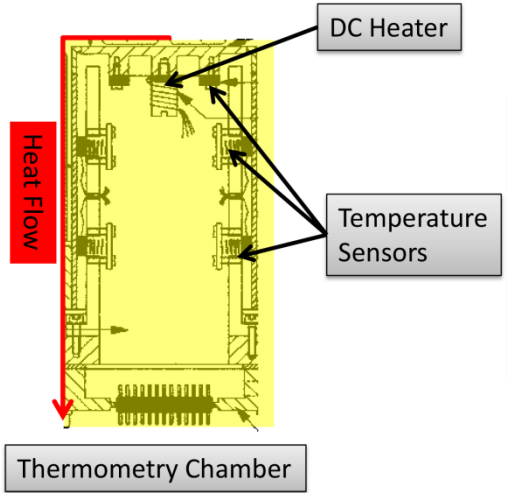

1. Temperature is set via DC heater
2. RF is switched on
3. Temperature increases
4. Power applied to DC heater is lowered to have same temperature on sample
5. Difference of heater power with and without RF is the power dissipated by RF

Resolution: sub-nΩ

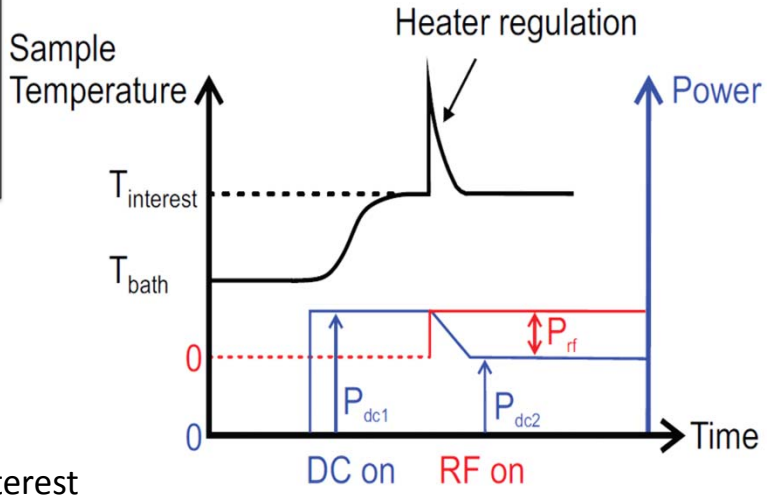

Temperature diodes: 12 mK absolute / 0.1 mK relative

- Heater voltage: 10 µV (relative)
- Transmitted power: ΔP = 3% (absolute)
- Pressure of helium bath: Changes the heat necessary for reaching Tinterest
- Pressure regulation system stabilizes ± 0.02 mbar
- Minimal heating of 0.1 mK depends on the thermal conductivity.
- 2.5 µW at 2 K lead to smallest detectable Rs change at 5 mT and 400 MHz

[S. Aull, "High Resolution Surface Resistance Studies", SRF 2013]

Quadrupole Resonator (CERN)

- Reactor grade bulk niobium sample
- Chemically etched
- 400 MHz

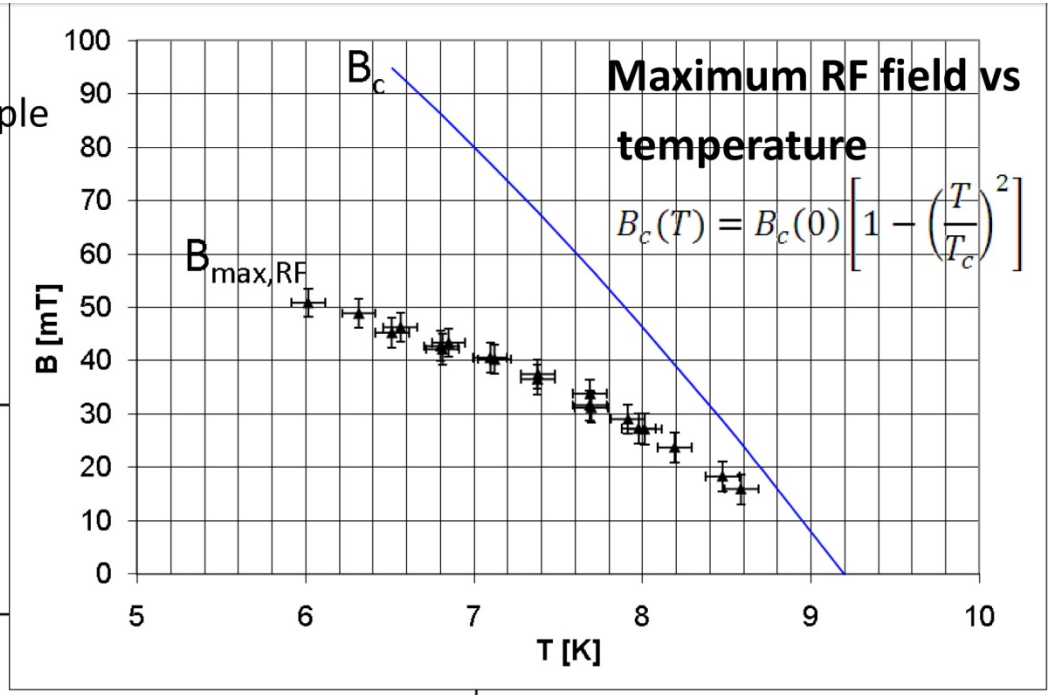

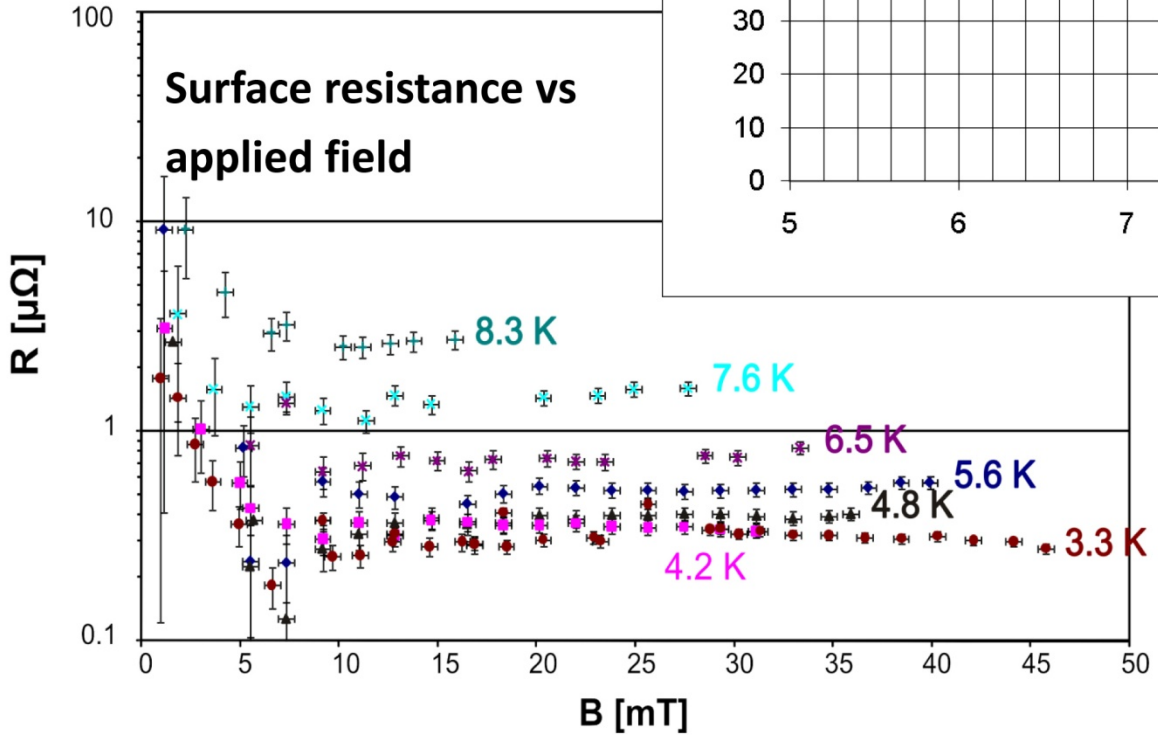

Quadrupole Resonator (CERN)

Penetration depth as a function of temperature

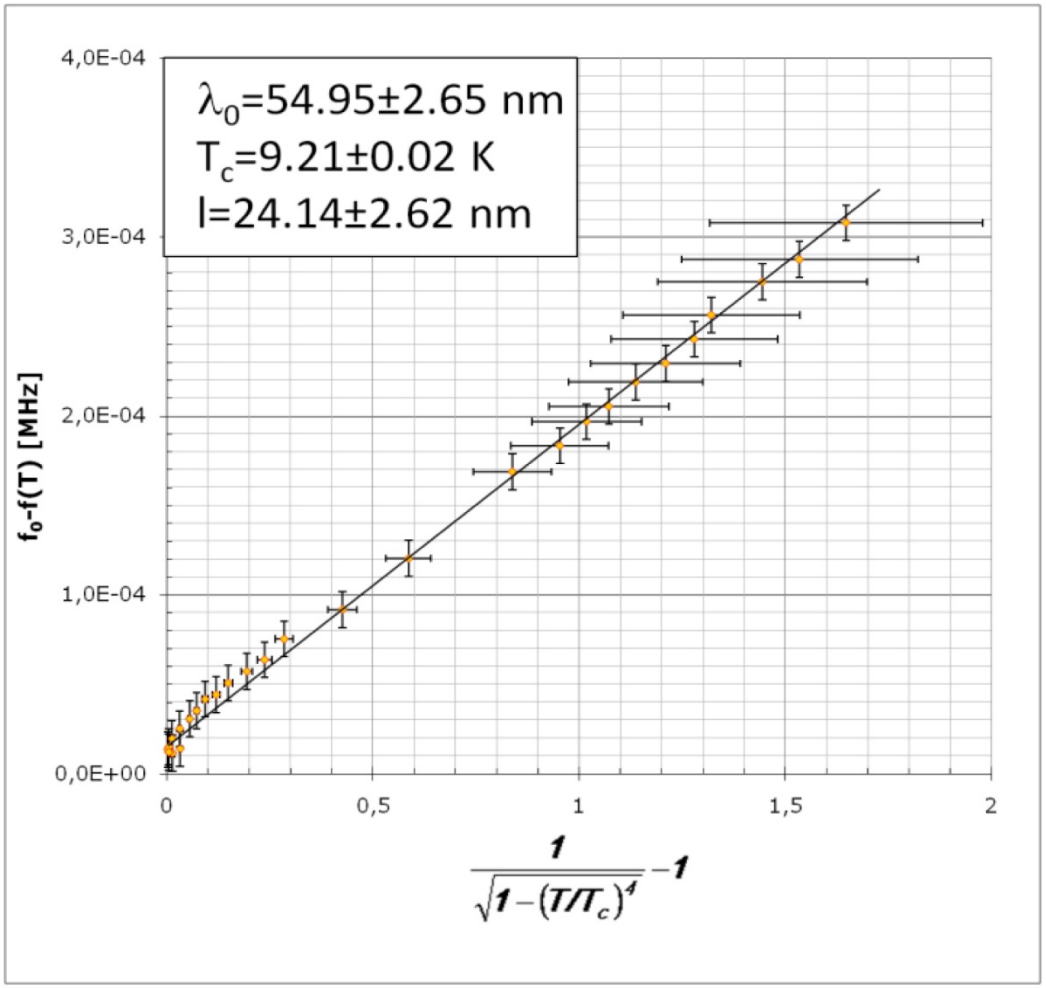

$$\Delta\lambda = -\frac{G}{\pi f^2 \mu_0}\Delta f$$

Fit using two fluid model

$$\Delta\lambda = \lambda_L \sqrt{1+\frac{\xi}{l}} \cdot \frac{1}{\sqrt{1-\left(\frac{T}{T_c}\right)^4}} - \lambda(T_0)$$

TE011 Cavity- Cornell

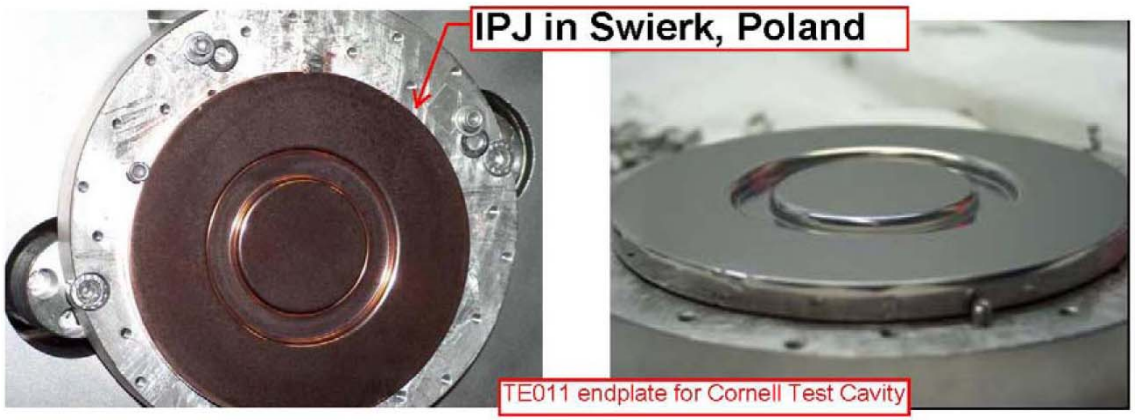

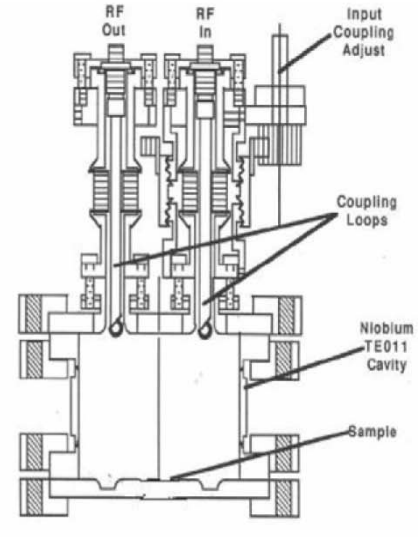

Figure 3: TE cavity schematic diagram.

TE_{011} cavity

- Replaceable endplate on Nb cavity

Romanenko Cornell SRF Wkshp 2005

f (GHz)	A_{Sample}	A_{rf}	$R_{sens}(\Omega)$	$B_{max\ (mT)}$
5.95	35 cm^2	35 cm^2	2e-6	45

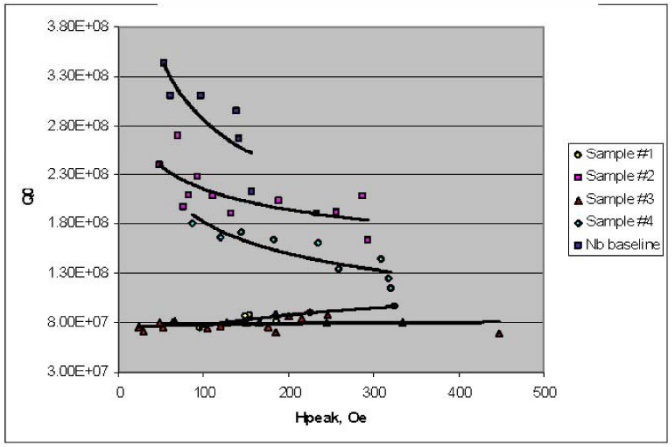

Figure 5: Q_0 versus peak magnetic field for different Nb/Cu end plates and a bulk Nb end plate.

CRYOGENIC MEASUREMENTS

Residual Resistivity Ratio

RRR is the ratio of the resistivity at 300K and 4.2K

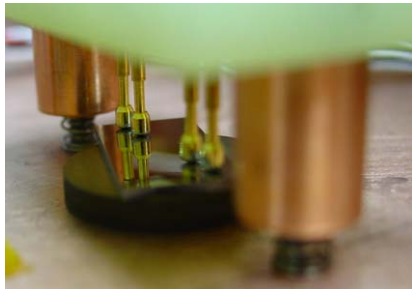

$$RRR = \frac{\rho_{300K}}{\rho_{4.2K}}$$

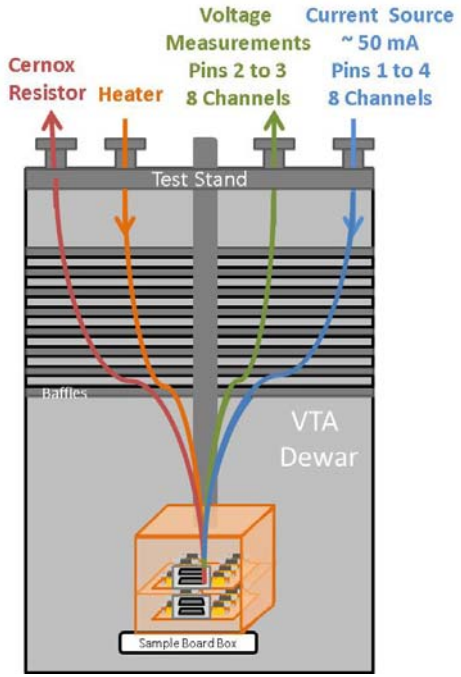

RRR is related to

Mean free path: for Nb, $l(T=4.2K)=27 \times RRR(Å)$

Thermal conductivity: for Nb: $l(T=4.2K)=RRR/4(W.m^{-1}.K^{-1})$

The measurement of RRR gives important information on the quality of the material especially if it is a film. The residual resistivity is a measure of impurity and lattice defects content.

Residual Resistivity Ratio (RRR)

Practically, $$RRR = \frac{\rho^{300K}}{\rho_{10K}}$$ (just above the transition point)

4-point probe method with the current being injected at the ends of the sample and the voltage taps being located further inwards such as to minimize the effect of non-uniform current distributions.
The 4-point resistance measurements : typically 100 nV precision after low-pass filtering. Thermo-voltages are eliminated by averaging over voltage readings obtained with alternating current polarities.
Typical measurement current :100 mA.

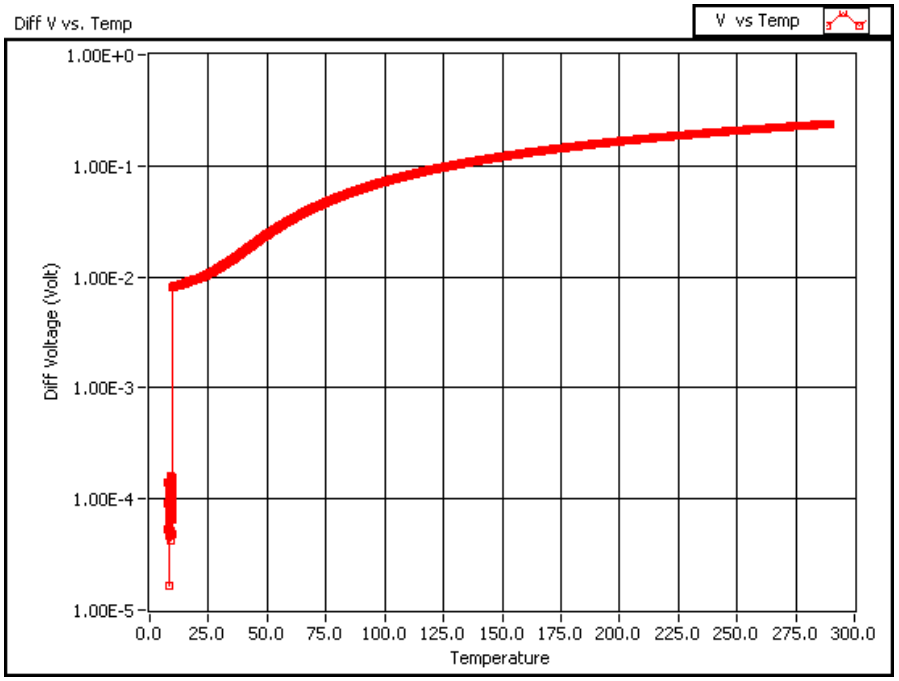

RRR Plot

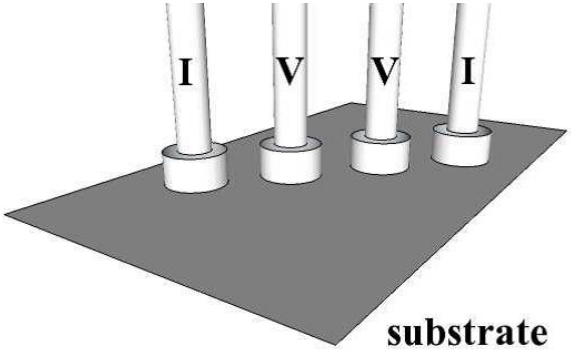

If the substrate has a much lower resistance than the film (like in the case of niobium on a copper substrate) the measure requires the removal of the substrate. For a better handling of the film, a kapton adhesive tape is glued on its free surface before dissolving the copper substrate in a nitric acid bath. The copper on the two extremities of the sample is protected with a resistant varnish to keep a good welding area.

Superconducting critical temperature Tc

Resistive measurement: 4-point probe as for RRR

Inductive measurement using Meissner effect:

The sample is placed between the primary and the secondary coil . Screening currents are induced on the sample surfaces by a low frequency field (2 Hz), generated by a primary (excitation) coil. The induced voltage in the secondary is recorded using a lock-in amplifier as function of the temperature. At transition the screening currents change inducing a voltage in a secondary (pick-up) coil.
The samples are cooled by He gas circulation and their temperature is controlled by changing the temperature of the He gas. The measurements are always performed in both directions (decreasing and increasing the temperature) to ascertain that there are no gradients between the sample and the thermometer.

T_c Plot

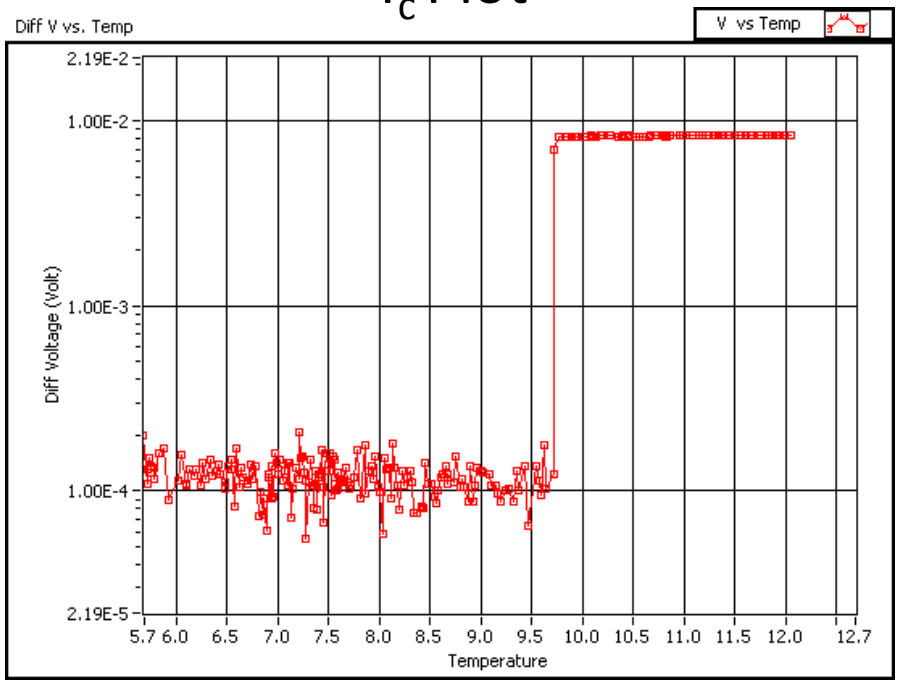

Near-field microwave microscopy

1) Stimulate Nb with a concentrated and intense RF magnetic field

2) Drive the material into nonlinearity (nonlinear Meissner effect)

Why the NLME? It is very sensitive to defects…

3) Measure the characteristic field scale for nonlinearity: J_{NL}

$$\lambda^2(T, J_{RF}) \approx \lambda^2(T,0)\left(1+\left(\frac{J_{RF}}{J_{NL}(T)}\right)^2\right)$$

4) Map out J_{NL}(x,y)

5) Relate J_{NL}(x,y) maps to ca

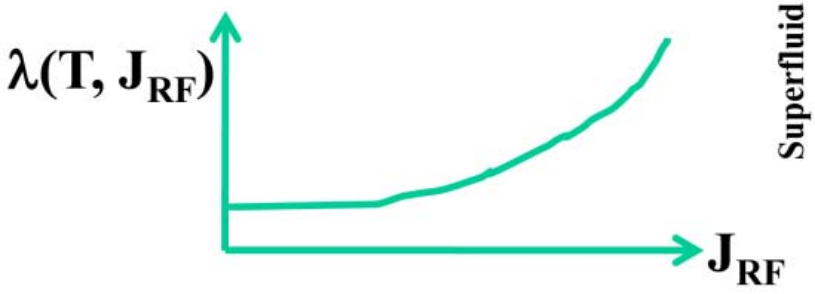

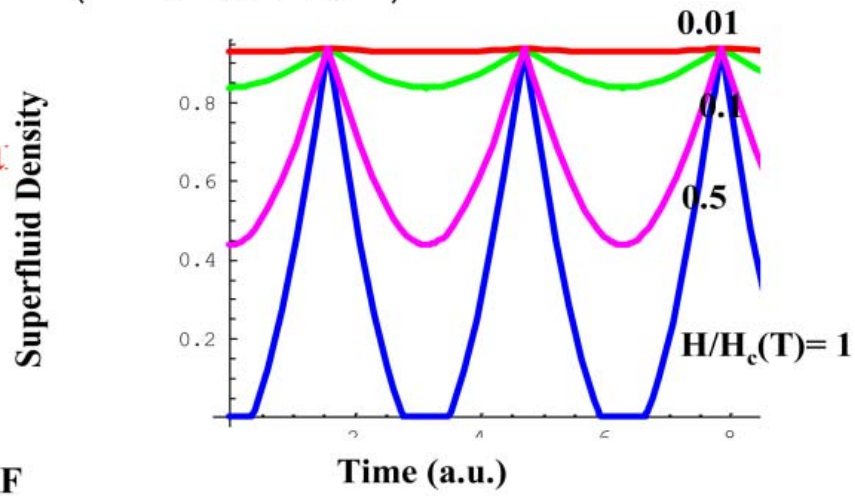

Near-field microwave microscopy

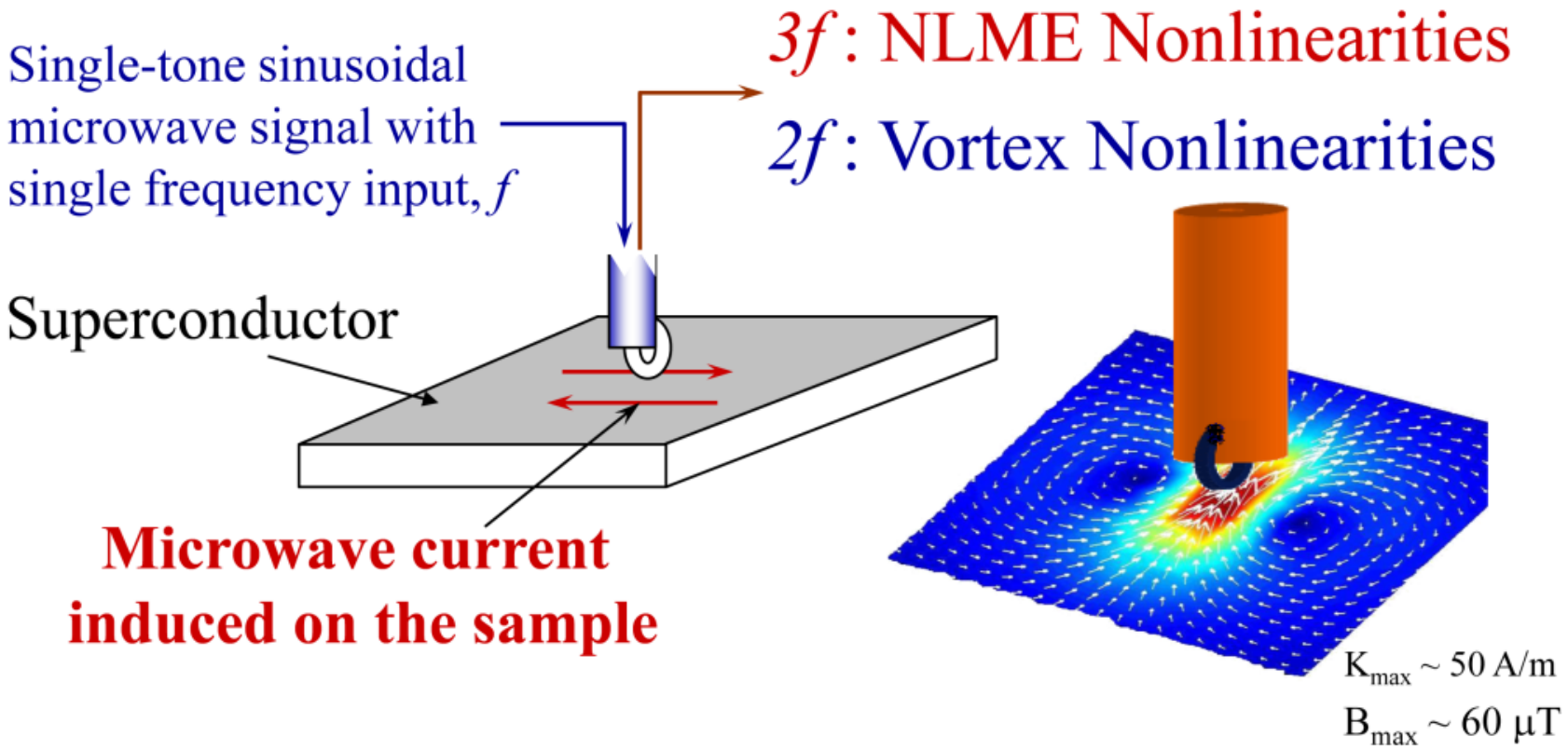

Create a sample with well-characterized defects and probe them with localized RF currents in the superconducting state

Near-field microwave microscopy

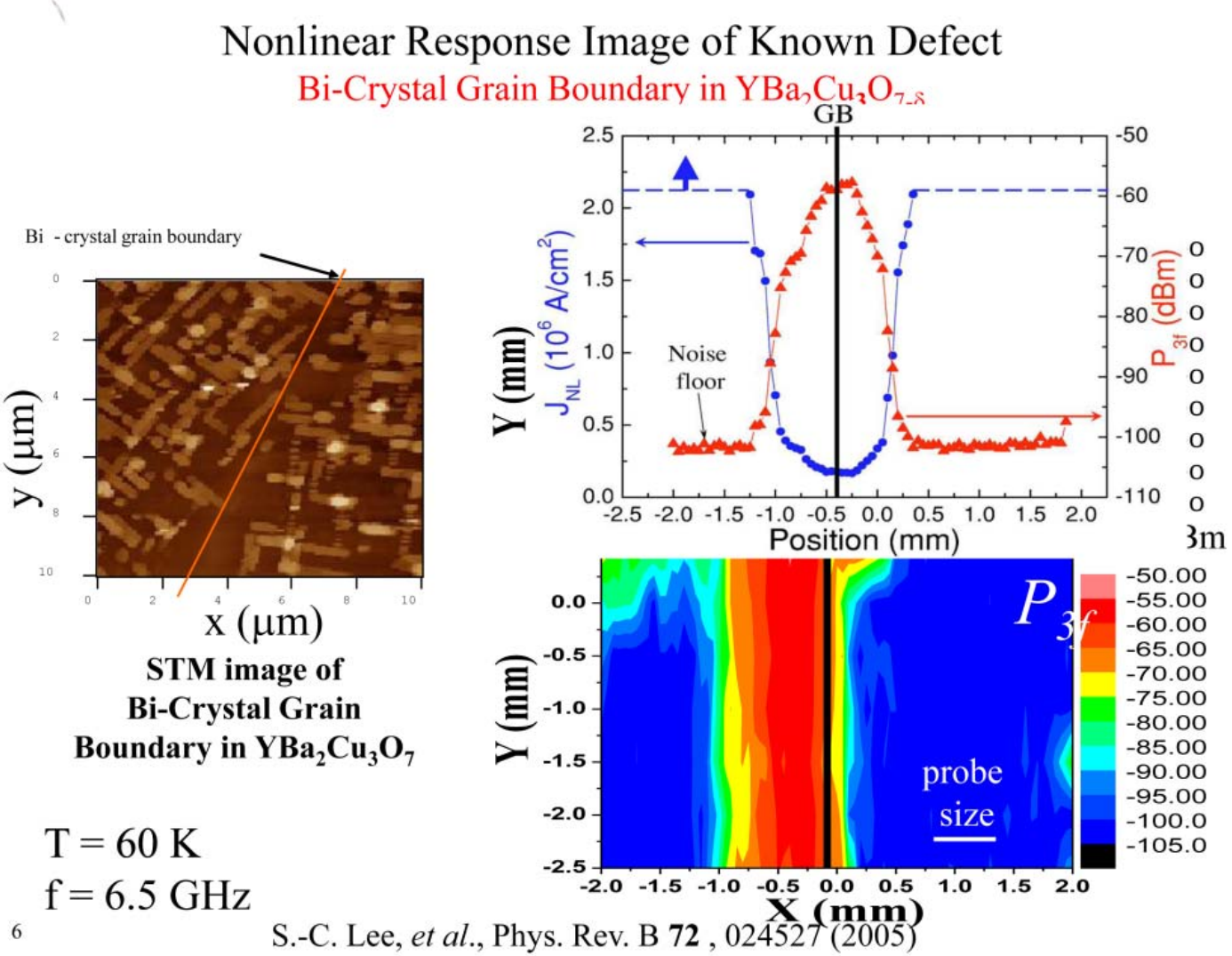

S.-C. Lee, *et al.*, Phys. Rev. B **72** , 024527 (2005)

Laser scanning microscopy

1) Create a compact resonant structure involving a Nb coupon
2) While exciting on resonance, scan a focused laser spot on sample
3) Image the Photo-Thermal effects:

   $J_{RF}(x, y)$ - RF current density in A/cm^2

   Thermo-Electric imaging

   $J_{NL}(x,y)$ – Nonlinearity current scale in A/cm^2

   RF vortex breakdown, flow, critical state

4) Relate these images to candidate defects

Laser scanning microscopy

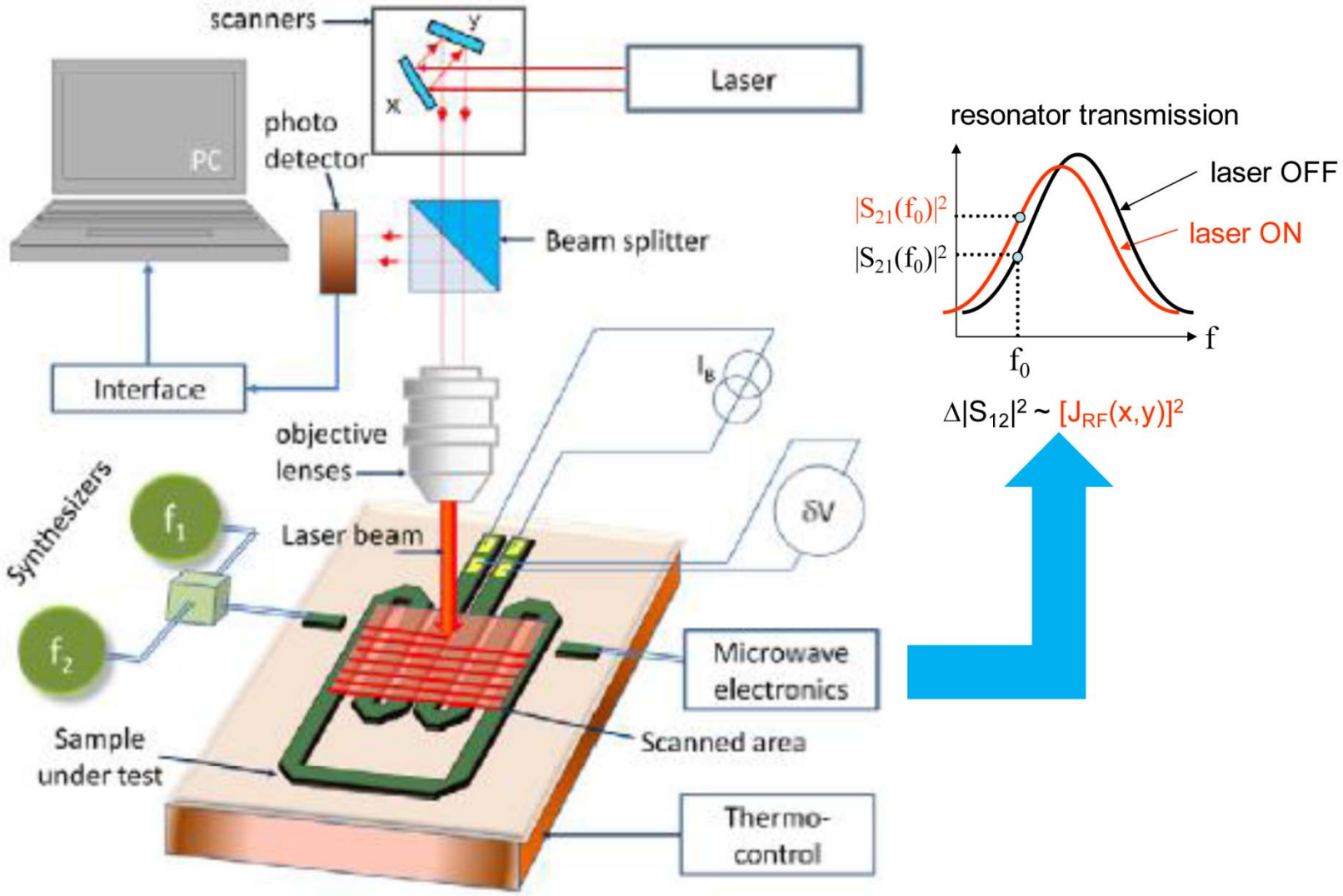

Preliminary Results ($YBa_2Cu_3O_7$)

Reflectivity Image

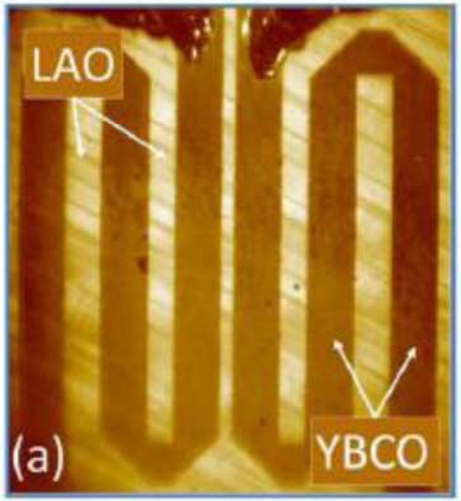

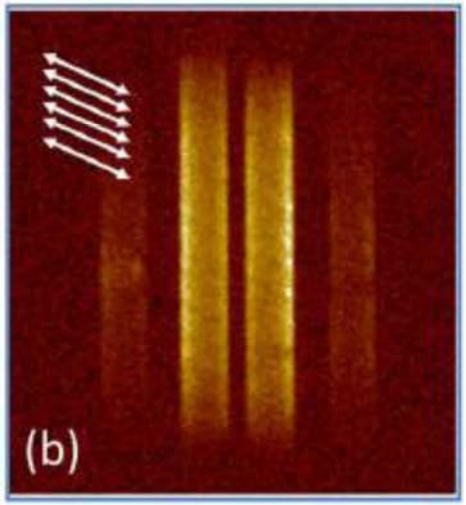

DC Critical State Image ($T < T_c$, $I > I_c$)

Thermo-Electric Image (room temperature)

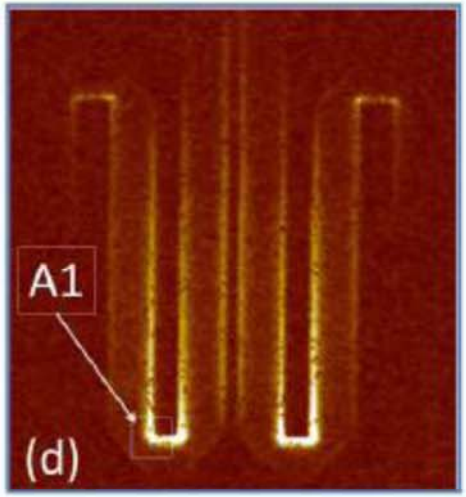

$J_{RF}(x,y)$ Image (5.5 GHz, $T < T_c$)

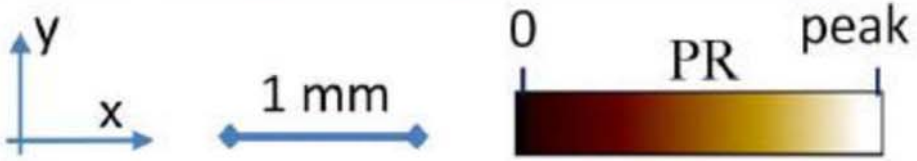

Laser scanning microscopy

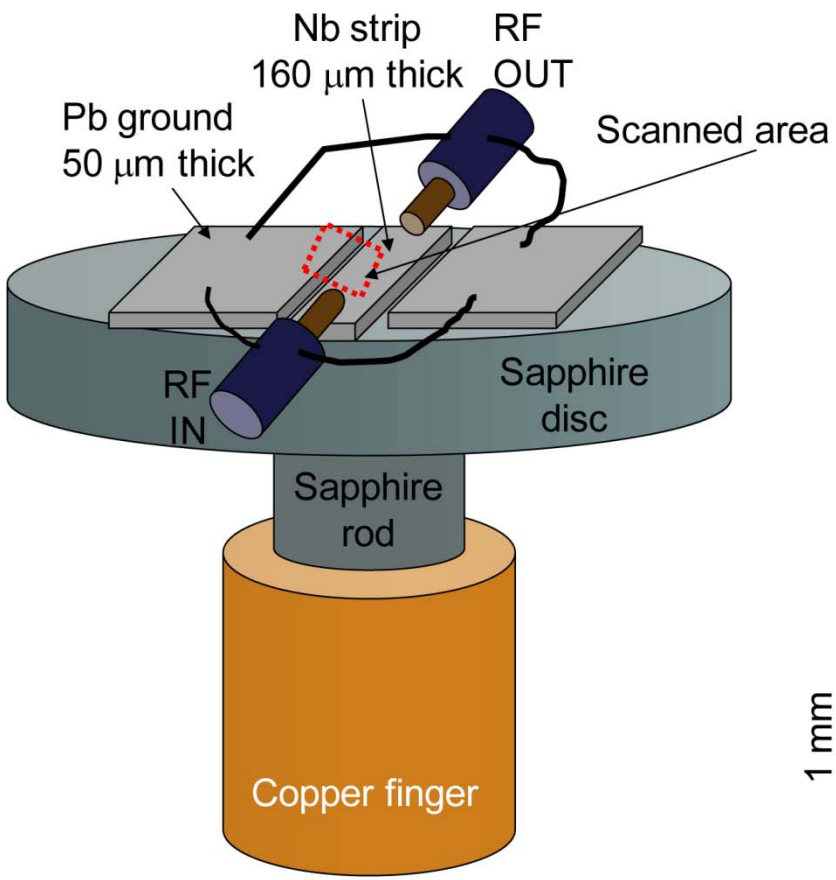

RF Defect Imaging in bulk Nb

reflectivity

F = 3.5 GHz

T = 4.3 K

P_{IN} = -15 dBm

P_{laser} = 1 mW

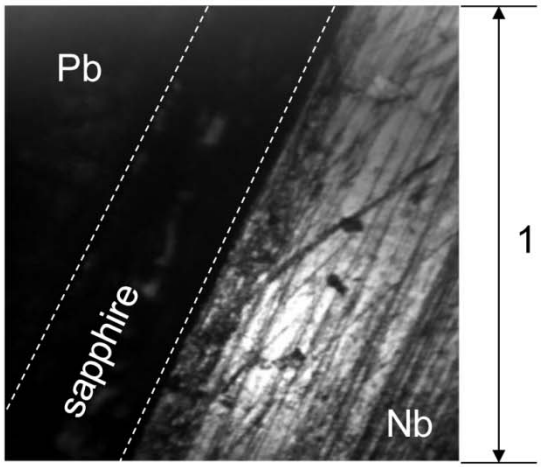

inductive

resistive

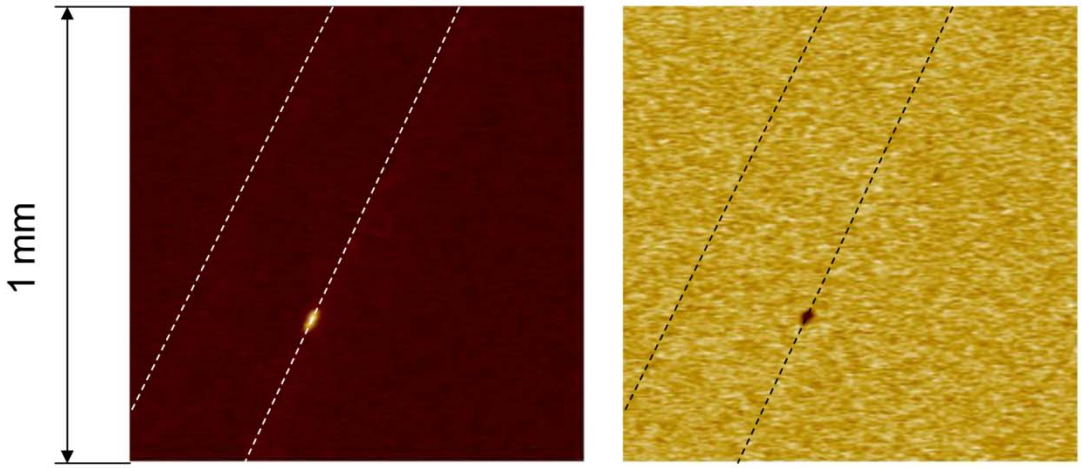

TM_{010} Resonant Mode Current Distribution

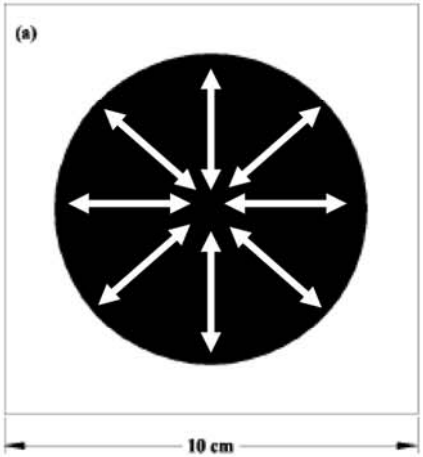

Candidate Resonant Structures

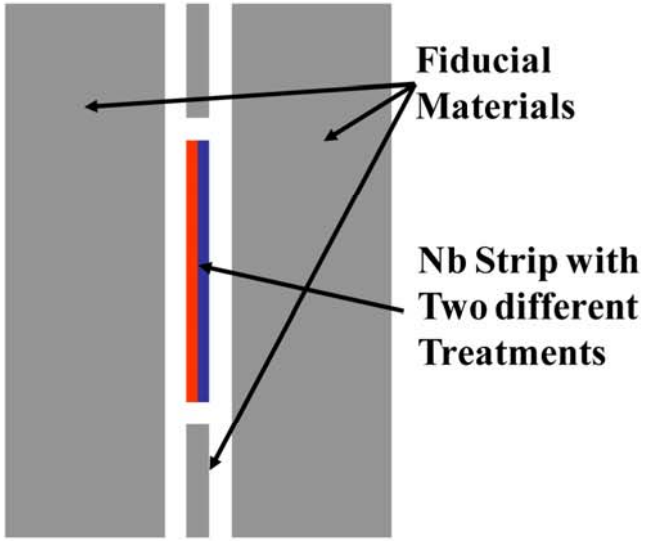

Bulk Nb "Short Sample" structures to measure RF breakdown fields and relate to defects and surface processing

Measure RF breakdown fields in SC / Ins / SC / Ins … multilayer samples

Gurevich, Appl. Phys. Lett. (2006)

Image variations in the thermal healing length to better understand the role of heat dissipation in RF performance

$$\ell_{thermal} = \sqrt{k / c\rho_m f_{Mod}}$$

MAGNETO OPTICAL IMAGING (MOI) OF SUPERCONDUCTORS

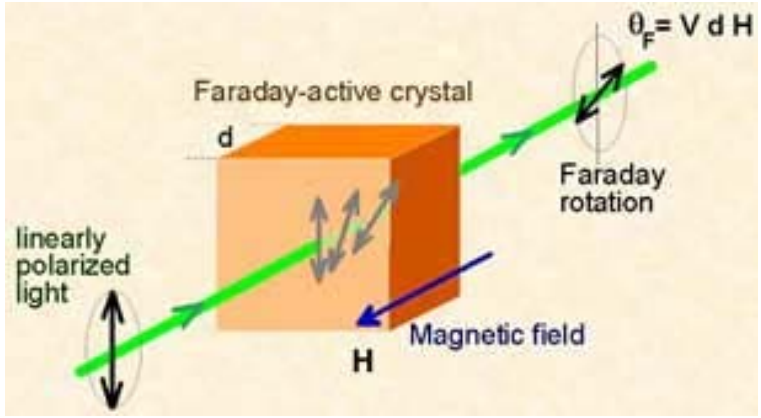

physical idea behind the magneto-optical imaging: **Faraday effect, i.e., rotation of the light polarization induced by magnetic field.**

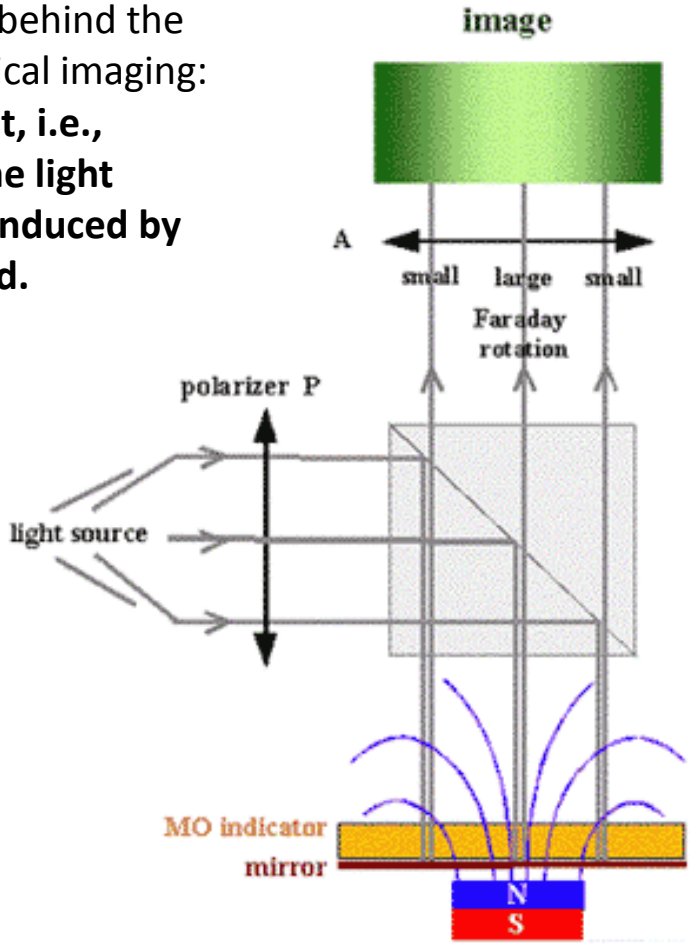

MO indicator is placed in the light beam path between a polarizer and an analyzer crossed by 90 degrees. If a magnetic field is present perpendicularly to the film, the magnetization of the Bi:YIG will be tilted out of the plane. The perpendicular component of the magnetization will cause a Faraday rotation of the light. The rotation angle will be small where the magnetic field is small, and large in regions of high fields. After leaving the analyzer the light will therefore have an intensity distribution that reflects the magnitude of the field in the plane of the indicator film.

MgB_2 film ID # MO 6006 from Brian Moeckly. Alumina substrate. ZFC T=5.3K. Dendridic flux instability

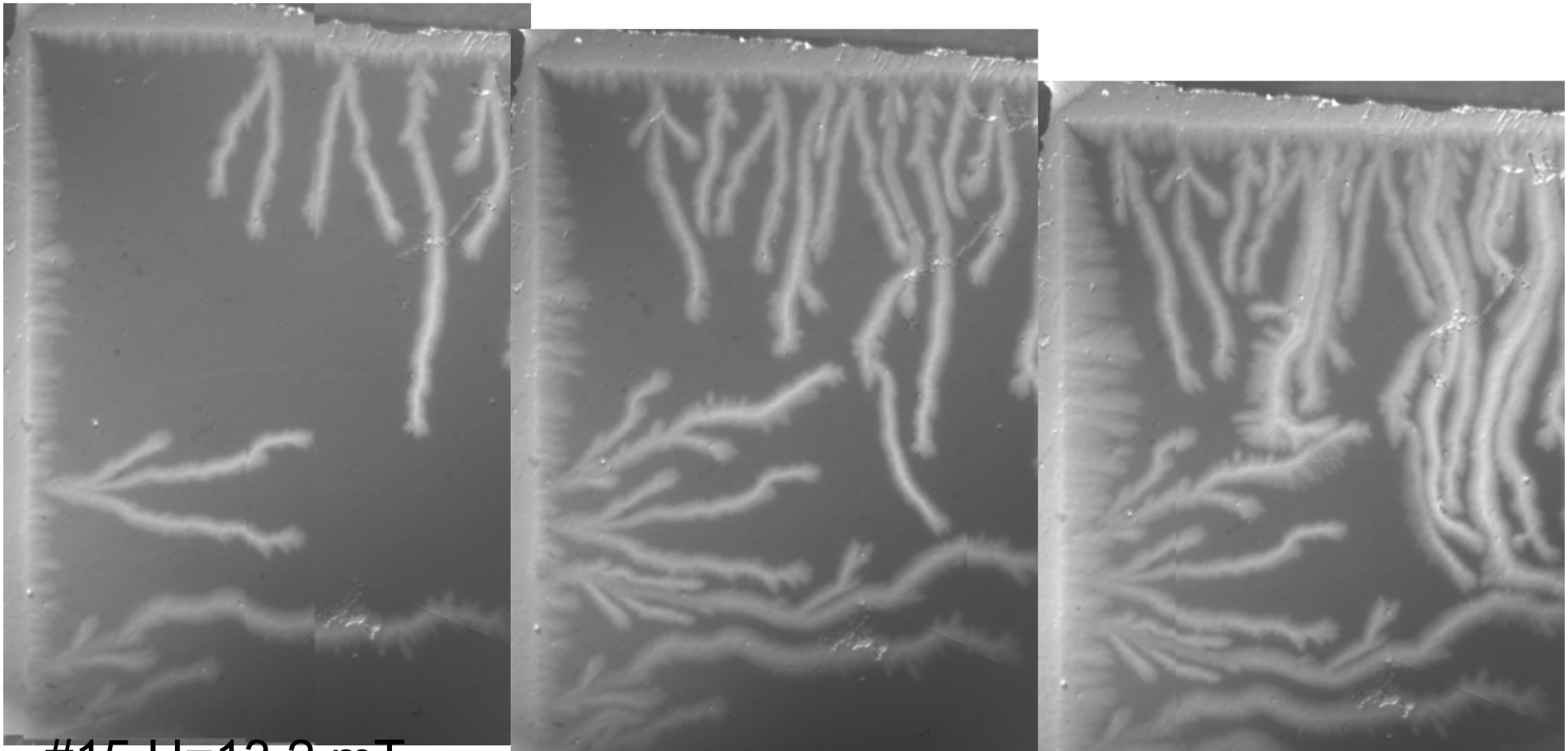

#15 H=13.2 mT

#19 H=20 mT

#23 H=32 mT

MgB_2 thin film on STOCBS 33-1-5 ZFC T=16K
Increasing H from 0 to 120mT Bean flux penetration

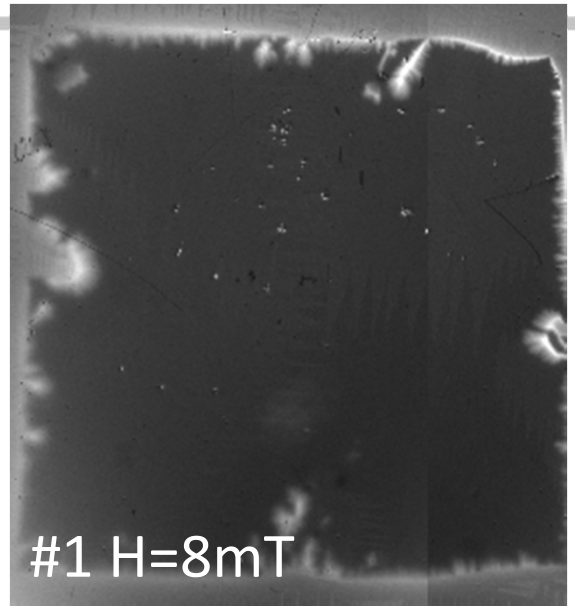

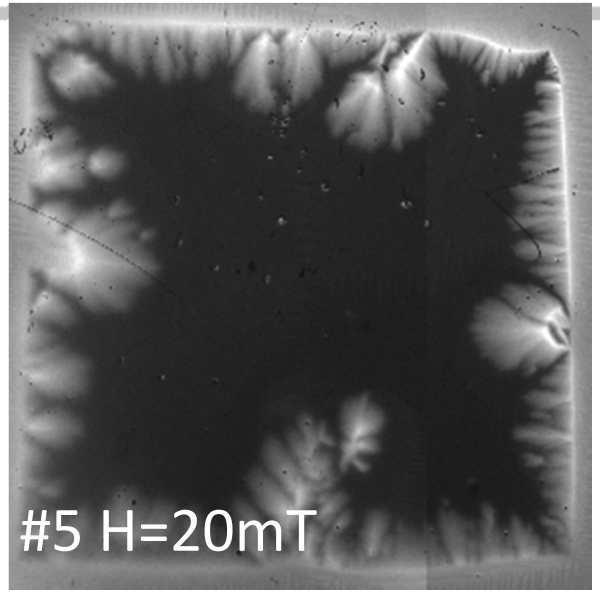

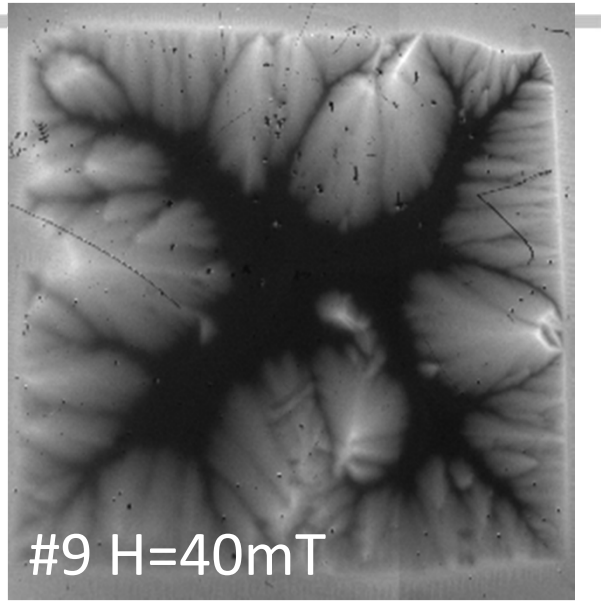

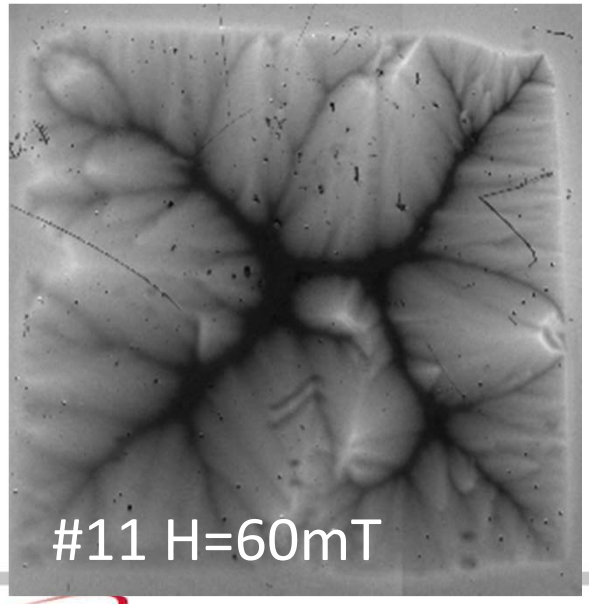

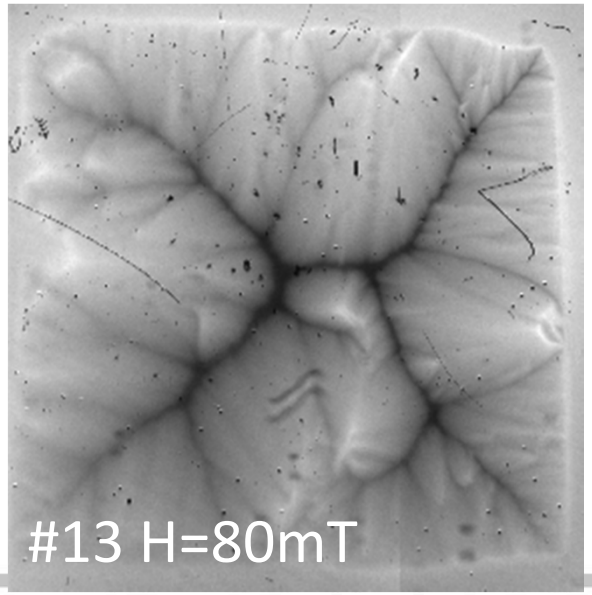

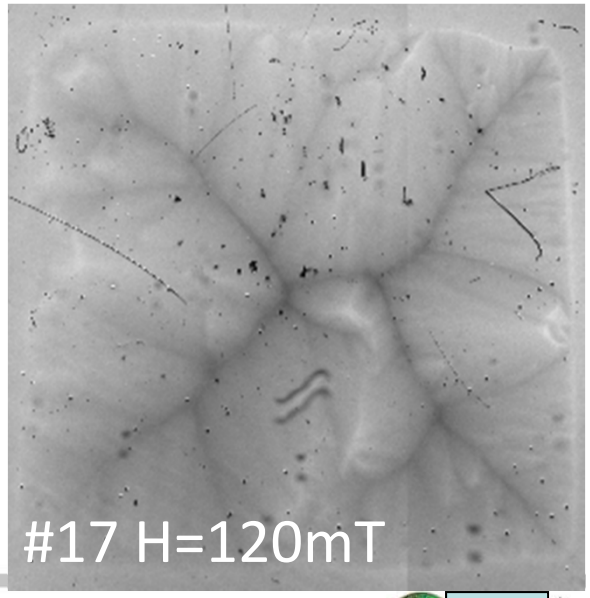

Magneto-optical Measurement

Flux instability in Nb thin film 25 μm, T=3.8 K

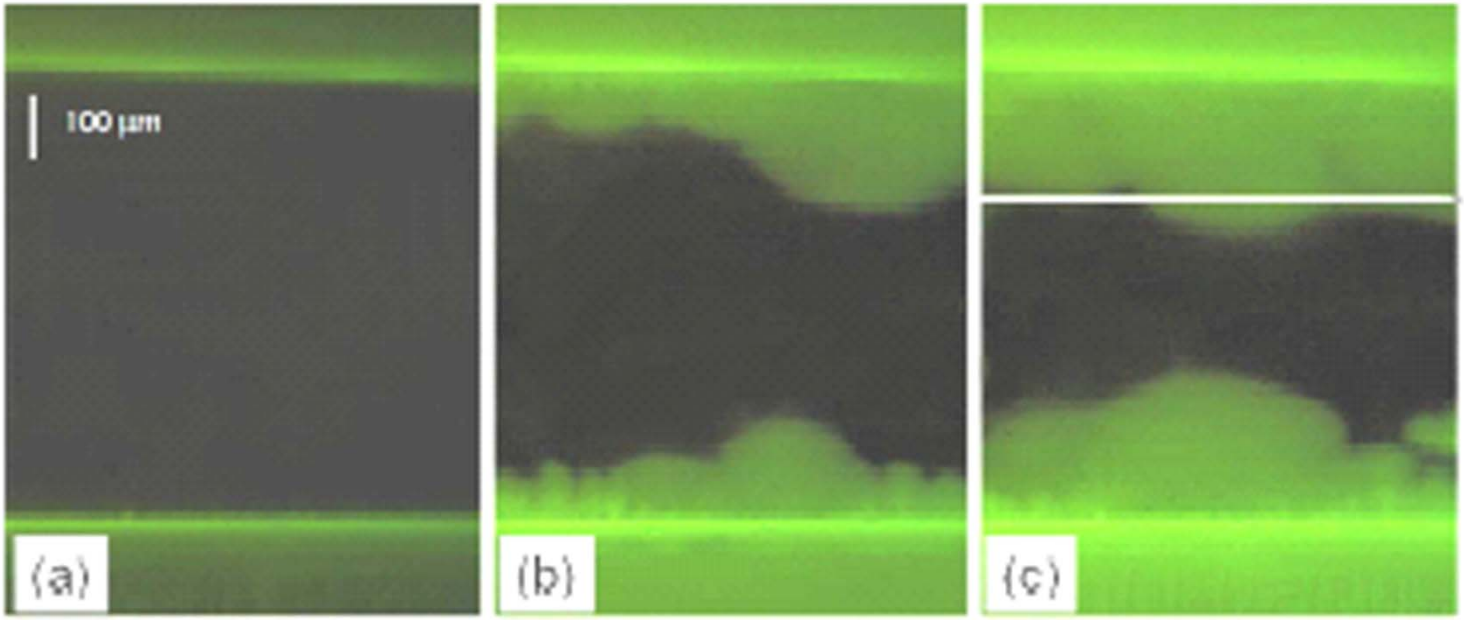

Ruslan Prozorov, Ames Nat. Lab

Magneto-optical Measurement

Flux instability in Nb thin film 25 μm, T=3.8 K

H = -320 Oe → H = -470 Oe → H = -740 Oe

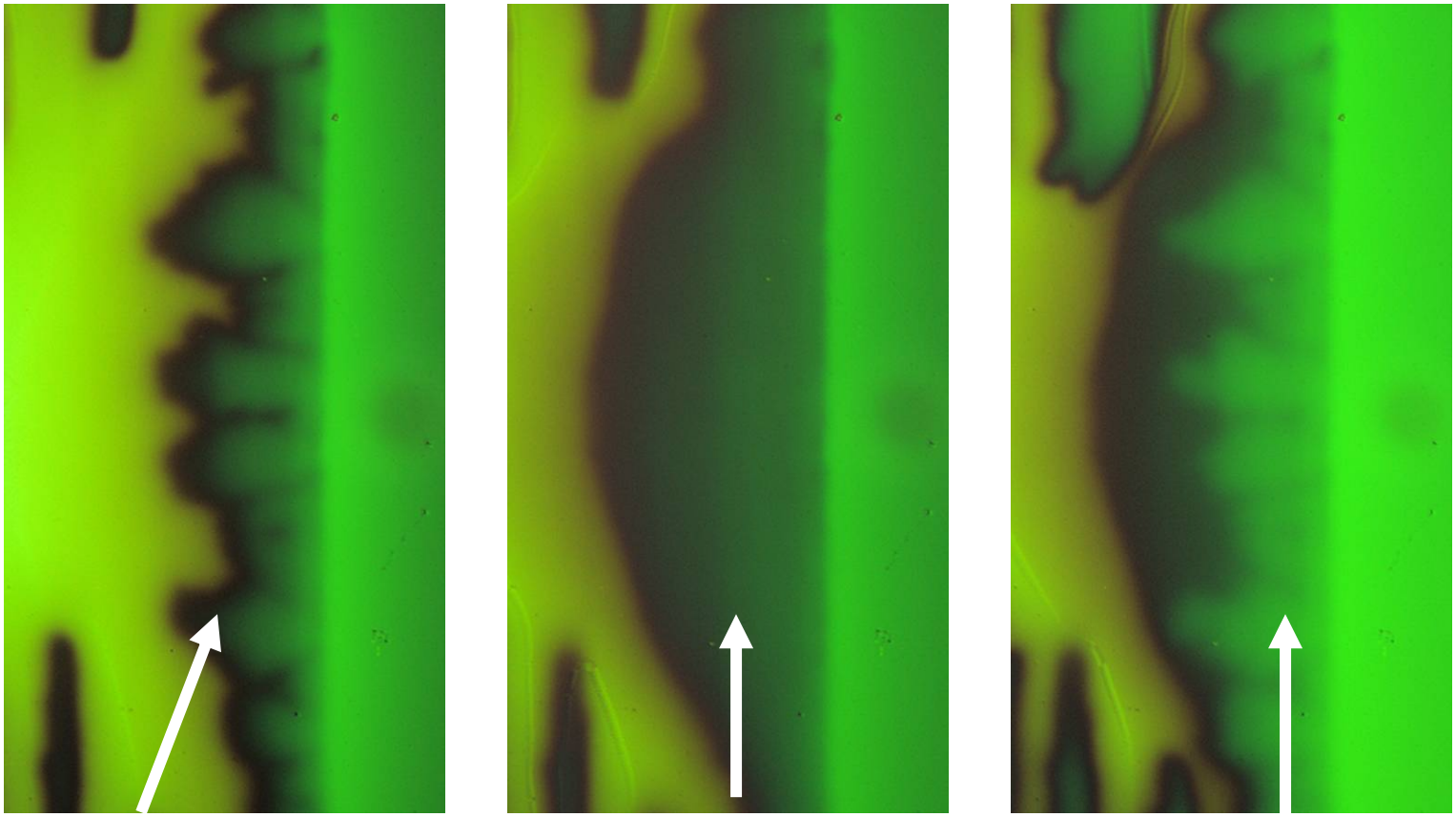

penetration of antiflux (green)

a uniform avalanche

secondary penetration

Ruslan Prozorov, Ames Nat. Lab

MOI of Vortex Penetration (FSU&FNAL)

A. Polyanskii & P. Lee – ASC/UW - FSU

- MOI of Nb bi-crystals cut from a Nb cavity.
- MOI reveals vortex penetration along grain boundaries

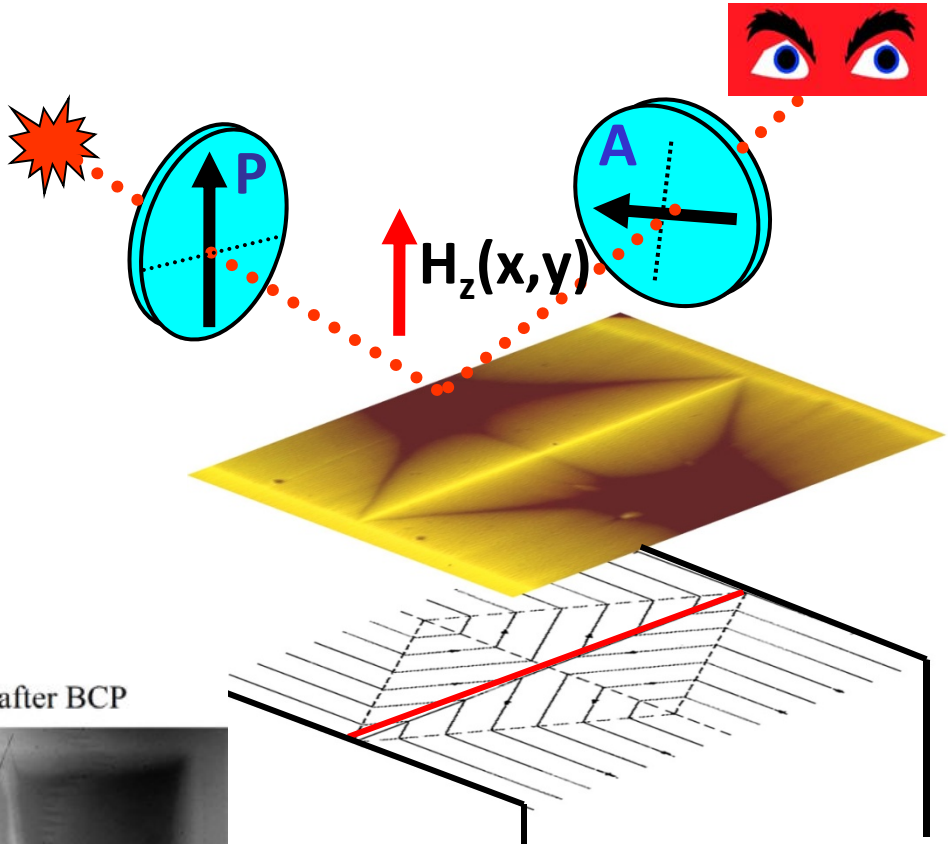

Faraday rotation of the light polarization angle

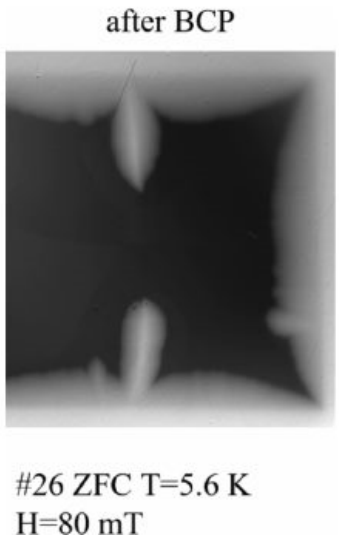

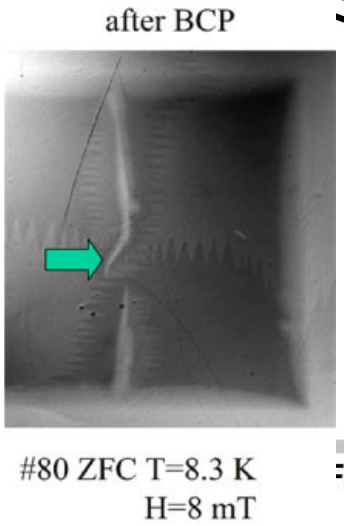

Point Contact Tunneling (PCT)

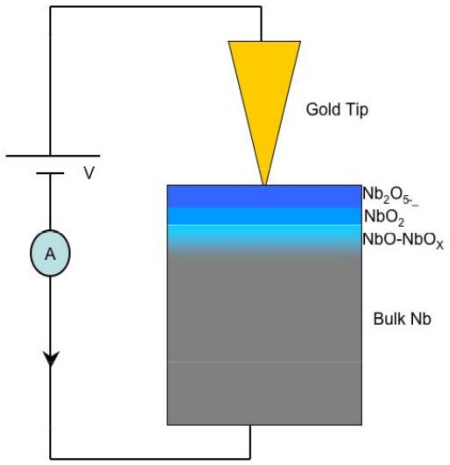

Tunnel junctions are formed by using a mechanical contact between the sample and an Au tip attached to a differential micrometer screw .

Measurement is typically conducted by forming a series of independent junctions in as single run (completely retracting the Au tip (~1 mm) and then re-advancing the tip until a tunnel current is observed).

Probe different regions over an area estimated to be greater than 10 μm^2.

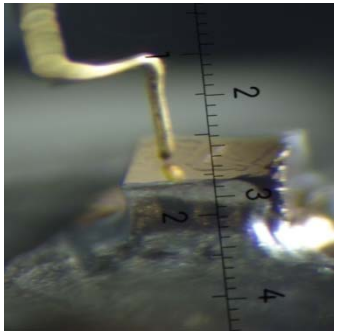

The data is analyzed using the tunnel current in superconductor-insulator- superconductor (S-I-S) and superconductor-insulator-normal metal (S-I-N) junctions written as

$$I(V) = c\int_{-\infty}^{\infty} |T|^2 \rho_1(E)\,\rho_2(E+eV)\,[f(E) - f(E+eV)]\,dE$$

ρ_1 (E), ρ_2 (E) quasi-particle DOS in the two electrodes

c proportionalityconstant

f (E) Fermi-Dirac distribution function describing thermal smearing

jTj2 is the tunneling matrix element

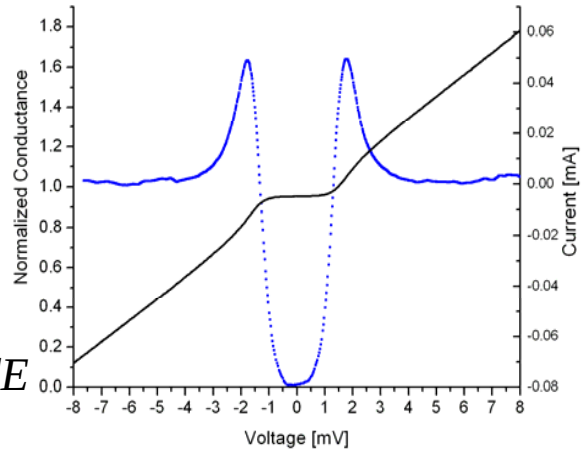

$$\frac{dI}{dV} = -\sigma_N \int N(E)\frac{\partial f(E+eV)}{\partial(eV)}dE$$

$$N(E) = \mathrm{Re}\left[\frac{|E| - i\Gamma}{\sqrt{(|E| - i\Gamma)^2 - \Delta^2}}\right]$$

Dynamic conductance curve (dI/dV versus V).

Point Contact Tunneling (PCT)

A typical spectrum on Nb single crystal and BTK fit

BTK (Blonder-Tinkham-Klapwijk) theory describes smooth transition from tunneling to Andreev reflection

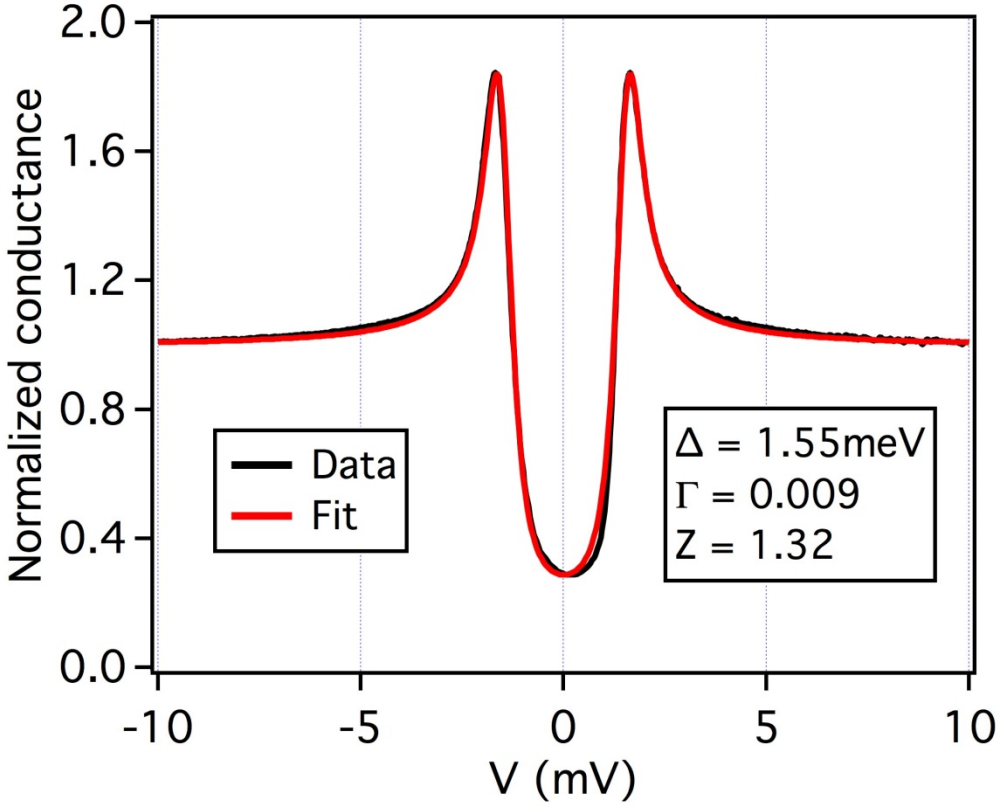

Δ Gap

Γ DOS Broadening

Z Barrier Strength

Point Contact Tunneling (PCT)

PCT on bulk niobium – High temperature treatment effect

P. Dhakal et al. - *Effect of high temperature heat treatments on the quality factor of a large-grain superconducting radio-frequency niobium cavity* – PRSTAB 2013 6

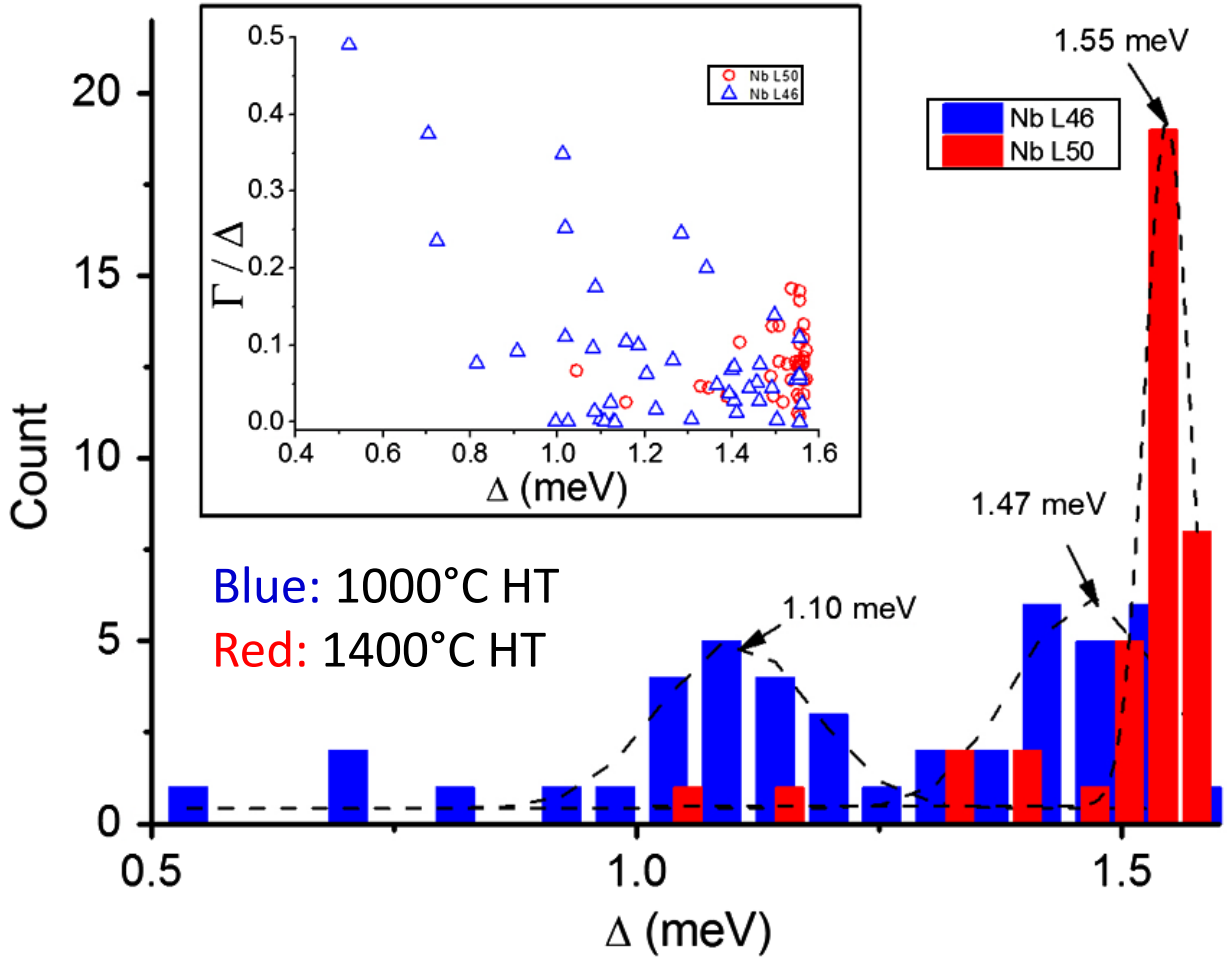

Higher temperature treatment (better RF performance) shows:

- ❑ less low energy gaps
- ❑ smaller Γ values (sharper distributions)

Muon Spin Rotation (μSR)

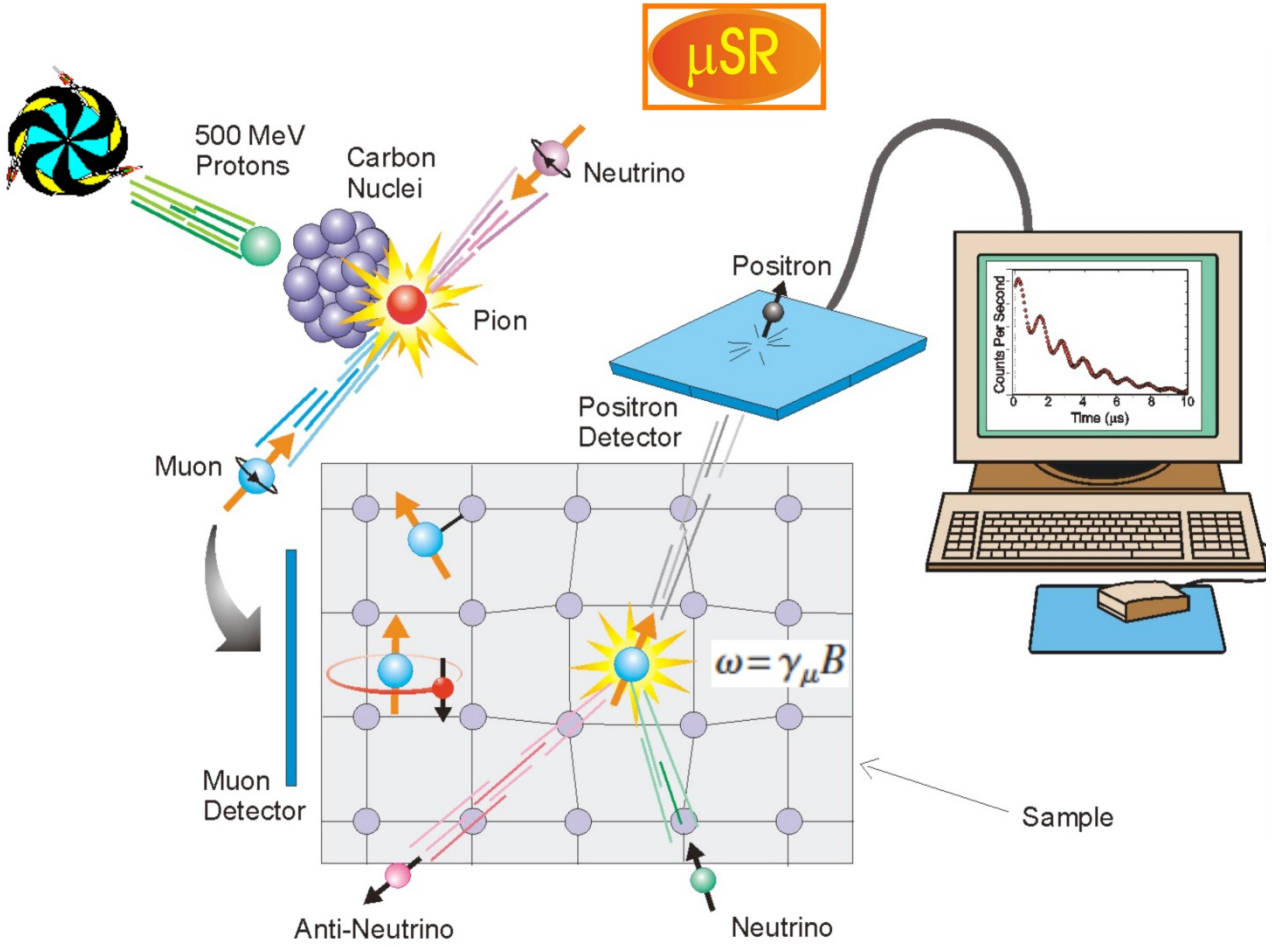

The Muon as a Probe

- Probing Magnetism: unequalled sensitivity
  - Local fields: electronic structure; ordering
  - Dynamics: electronic, nuclear spins
- Probing Superconductivity: (esp. HT_cSC)
  - Coexistence of SC & Magnetism
  - Magnetic Penetration Depth λ
  - Coherence Length ξ

Muon Spin Rotation (μSR)

Transverse-Field μSR

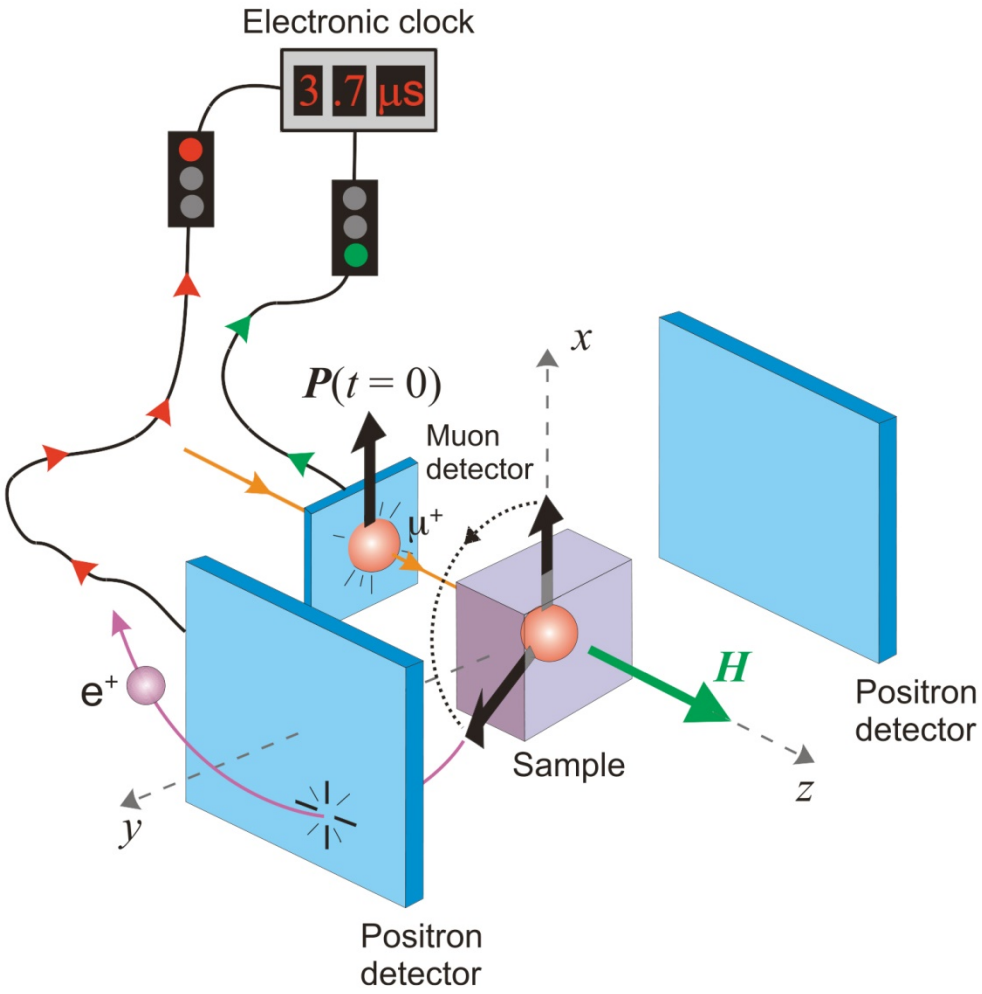

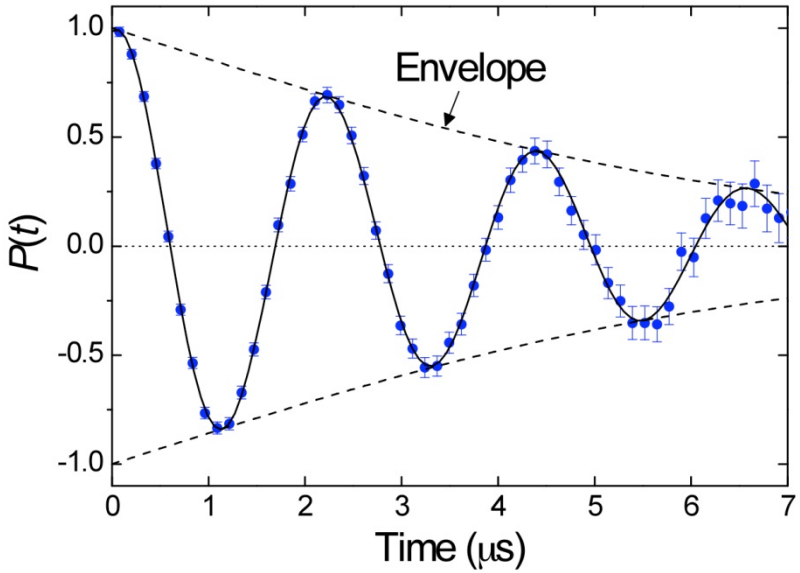

The time evolution of the muon spin polarization is described by:

$$P(t) = G(t)\cos(\gamma_\mu B_\mu t + \phi)$$

where $G(t)$ is a relaxation function describing the ***envelope*** of the TF-μSR signal that is sensitive to the width of the static field distribution or temporal fluctuations.

Muon Spin Rotation (μSR)

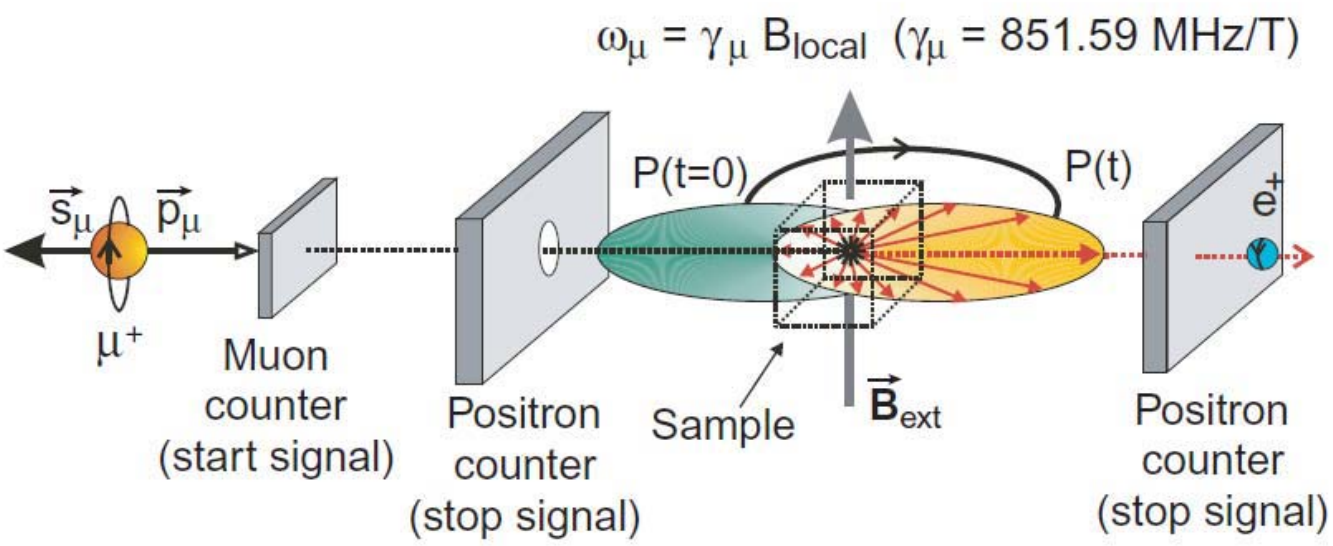

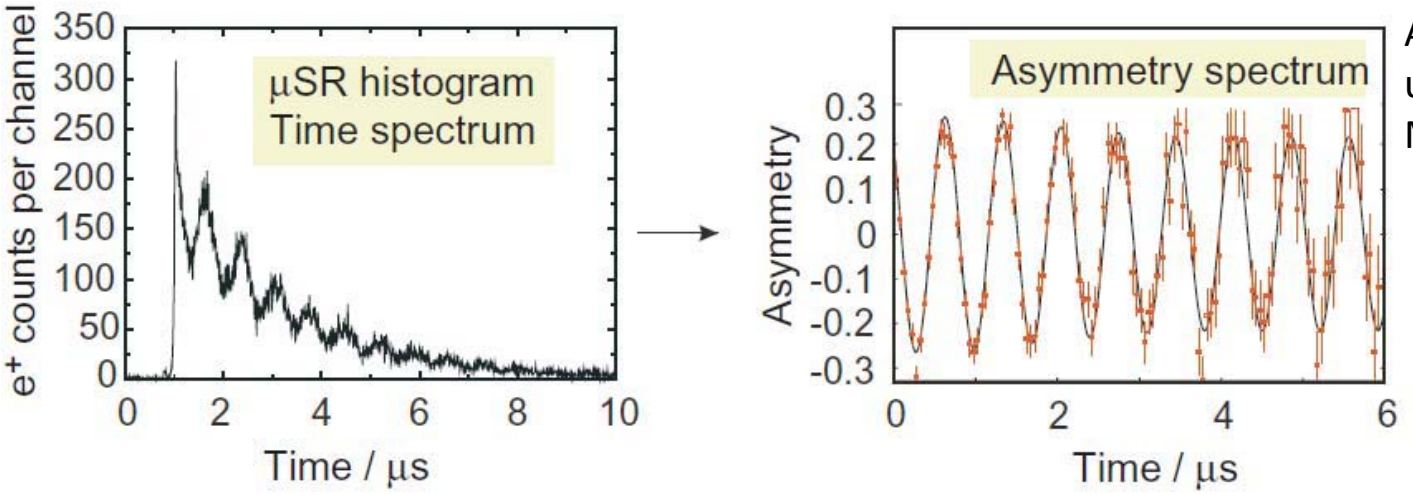

The muon is sensitive to the **vector sum** of the local magnetic fields at its stopping site. The local fields consist of:

- those from **nuclear** magnetic moments
- those from **electronic** moments (100-1000 times larger than from nuclear moments)
- **external** magnetic fields

As a local probe, μSR can be used to deduce Magnetic volume fractions.

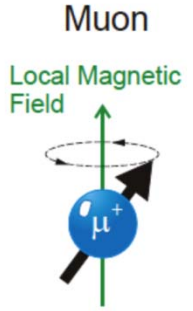

Muon Spin Rotation (μSR)

Method:

- Implant and thermalize ~100% polarized muons in matter (stopping time in solid ~ 10 ps, no initial loss of polarization, stop site: generally interstitial). P(0) =1
- Magnetic moment of muon interacts with local magnetic fields (moments, currents, spins) → P(t)
- P(t) is characterized by precession and/or depolarization/relaxation.
- Observe time evolution of the polarization P(t) of the muon ensemble via asymmetric muon decay: (positrons preferentially emitted along muon spin).
- P(t) contains information about static and dynamic properties of local environment (fields, moments,..)

$$\frac{d\vec{\mu}_\mu}{dt} = \gamma_\mu \left(\vec{\mu}_\mu \times \vec{B}(t)\right) \qquad \vec{P} = \frac{<\vec{s}>}{\frac{1}{2}\hbar}$$

$$\frac{d\vec{P}}{dt} = \gamma_\mu \left(\vec{P} \times \vec{B}(t)\right)$$

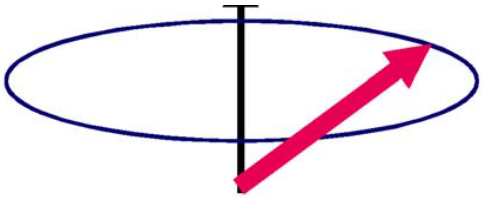

$$\omega_L = \gamma_\mu B_{loc}$$

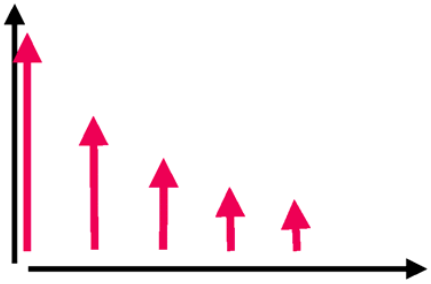

Muon Spin Rotation (LEμSR)

Low energy:0.5-30 keV vs. 3-4 MeV for conventional)

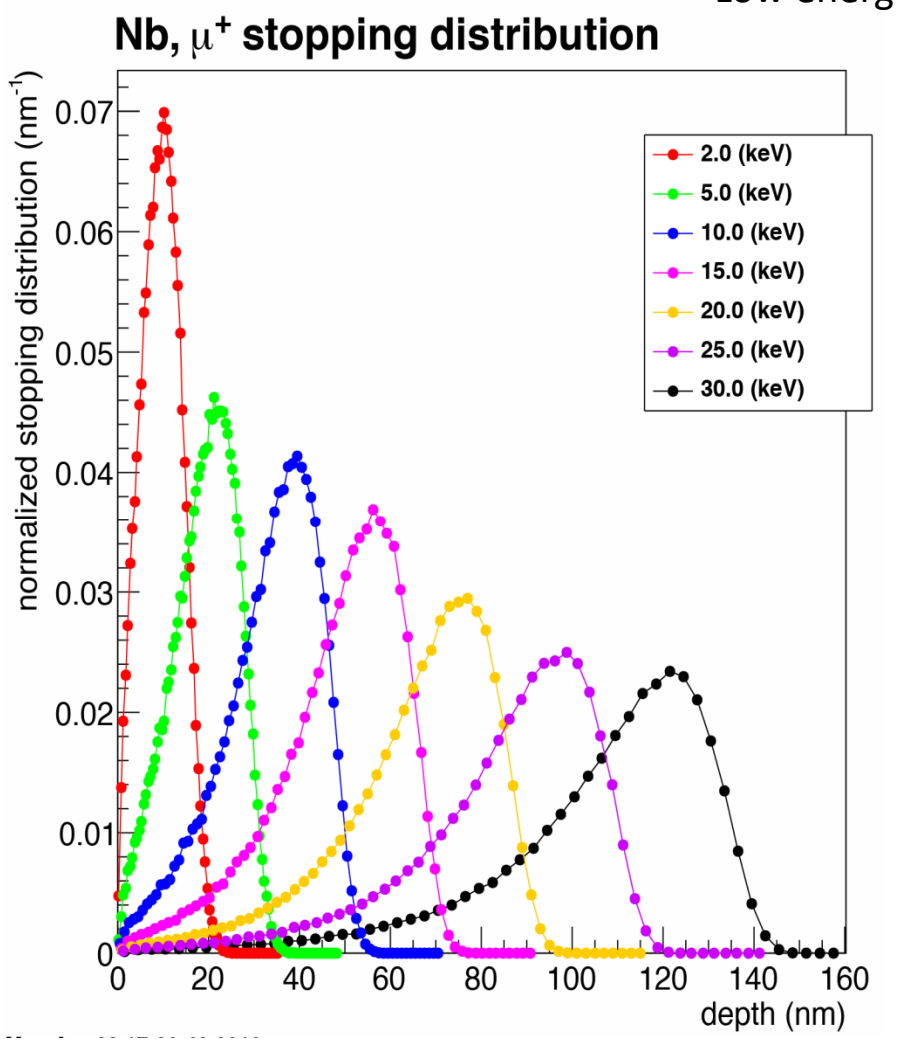

"Local" extremely sensitive magnetic field probe (vs magnetization etc)

- Can implant at different depths: can study surface vs bulk
- Can be used to study thin films, surfaces and multi-layered compounds
- Can answer several questions:

1. Is HFQS due to early flux penetration?

2. Role of trapped flux on HFQS and/or MFQS ?

3. Field dependence of penetration depth and coherence length?

4. Magnetic impurities?

Muon Spin Rotation (μSR)

The muon is sensitive to the **vector sum** of the local
magnetic fields at its stopping site. The local fields
consist of:

- those from **nuclear** magnetic moments
- those from **electronic** moments
(100-1000 times larger than from nuclear moments)
- **external** magnetic fields

As a local probe, μSR can be used to deduce Magnetic volume fractions.

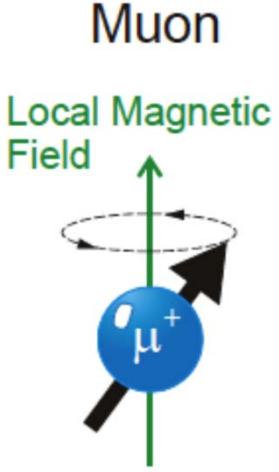

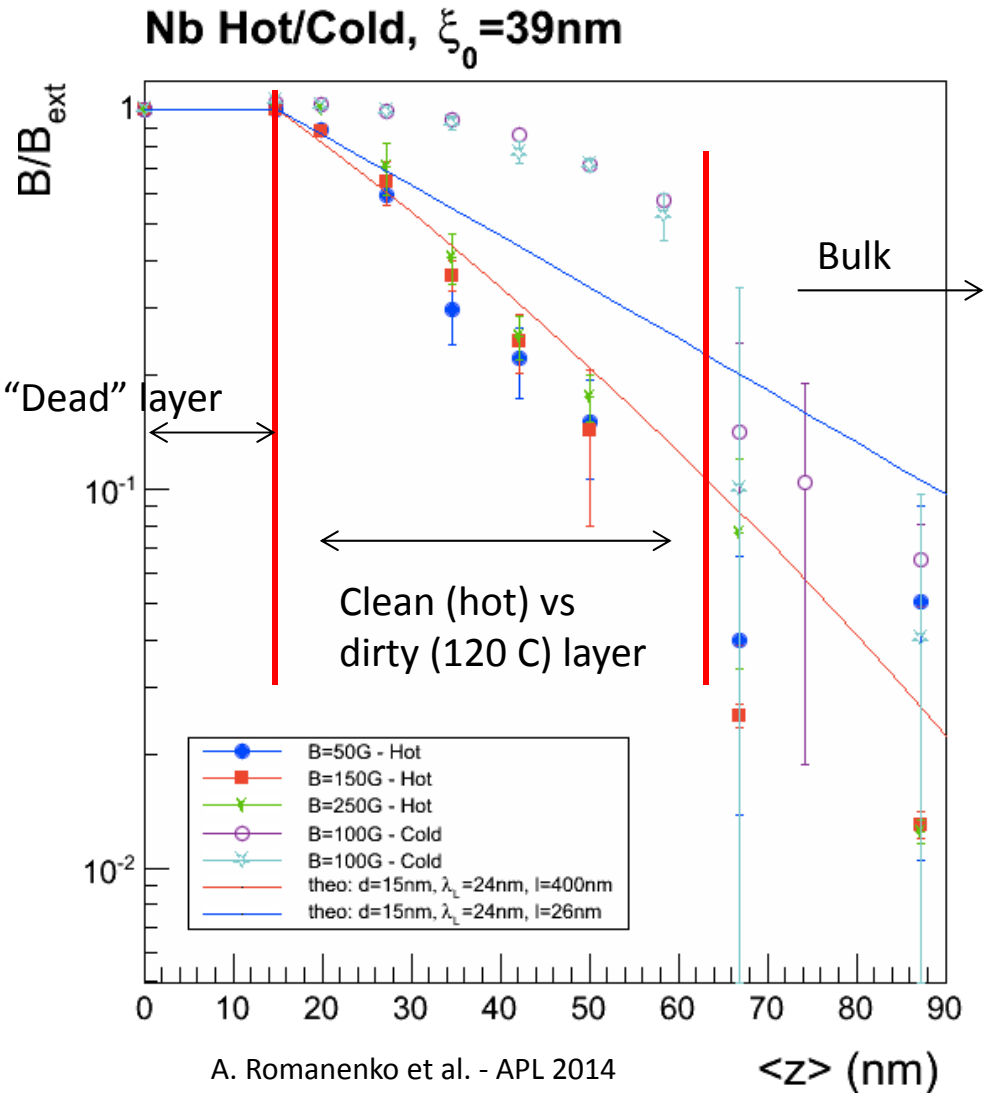

A. Romanenko et al. - APL 2014

Muon Spin Rotation (μSR)

A. Romanenko et al. - Strong Meissner screening change in superconducting radio frequency cavities due to mild baking – APL 2014

LE μ SR (low energy muon spin rotation) on bulk Nb

Magnetic field profile at 25 mT

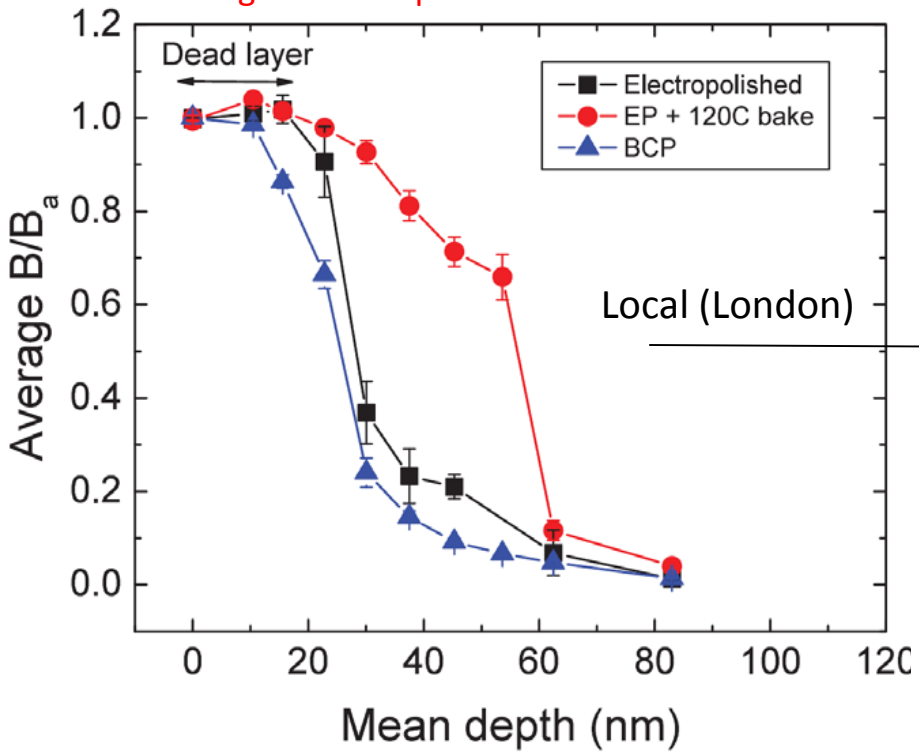

Local (London)

Non-local (Pippard)

Average normalized field vs. mean muon stopping depth

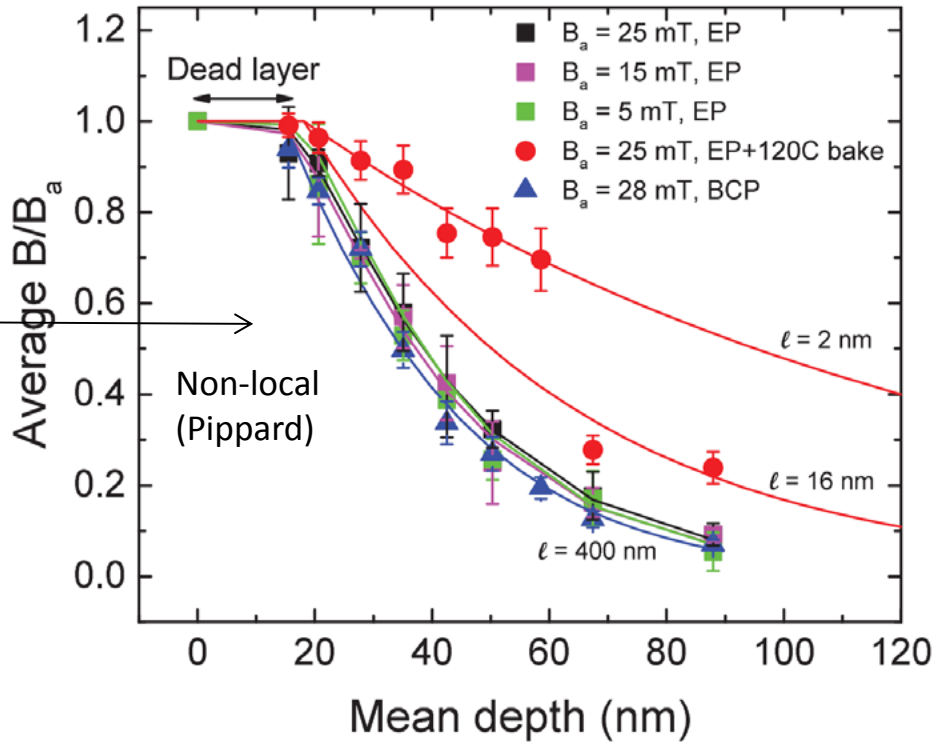

Non exponential penetration

- Taking non-locality into account exponential fit possible
- Cold region of 120°C baked sample shows a strong change in Meissner screening with depth

SQUID Measurements

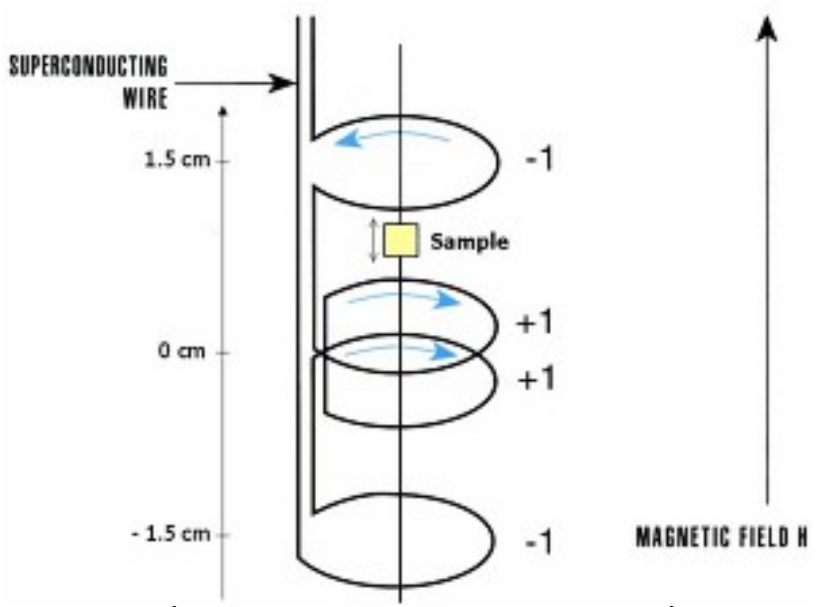

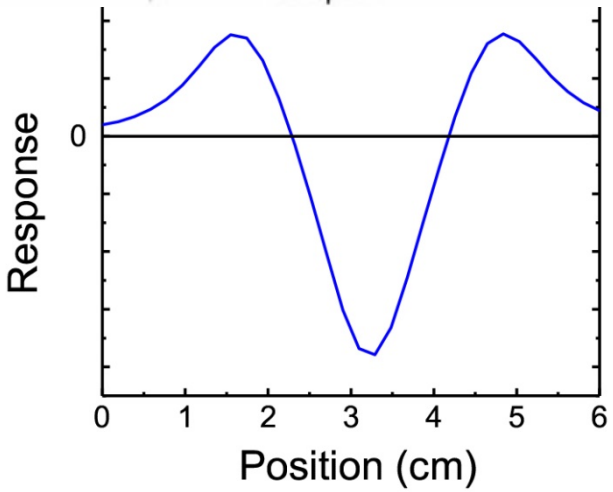

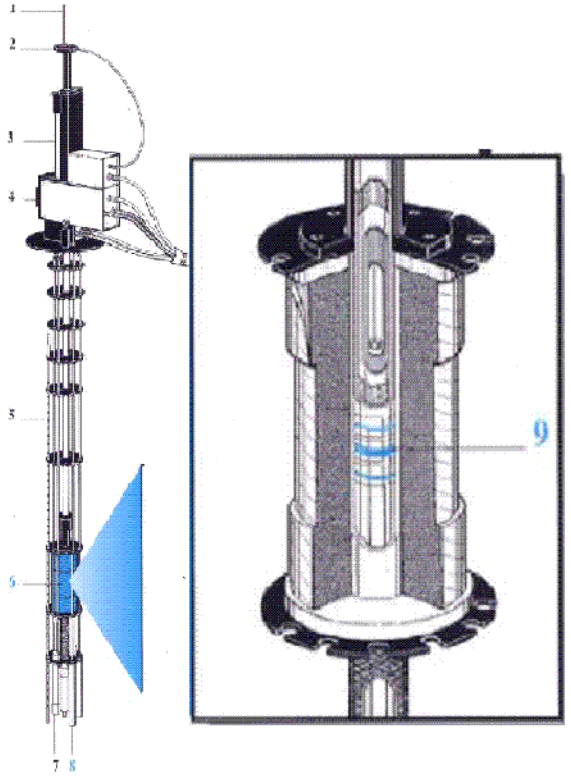

1. Sample rod
2. Sample rotator
3. Sample transport
4. Probe assembly
5. He level Sensor
6. Superconducting Solenoid
7. Flow Impedance
8. Squid capsule with magnetic shield
9. Superconducting pick-up coil

Current proportional to magnet flux changes
Issue: sample needs to be large compared to the coils to avoid edge effects

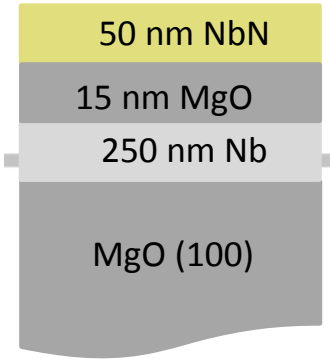

SQUID Measurements

Any misalignment sample surface /direction of the applied field →decreased value for the measured critical field.

Field measured represent a lower limit of Hc1 (perpendicular component of the applied field promotes earlier vortex penetration.)

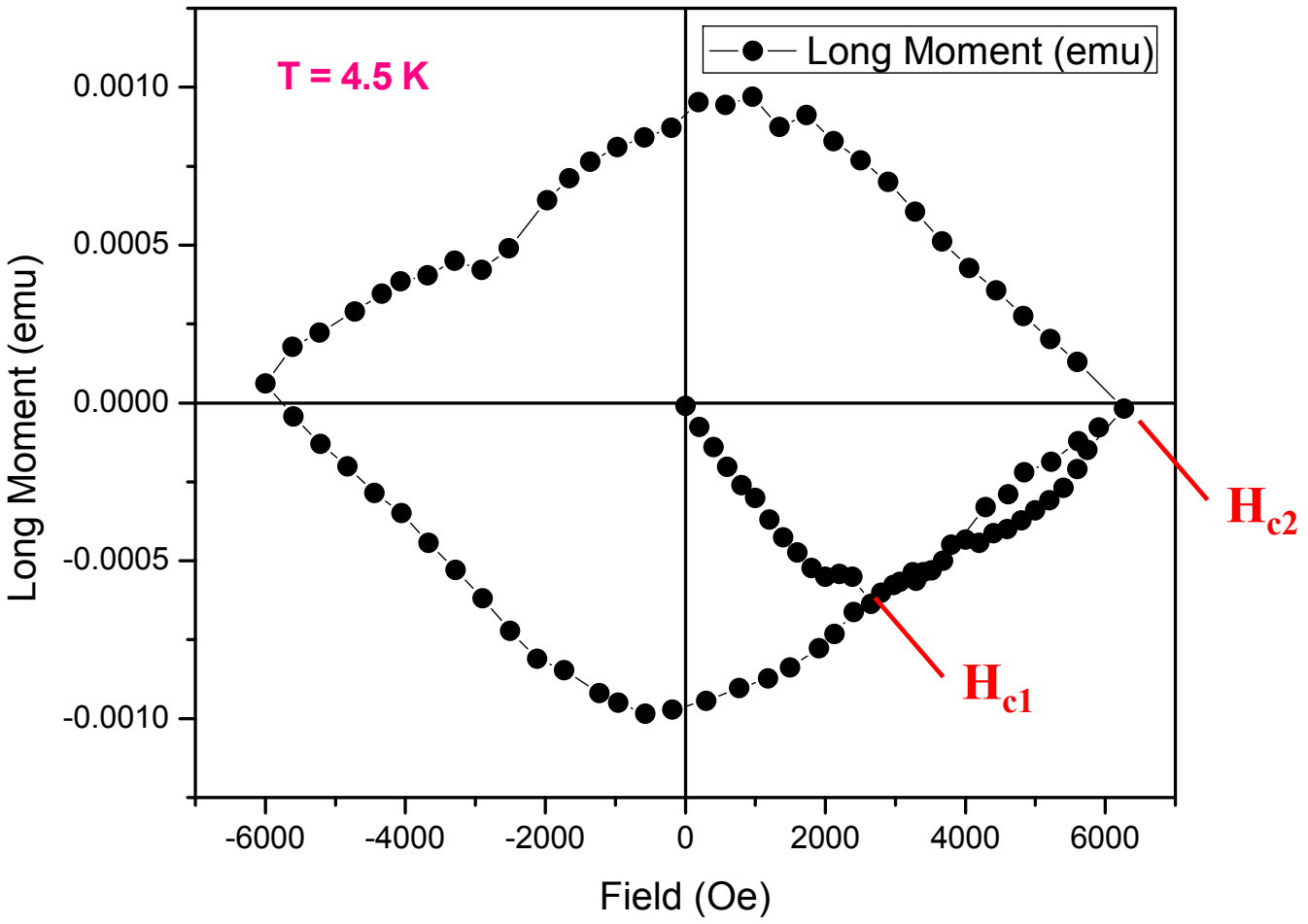

"Magnetic Shielding Larger than the Lower Critical Field of Niobium in Multilayers" W. M. Roach, D. B. Beringer, Z. Li, C. Clavero, and R. A. Lukaszew, *IEEE Trans. Appl. Supercond.* **23**, 8600203 (2013).

$H_{c1\text{-NbN-based-Multilayer}}$ ~ 220 mT!

$H_{c1\text{-bulk Nb}}$ = 170 mT

SQUID Measurements

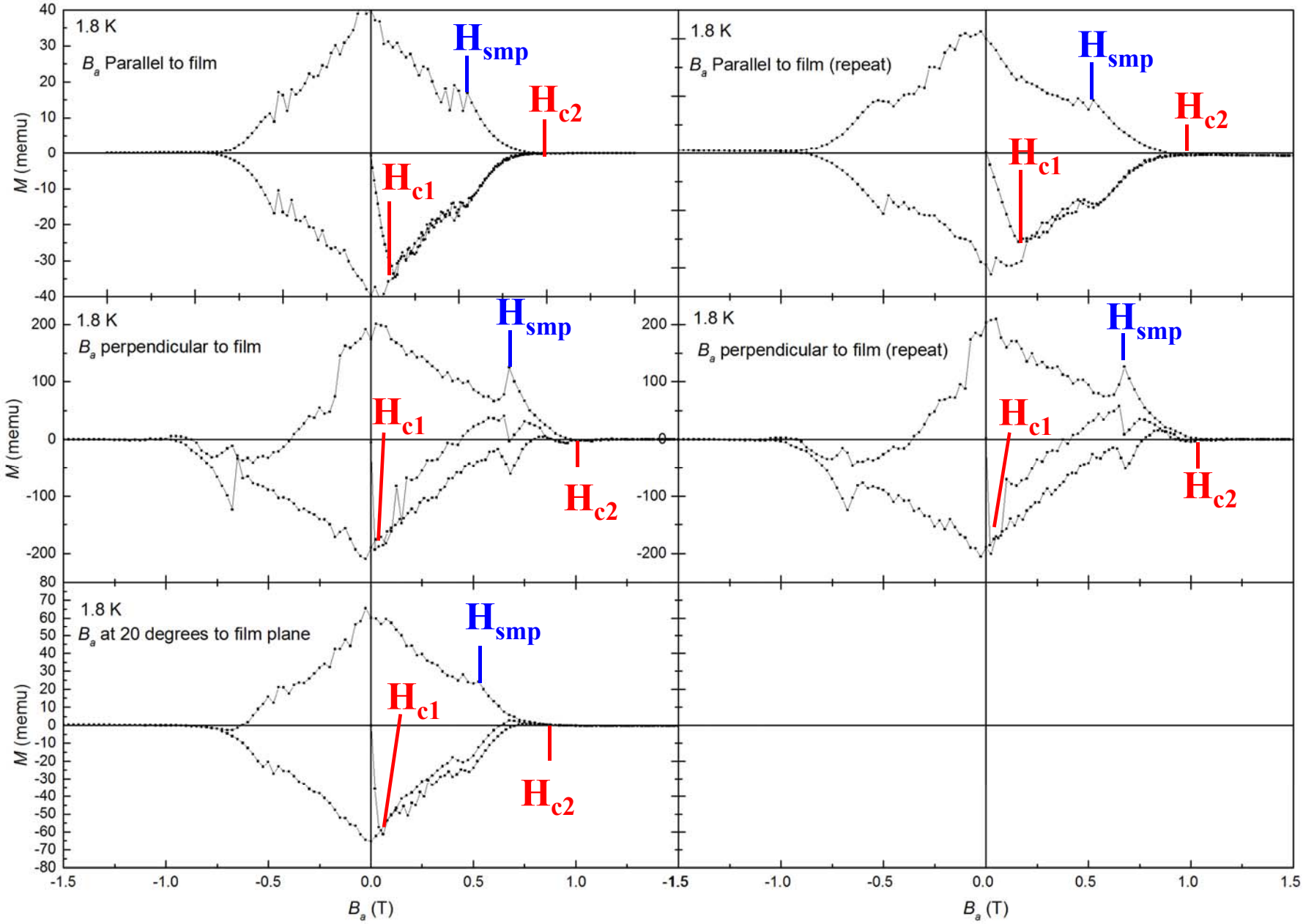

OTHER

Field Emission

Fowler-Nordheim model

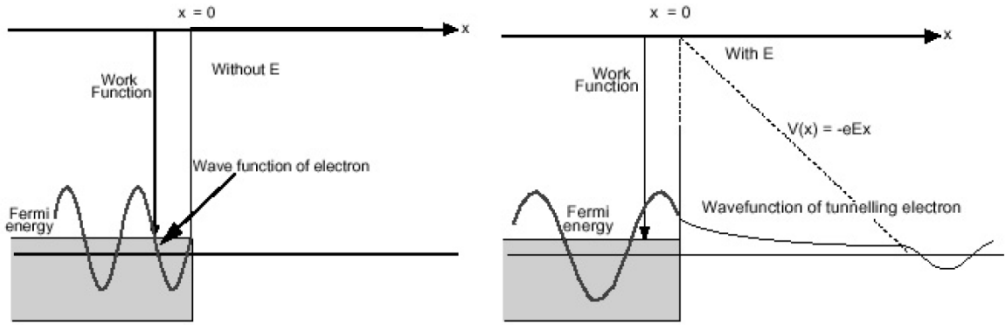

$$I(E) = \frac{1.54\times10^{6}\ Ae\left(\beta_{FN}E\right)^{2}}{\phi}\exp\left[-\frac{6.83\times10^{3}\ \phi^{\frac{3}{2}}}{\beta_{FN}\ E}\right]$$

$\phi = work\ function$

$A_e = Effective\ Emitter\ Surface\ Area$

$E = Electric\ Field$

$\beta_{FN} = Field\ Enhancement\ Factor$

Smooth particles show little field emission

Simple protrusions are not sufficient to explain the measured enhancement factors

Possible explanation: tip on tip (compounded enhancement)

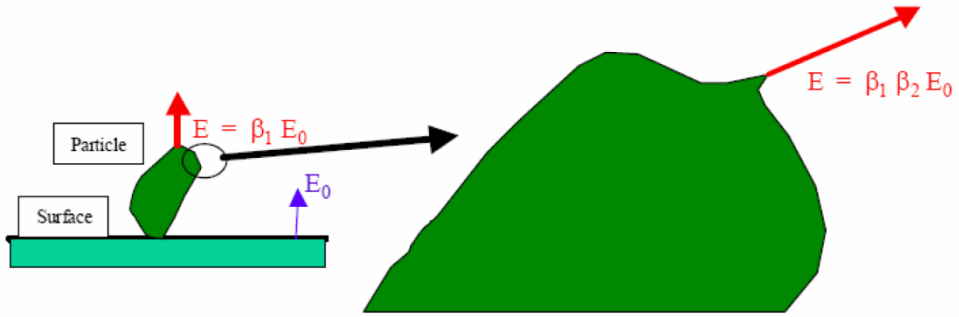

Field emission scanning microscope (FESM)

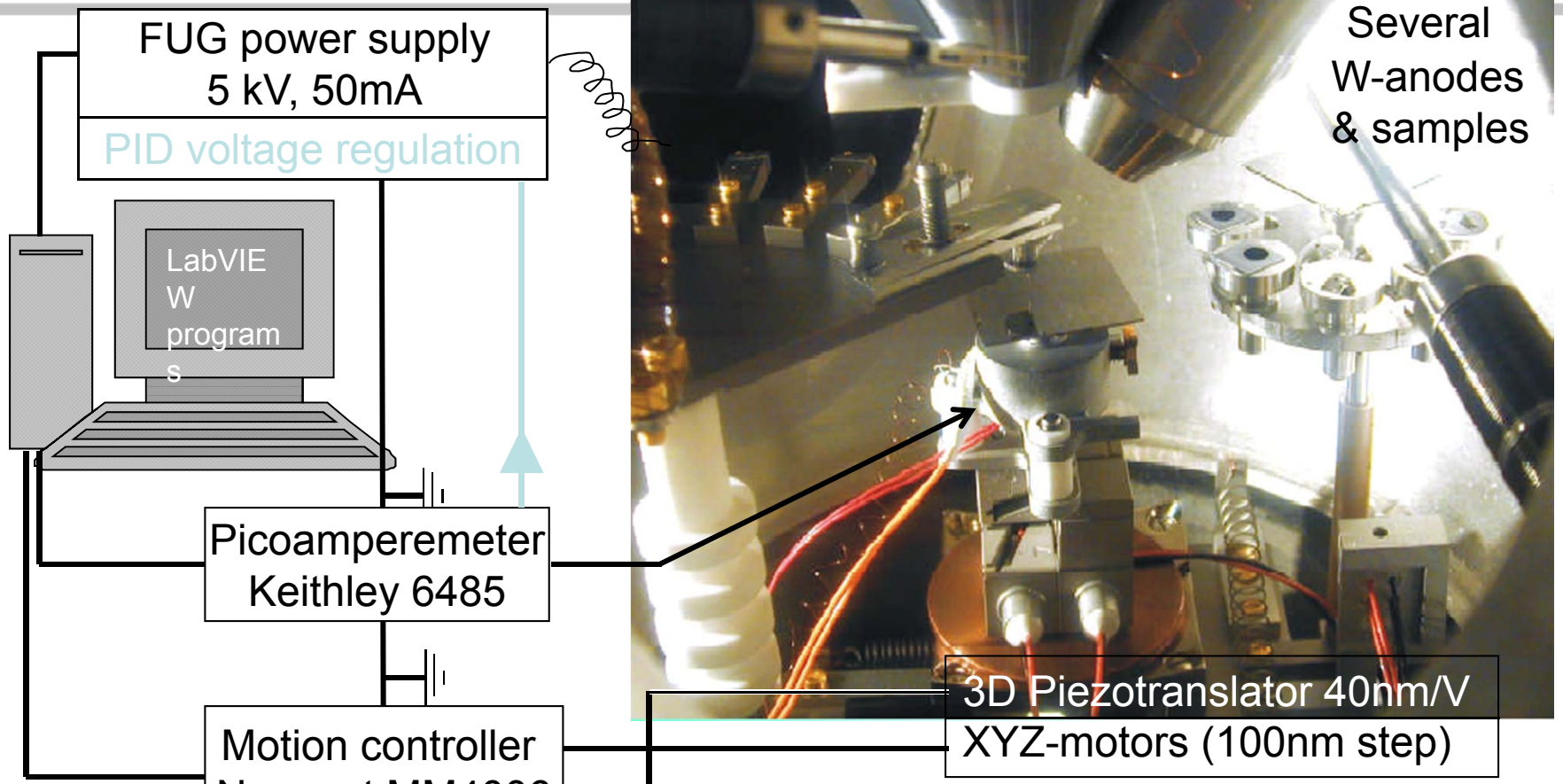

UHV system typically at $2 \cdot 10^{-7}$ Pa

LabVIEW automated scans of U(x,y) for 2 nA

Scanning speed: (100×100) pixels in 1 hr

I/V curves and localization of stable emitters

FE suppression of SC and LG Nb samples by DIC (dry ice cleaning)

A. Dangwal et al., J. Appl. Phys. 102, 044903 (2007)

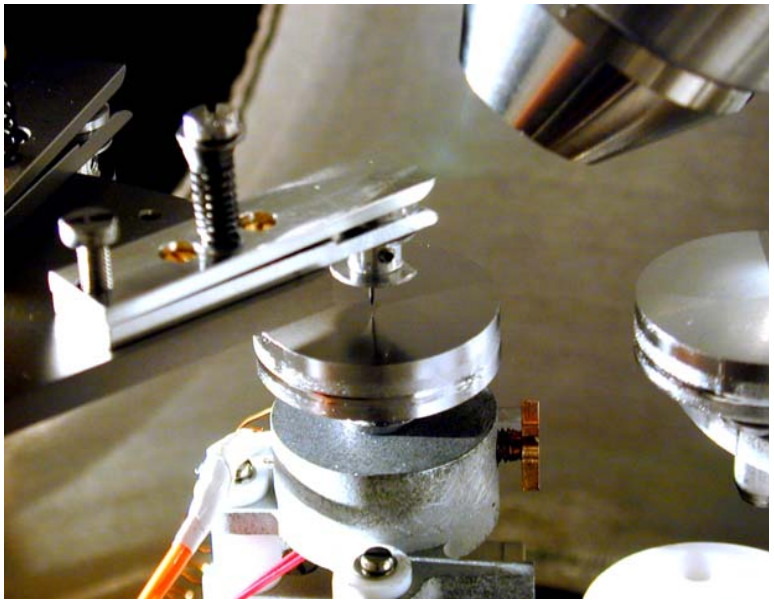

Mirrorlike SCNb sample of Ø 28 mm under W tip anode, 1 μm apex radius

PID-regulated voltage maps U(x,y) for 2 nA scan area = 5×5 mm^2, flat W anode $Ø_a$= 100 μm U_{max} = 5000 V, electrode spacing Dz = 25/20

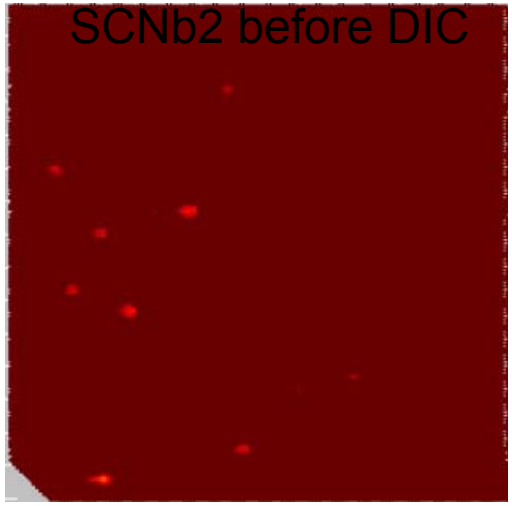

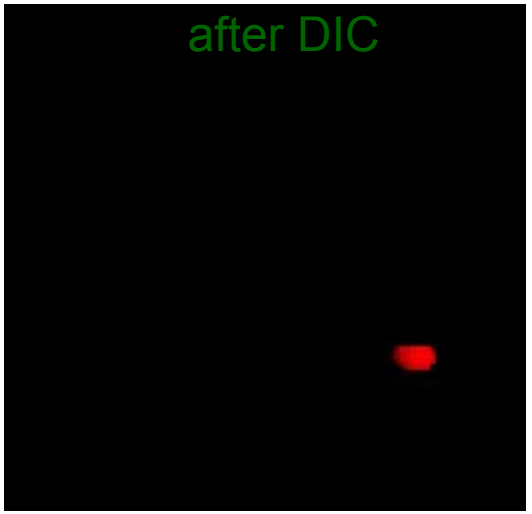

no FE @ 120 MV/m no FE @ 150 MV/m
9 emit. @ 200 MV/m 1 emit. @250 MV/m

Samples LGNb1, LGNb2, SCNb1 yielded before and after DIC
0, 2, 0 @ 120 MV/m no FE @ 150 MV/m
10,12, 5 @ 200MV/m 2, 0 @ 250MV/m

DIC statistically suppresses FE on all type of samples (Cu, Nb)

In-situ bakeout at 150 ºC effects on LGNb3 and SCNb4

PID-regulated U(x,y) for 2 nA scanned area = 5×5 mm^2

flat W-anode Ø$_a$ = 100 µm, U$_{max}$ = 5000 V, Dz = 25, 20, 16.6 µm

LGNb3

before baking

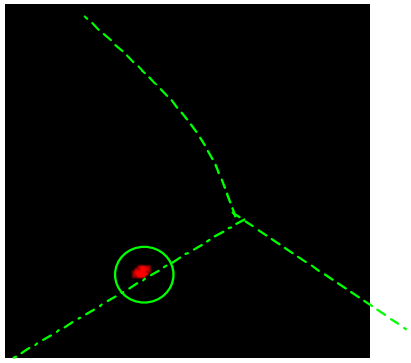

250 MV/m

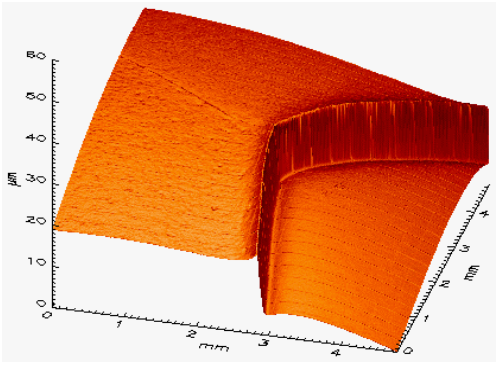

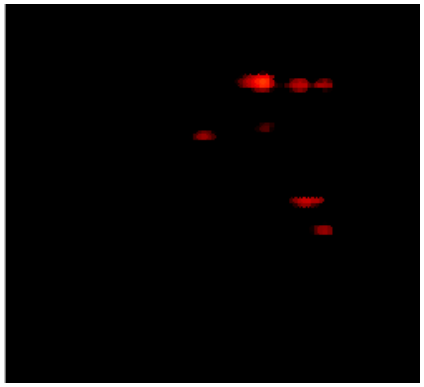

250 MV/m

SCNb4

before baking

after 14 h baking at 150 ºC

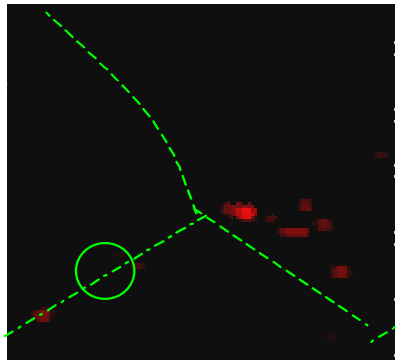

250 MV/m

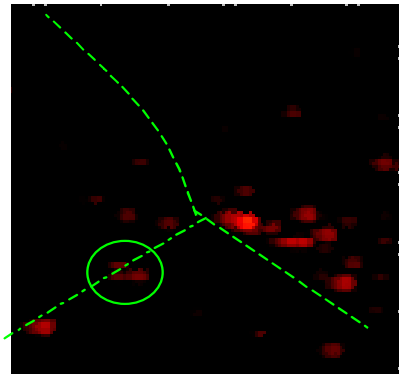

300 MV/m

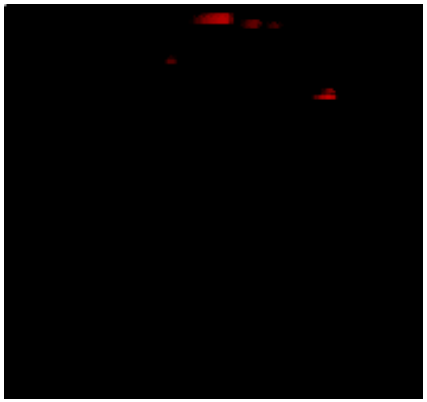

250 MV/m

after 8 h baking at 150ºC

After Baking more emitters appear for LG but not for SC at E > 250MV/m

⇒ evidence for impurity segregation to grain boundaries

Scanning Field Emission Microscope - SFEM

- Coupled with SEM, EDX, and EBSD.
- Large scan area 25mm with 2.5µm lateral resolution
- Emitters can be examined before and after field emission
- Sample treatment chamber (heated up to 1400°C)

Emitter #: 140

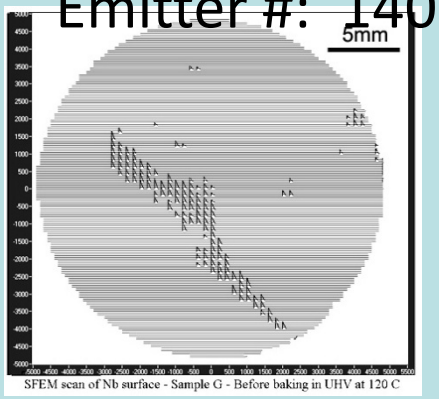

Before Baking

67

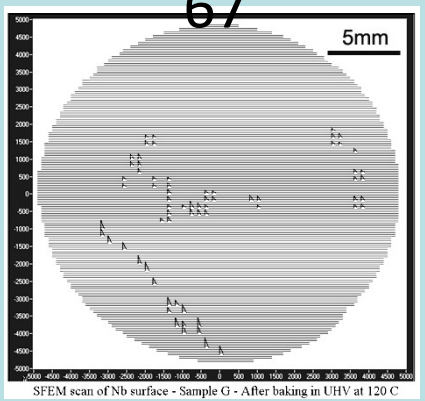

After Baking

BCP

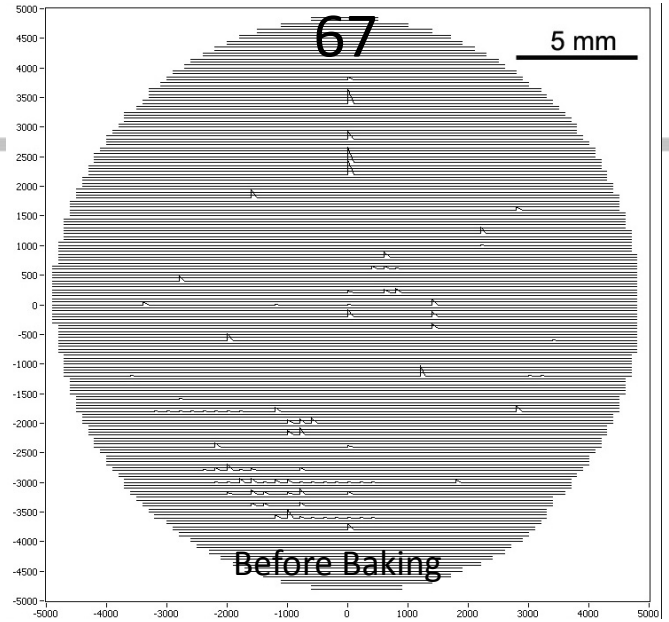

BEP

Emitters on BEP treated Nb surface is significantly less before baking

A. Wu

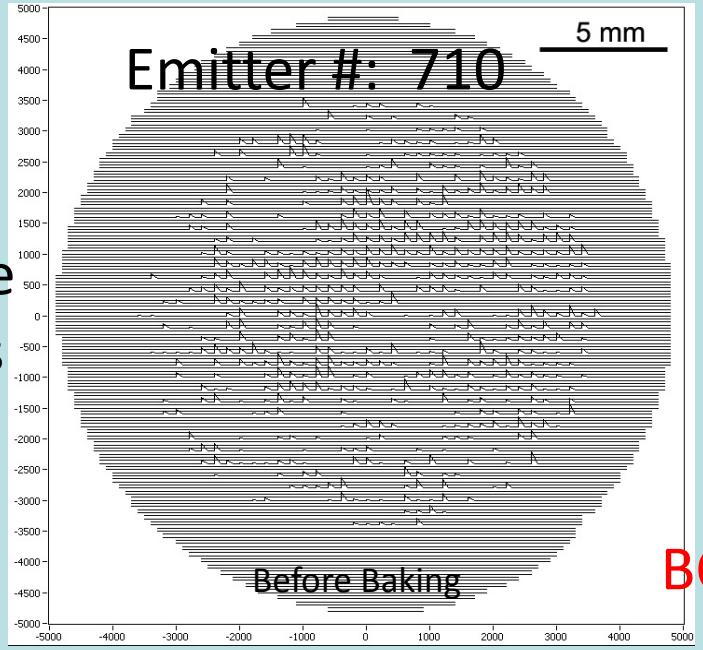

BCP